MASS DIFFUSION OVER WIND WAVES

by

H. T. Liu and S. Karaki

Prepared Under

Contract No. AT(11-1)-1813

Atomic Energy Commission

Fallout Studies Branch

Fluid Dynamics and Diffusion Laboratory
College of Engineering
Colorado State University
Fort Collins, Colorado

May 1972

CER71-72HTL-SK46

ABSTRACT

MASS DIFFUSION OVER WIND WAVES

The mass diffusion process from an elevated point source over a wind-disturbed water surface was investigated experimentally and numerically. The diffusion model which generated from this study was used also to compare experimental with calculated concentration distributions for diffusion in the boundary layer of a flat plate and over a mechanically-generated water wave.

An optical device was developed to measure mean and fluctuating concentrations of small aerosol particles in the wind field. The frequency response and sampling volume of the optical device were found to be adequate for this study and comparable approximately to those for a hot-wire anemometer. A steady stream of aerosol particles was generated by atomization of a heavy oil (Dioctyl Phthalate).

Velocity measurements indicated that the flow conditions, that is, the normalized mean velocity U/U_∞ and relative turbulent intensities $\sqrt{\overline{u'^2}}/U_\infty$ and $\sqrt{\overline{w'^2}}/U_\infty$ were distributed similarly for flow over wind waves for $U_\infty \simeq 10$ fps and over a flat plate for $U_\infty \simeq 10$ and 20 fps. Comparisons of normalized mean velocity distributions indicated that net momentum was transferred from the air stream to water waves and the amount transferred was proportional to the wind speed. However, there was less net momentum transfer from the air stream to mechanically-generated water waves. The relative turbulent intensities increased with increasing wind speed over wind waves. Comparatively large vertical gradients of $\sqrt{\overline{u'^2}}/U_\infty$ and $\sqrt{\overline{w'^2}}/U_\infty$ characterized the flow over mechanical waves.

Results of concentration measurements indicated that the diffusion process is directly proportional to turbulent intensities. The influences of turbulent diffusion, wind shear, and surface reflection resulted in shifting the maximum mean concentration toward the lower boundary while the turbulent diffusion shifted the maximum root-mean-square concentration upward and laterally. The mean concentration distributions over wind waves for $U_\infty \simeq 10$ fps were similar to those over a flat plate for $U_\infty \simeq 20$ fps. The comparatively large vertical gradients of the relative turbulent intensities caused a large concentration accumulation at the mean water level over mechanical waves.

Revised diffusivity models, based on those given by Hino (1968), are proposed. These models are dimensionally correct as opposed to the dimensionally incorrect Hino models and incorporate local conditions by introducing dependency on the boundary layer thickness. The diffusion equation was solved numerically, utilizing an improved finite-difference technique and by using measured flow conditions. The water surface was viewed, in the mean, as a flat surface with wave influences incorporated implicitly into the diffusivity models. With the net vertical mean velocity properly adjusted, general agreement was observed between numerical solutions and corresponding experimental data.

ACKNOWLEDGMENTS

The authors wish to express their appreciation to Professor J. Gessler and Dr. R. L. Drake for their critical reviews of the manuscript. Special appreciation is expressed to Professor E. J. Plate for his early interest in this work prior to his departure to his new post at Karlsruhe, Germany, and to Mr. P. Brawn for his contributions leading to the development of the optical probe for measurement of concentration fluctuations. We are grateful to Mrs. Carolyn Card for typing the manuscript and for her persistence with the details leading to printing of this manuscript.

We are most grateful to the U. S. Atomic Energy Commission for the financial support provided through Contract No. AT(11-1)-1813, to the National Center for Atmospheric Research for use of their computer facilities and to the Department of Civil Engineering, Colorado State University for financial assistance to meet over-runs in computer costs.

TABLE OF CONTENTS

TABLE OF CONTENTS - Continued

TABLE OF CONTENTS - Continued

TABLE OF CONTENTS - Continued

LIST OF TABLES

LIST OF FIGURES

LIST OF FIGURES - Continued

LIST OF FIGURES - Continued

LIST OF SYMBOLS

Symbol	Definition
A,B	Parameters defined in Eq. (2-12)
A_1,B_1,B_2	Constants defined in Eq. (2-27)
A_2,B_3	Constants defined in Eq. (3-7)
a_o	Constant defined in Eq. (6-1)
a_1,b_1,c_1	Polynomial coefficients defined in Eq. (3-6)
a_2,b_2,c_2	Polynomial coefficients defined in Eq. (3-6)
a_y,a_z	Constants defined in Eqs. (2-10) and (2-11), respectively
C	Mean concentration at a point in space
C_{max}	Maximum mean concentration at a given station
C_p	Weighted mean concentration
CREF	Maximum concentration at $x - x_s = 1.83$ ft
c'	Concentration fluctuation
f	Frequency in Hertz (Hz)
$f(\zeta)$	Universal function describing velocity variation
i,j,k	Indices of mesh system in x, y, and z directions, respectively
K	Constant diffusivity
K_2	Diffusivity defined in Eq. (2-20)
K_x,K_y,K_z	Turbulent mass diffusivities in x, y, and z directions, respectively
L	Monin-Obukhov stability length scale
m,n	Constant exponents
m_p	pth moment of concentration distribution
n_1,n_2	Exponents defined in Eqs. (2-27) and (3-7)
p	Integer exponent (Aris moment method), 0, 1, 2, 3, . . .

Symbol	Definition
Q	Discharge rate of aerosols from a point source
Q'	Discharge rate of a point source corrected for the cumulative rate of adsorption by the lower boundary
$\sqrt{\overline{q^2}}$	Root-mean-square turbulent kinetic energy
R	Inside Radius of a pipe
Re	Reynolds number
$R(\xi)$	Autocorrelation function
r	Radial coordinate from the center of pipe
S	Surface area normal to the x direction
T	A general dependent variable as in Eqs. (4-1) and (4-6)
t	Time
U,V,W	Mean velocity components in x, y and z directions, respectively
U_1	Mean wind speed at height z_1
U_2	Mean wind speed at height z_2
U_{max}	Maximum wind speed of pipe flow or freestream velocity, also designated by UMAX
U_∞	Freestream velocity
$\overline{U}$	Average velocity of pipe flow
u_*	Friction velocity, $\sqrt{\tau_0/\rho}$
u',v',w'	Velocity fluctuations in x, y, and z directions, respectively
V_p	Photomultiplier mean voltage output
v'_t	Random component of the velocity fluctuation v'
$v'(t)$	Velocity of a particle
$\tilde{v}$	Wave induced component of the velocity fluctuation v'

Symbol	Definition
W_f	Particle fall velocity
x,y,z	Distances in longitudinal, lateral, and vertical directions, respectively
x_o	X-coordinate at which an initial Gaussian concentration distribution is assumed for numerical calculations
x_1,x_2,x_3	Distances in x, y, and z directions, respectively
x_s,y_s,z_s	Coordinates of point source in x, y, and z directions, respectively
y_{max},z_{max}	Limits for the computational domain in y and z directions, respectively
z_o	Aerodynamic roughness height
z_1	Reference height at which $U = U_1$
z_2	Reference height at which $U = U_2$
z_*	Reference height for mass diffusivity models
α	Adsorbency coefficient
δ	Boundary layer thickness at which $U = .99U_\infty$
δ_2	Momentum thickness
δ_*	Displacement thickness
δ_j	Central-differencing operator
$\Delta x,\Delta y,\Delta z$	Increments of x, y, and z, respectively
η	Water surface perturbation relative to the mean water level
ν	Kinematic viscosity of air
Γ	Gamma function as in Eq. (2-12)
γ	Parameter of the mixed finite-difference scheme
k	Wave number

Symbol	Definition
κ	von Kármán constant
L	Lagrangian integral scale
λ	Half width of a diffusing plume at which C = .5 C_{max}
ρ	Density of air
σ	Constant coefficient of a partial differential equation
$\sigma_1, \sigma_2, \sigma_3$	Constant coefficients of a partial differential equation
$\sigma_{x_1}, \sigma_{x_2}, \sigma_{x_3}$	Standard deviations of the spread of a diffusing plume in x, y, and z directions, respectively
σ_y	Standard deviation of the spread of a diffusing plume in y direction
t	Time constant
τ	Local shear stress
τ_o	Wall shear stress
θ	Parameter of a finite-difference scheme
x	Transformed longitudinal coordinate, x - Ut
ξ	Time lag
ζ	Nondimensional height, z/L
ζ'	Height from the ground surface
ζ'_*	Reference height from the ground surface

Chapter I

INTRODUCTION

In recent years, concern with air pollution has indicated need for better understanding of the atmospheric mass diffusion process. In order to gain better knowledge of the diffusion process, both experimental and numerical investigations have been conducted extensively in the last few decades. Experimental investigations include field observations and laboratory measurements. Field studies provide overall appreciation of the atmospheric diffusion process and thus furnish constraints for laboratory and numerical models. However, in order to study the mechanism of mass diffusion, laboratory studies under controlled conditions must be made. Numerical investigations utilize the knowledge gained from experimental investigations and are used to predict quantitatively the distributions of diffusing pollutants under specified conditions. At the present time, it cannot be stated that the mass diffusion process is thoroughly understood. This is evidenced by the inability to calculate the spread of diffusing particles for general atmospheric conditions.

1.1 Motivations of the Present Study

The atmospheric mass diffusion process is governed by a number of complex factors, such as turbulent intensities, thermal stratification in the surface layer, type of pollution source, properties of the pollutant, velocity profiles and surface conditions. Individual influences of these factors, which interact with one another, are difficult to separate. By appropriate modeling, laboratory investigations can isolate certain of these factors. The advantage of controlled experiments is that the diffusion process may be investigated systematically to understand various influences. With the individual influences better understood, a comprehensive diffusion model is possible to provide accurate prediction of particle concentration distributions downwind from various sources under a variety of atmospheric conditions. As a result, realistic constraints may be specified with regard to release of particulate matter in the atmosphere.

Many investigations of mass diffusion over rigid surfaces such as a flat plate or natural topography have been reported in the literature. Mass diffusion over water surfaces on which wind-driven waves are present have had less attention. The present study attempts to provide a mechanistic understanding of the diffusion process over water surfaces, and a computational model to predict concentration distributions downwind from a point source. Because many industrialized areas are adjacent to large bodies of water, it would seem important to investigate the mass diffusion process over a water surface.

The presence of water waves substantially changes the turbulent structure in the surface layer, and it is the turbulent structure which has dominant influence on the mass diffusion process. The results of the present study will provide better understanding of the wind-wave interaction with regard to the diffusion process.

1.2 Scope and Limitations of the Present Study

The main objective of the present study was to investigate experimentally and numerically the mass diffusion process from an elevated point source over a wind-disturbed water surface (wind waves). Experiments for flow over mechanically generated waves (mechanical waves) superimposed on wind waves were limited. The mechanical waves were of low frequency (2.5 Hz) and had comparatively large amplitudes. The basis for comparison of these experiments was a set of measurements over a flat plate suspended at water level in the same wind-water tunnel.

To enable measurement of concentration of mean and fluctuating quantities, an optical device, which measured scattered light from small particles, was developed. The diffusion particulate matter was generated by atomization of a heavy oil (Dioctyl Phthalate). These particles with average sizes of a few microns were considered to be passive.

The free stream velocity varied from approximately 10 to 30 feet per second (fps). The test section was limited to a 20-ft section in which the deviation from two-dimensional mean flow was small. The aerosol particles were released 12 feet downstream from flow-straighteners near the entrance of the tunnel. The source height was 2 in. above the mean water level which was within the momentum boundary layer ($\gtrsim$ 3 in.). Pressure gradients and secondary flows were present in the flow field as they are in any other noncircular wind tunnel with constant cross-sectional flow area.

Data were taken at fixed probe positions; accordingly, measurements could be made only down to the level of the highest wave crest over the water surface. All conditions were assumed to be statistically stationary during the measurements. The total time period for determination of average values at a given elevation was at least 2.5 minutes.

Revised diffusivity models (Eq. 3-7) based on those given by Hino (1968) were proposed. The diffusion equation was solved numerically utilizing a finite-difference technique and with the aid of a CDC 7600 digital computer located at the National Center for Atmospheric Research, Boulder, Colorado. In the numerical calculations, measured flow conditions were provided and the water surface was viewed, in the mean, as a flat surface. The influences of the wavy surface were implicitly incorporated into a "recovered" turbulent kinetic energy (Sec. 4.4.2) which is one of the independent variables of the diffusivities. To improve calculation efficiency, a variable grid-size system was adopted. The grid system was designed to expand with the spread of the diffusing plume.

Chapter II

BACKGROUND

The diffusion of an aerosol or a gas plume from a continuous point source into a turbulent wind field has been the subject of considerable study in recent years. The diffusion mechanism is governed by a number of complex factors in a turbulent wind field, such as the mean convective velocity profile, turbulence intensity, surface conditions and thermal stratification. Theoretical treatments, which cannot as yet rigorously include all of these natural factors, are limited to a relatively few simple cases. As a result, study of the diffusion mechanism relies primarily on experimental and numerical studies. In this chapter, attempts are made to review relevant literature concerning turbulent diffusion of particulate matter in a neutrally stable boundary layer.

The present study considers the air-water interface formed by a water body as the lower boundary. Therefore, pertinent aspects of the interaction between the wind and the water surface will be reviewed. Prior experimental data appear to be non-existent in the literature, thus measurements were required in this study. For this purpose, an optical device was developed to measure relative concentration of particles in the air stream above the water surface. A brief review of the basic principles of light-scattering from small particles relevant to the design of the optical device seems pertinent and will be discussed in the last section.

2.1 Mass Diffusion Theories

The concept of mass diffusion over solid boundaries such as flat plates or natural topography has been studied extensively both theoretically and experimentally. A comprehensive review of literature on the subject has been made by Slade (1968). A more recent survey has been given by Rao et al. (1971). Only the studies directly pertinent to this investigation will be included here.

In general, there are two distinct approaches to describe the diffusion process, the Eulerian and the Lagrangian (or statistical) descriptions of diffusion. The former describes the diffusion process relative to a spatially fixed coordinate system and the latter considers motion of the separate particles.

2.1.1 Eulerian Description of Diffusion (The K-Theory)

Consider a cartesian coordinate system with component axes x, y and z. The x axis coincides with the mean flow direction and the z axis, vertically upward, is normal to the lower boundary. Let U, V and W be the mean velocity components and u', v' and w' be the corresponding velocity fluctuations in the x, y and z directions, respectively. The diffusion equation, based on conservation of mass may be written in the following form:

$$\frac{\partial C}{\partial t} + U\frac{\partial C}{\partial x} + V\frac{\partial C}{\partial y} + W\frac{\partial C}{\partial z} = \frac{\partial}{\partial x}\left(K_x \frac{\partial C}{\partial x}\right) + \frac{\partial}{\partial y}\left(K_y \frac{\partial C}{\partial y}\right) + \frac{\partial}{\partial z}\left(K_z \frac{\partial C}{\partial z}\right) , \qquad (2\text{-}1)$$

where C is the mean concentration and K_x, K_y and K_z are the exchange coefficients for mass transfer or mass diffusivities. These diffusivities are derived from the assumption of proportionality between the flux of mass and concentration gradients,

$$\overline{u'c'} = -K_x \frac{\partial C}{\partial x}, \overline{v'c'} = -K_y \frac{\partial C}{\partial y}, \overline{w'c'} = -K_z \frac{\partial C}{\partial z} , \qquad (2-2)$$

where c' is concentration fluctuation. The diffusion process is called Fickian when the diffusivities are equal to a constant. In general, the diffusion equation, Eq. (2-1), is a nonlinear partial differential equation because the diffusivities may be functions of the concentration and its gradients. A general solution to Eq. (2-1) is thus, as yet, nonexistent. For practical applications, methods with certain assumptions regarding the flow field and various simplifications to determine the eddy diffusivities have been developed over many years [Pasquill (1966), Priestley (1959) and Sutton (1953)]. The resulting "working" formulae enable us to estimate mass diffusion analytically or numerically under specified conditions.

If the flow is considered to be two-dimensional where V = 0, and if the longitudinal diffusion term is neglected, being much smaller than the convective term, Eq. (2-1) becomes

$$\frac{\partial C}{\partial t} + U\frac{\partial C}{\partial x} + W\frac{\partial C}{\partial z} = \frac{\partial}{\partial y} (K_y \frac{\partial C}{\partial y}) + \frac{\partial}{\partial z} (K_z \frac{\partial C}{\partial z}) . \qquad (2-3)$$

Furthermore, if the flow is steady, Eq. (2-1) reduces to

$$U\frac{\partial C}{\partial x} + W\frac{\partial C}{\partial z} = \frac{\partial}{\partial y} (K_y \frac{\partial C}{\partial y}) + \frac{\partial}{\partial z} (K_z \frac{\partial C}{\partial z}) . \qquad (2-4)$$

Analytical solutions* to Eq. (2-4) exist only for few standard functional forms of velocities and diffusivities. Thus, even in its simplified form, Eq. (2-4) must be solved numerically for general forms of velocities and diffusivities.

---

*Solution of a differential equation is understood to involve the boundary conditions.

Roberts (1923) obtained a solution to Eq. (2-4), with W = 0, for the case of constant diffusivity and wind velocity independent of height. Let x_s, y_s and z_s be the source coordinates and z = 0 be the level of the lower boundary. The associated boundary conditions are:

$$\begin{aligned}
&1.\ C \to 0 \text{ as } y \to \infty \text{ or } z \to \infty \\
&2.\ C \to 0 \text{ as } x \to x_s \text{ for all } z \neq z_s \text{ and } y \neq y_s \text{ but} \\
&\quad C \to \infty \text{ as } x \to x_s,\ y \to y_s \text{ and } z \to z_s, \text{ and} \\
&3.\ K\frac{\partial C}{\partial z} \to 0 \text{ as } z \to 0 \text{ for all } y \text{ and } x > 0 \ .
\end{aligned} \tag{2-5}$$

The solution with $x_s = y_s = 0$ is written as

$$C = \frac{Q}{4\pi K}\frac{1}{\sqrt{x^2+y^2+(z-z_s)^2}}\left[\exp\left(-\frac{U}{2K}\left(\sqrt{x^2+y^2+(z-z_s)^2} - x\right)\right)\right.$$

$$\left. + \exp\left(-\frac{U}{2K}\left(\sqrt{x^2+y^2+(z+z_s)^2} - x\right)\right)\right] \tag{2-6}$$

where Q is the discharge rate of particulate matter which is defined as

$$Q = \int_{-\infty}^{\infty}\int_{0}^{\infty} UCdzdy \ . \tag{2-7}$$

The above solution, Eq. (2-6), however, does not conform with laboratory and field observations. The discrepancy is because diffusivities and wind velocity vary considerably with height in laboratory and atmospheric surface boundary layers.

Bosanquet and Pearson (1936) solved Eq. (2-4), again with W = 0, by assuming a linear variation of K_y and K_z with height in a uniform wind field. The effect of wind shear was taken into account by Roberts [see Calder (1949)] who obtained a solution to the problem for a steady, infinite line source with the governing equation

$$U\frac{\partial C}{\partial x} = \frac{\partial}{\partial z}\left(K_z \frac{\partial C}{\partial z}\right) , \tag{2-8}$$

and the boundary conditions are the same as given by Eq. (2-5) but with no dependency on y. In Eq. (2-8), it was assumed that $U \sim z^m$ and $K_z \sim z^n$ where m and n are constants. Assuming a power-law profile, the mean velocity distribution takes the form

$$U = U_1 \left(\frac{z}{z_1}\right)^m \tag{2-9}$$

where U_1 is the mean velocity at height z_1. Many experiments [Schlichting (1968)] show that m = 1/7 in turbulent flows over smooth surface for a wide range of Reynolds number ($Re < 10^5$). By applying Taylor's continuous movement theory, discussed in the next section, Prandtl's mixing length theory, and Reynolds analogy, Sutton (1934) obtained the so-called "conjugate power law" for the vertical diffusivity

$$K_z = a_z U_1^{1-n} z^{1-m} \tag{2-10}$$

where a_z is a constant. The analytical solution to Eq. (2-8) based on Eqs. (2-9) and (2-10) showed good agreement with experiments [Himus (1929) and Hine (1924)]. The discrepancy was that the predicted height of the plume, which is the distance above ground at which the concentration falls to one-tenth of the local maximum value, was in marked disagreement with observed height. Calder (1949) accounted for surface roughness effects on the velocity profiles in the above analysis. Calder's results, using Reynolds analogy and the assumption of constant horizontal shear stress in the surface layer, was found to agree well with the data.

Significant improvement was made by Davies (1950a, 1950b), who introduced a variable lateral diffusivity to extend the above analysis for the diffusion problem from a continuous point source at ground level. Furthermore, Davies (1952) assumed a dependency of K_y on y such that

$$K_y = a_y U_1^{1-n} z^m y^{1-2m} \tag{2-11}$$

where a_y is a constant and $m = n/(2-n)$. Davies obtained an analytical solution to Eq. (2-4) together with Eqs. (2-9), (2-10), (2-11), and the boundary conditions of Eq. (2-5), given by

$$C = B_o x^{-\frac{2+m}{1+2m}} \exp[-(\frac{1}{A(1+2m)^2})(\frac{z^{(1+2m)}}{x})] \cdot$$

$$\exp[-(\frac{1}{B(1+2m)})(\frac{y^{(1+2m)}}{x})] \tag{2-12}$$

where $A = a_z z_1^m / U_1^n$, $B = a_y z_1^m / U_1^n$,

$$B_o = \frac{Q z_1^m (1+2m)[A(1+2m)^2]^{-(1+m)/(1+2m)}}{2U_1 B^{-(1+2m)} \Gamma(\frac{1}{1+2m}) \Gamma[(1+m)/(1+2m)](1+2m)^{(1-2m)/(1+2m)}} ,$$

and $\Gamma(m) = \int_0^\infty e^{-x} x^{m-1} dx$.

The relation between a_y and a_z is

$$\left\{\frac{a_y}{a_z} = \frac{\overline{v'^2}}{\overline{w'^2}}\right\}^{(1-n)} . \tag{2-13}$$

The solution agreed well with experiments [Calder (1949)] for cloud height and width in a neutrally stable condition.

Instead of seeking a direct solution to Eq. (2-4), Aris (1956) investigated the transformed equation by using the Aris' moment transformation

$$C_p(y,z) = \int_{-\infty}^{\infty} x^p C(x,y,z;t) dx \tag{2-14}$$

and $$m_p = \frac{1}{S} \iint_S C_p dydx \tag{2-15}$$

where C_p is the concentration in the transformed system, p is an integer, S is the area normal to the x-direction, and m_p is the pth moment of the distribution of concentration.

Substituting Eq. (2-14) into Eq. (2-4) in the transformed coordinate system (x = x - Ut), solutions to the moments m_0, m_1, m_2, etc. can be obtained. Although these solutions do not give the actual concentration profiles, they can be used to assist in understanding certain aspects of the diffusion process in considerable detail. Fischer (1964), Sayre (1968), and Atesman (1970) extended Aris' moment method in open channel and pipe flows. Applications of Aris' moment method to atmospheric diffusion have been made by Smith (1957), Saffman (1962), and Chatwin (1968) with some degree of success. Some of their results will be incorporated into the numerical modeling in this investigation.

2.1.2 Langrangian Description of Diffusion (The Statistical Theory)

Based on the random walk model, Taylor (1921) developed a statistical theory of turbulent diffusion. Instead of studying the concentration at a fixed point in space, the statistical approach involving the history of the motion of individual particles is studied and properties necessary to represent diffusion are determined.

Consider a homogeneous and stationary turbulent flow field with zero mean, the autocorrelation function is defined as

$$R(\xi) = \frac{\overline{v'(t)v'(t+\xi)}}{\overline{v'^2}} \tag{2-16}$$

where v'(t) is the velocity of a particle and the overbar designates average values with respect to time, t. Taylor (1921) derived the variance of a spreading smoke plume to be

$$\sigma_y^2(t) = 2\overline{v'^2} \int_0^t \int_0^{t'} R(\xi)d\xi dt'. \tag{2-17}$$

Two limiting cases follow immediately from the above equation:

1. For small diffusion time, $R(\xi) \to 1$, then

$$\sigma_y^2(t) \simeq \overline{v'^2}t^2 \ . \tag{2-18}$$

2. For large diffusion time, $\overline{v'^2} \int_0^{\infty} R(\xi)d\xi = K_2$, then

$$\sigma_y^2(t) = 2K_2 t \ . \tag{2-19}$$

It is noted that

$$K_2 = \frac{1}{2} \frac{d\sigma_y^2(t)}{dt} \tag{2-20}$$

where K_2 is the eddy exchange coefficient. The Fickian diffusion, where the diffusivity is a constant, corresponds to the case in which the turbulent flow contains only eddies of fixed sizes. However, the shear layer in the atmosphere contains eddies of all sizes.

Sutton (1953) reasoned that the Lagrangian single particle auto-correlation function, $R(\xi)$, must depend on the intensity of turbulence, $\overline{w'^2}$, on viscosity, ν , and on ξ. Simply on dimensional grounds, Sutton proposed

$$R(\xi) = \left(\frac{\nu}{\nu+\overline{w'^2}\xi}\right)^n \quad 0 < n < 1 \ . \tag{2-21}$$

Substituting Eq. (2-21) into Eq. (2-17) and assuming ν is much smaller than $\overline{w'^2}t$, the variance becomes

$$\sigma_{x_i}^2(t) = \frac{1}{2} C_i^2 (Ut)^{2-n} \quad i = 1,\ 2,\ \text{and}\ 3 \tag{2-22}$$

where $$C_i = \frac{4\nu^n}{(1-n)(2-n)U^n}\left(\frac{\overline{u_i'^2}}{\overline{u'^2}}\right)^{1-n} \qquad i = 1,\ 2 \text{ and } 3 \qquad (2\text{-}23)$$

called the virtual diffusion coefficient. The value of n may be evaluated from the wind profile

$$\frac{U_1}{U_2} = \left(\frac{z_1}{z_2}\right)^{n/(2-n)} \quad . \qquad (2\text{-}24)$$

Unfortunately, the Lagrangian integral scale, L, with $R(\xi)$ defined in Eq. (2-21) leads to

$$L = \int_0^\infty \left(\frac{\nu}{\nu+\overline{w'^2}t_1}\right)^n dt_1 \rightarrow \infty \ , \qquad (2\text{-}25)$$

which implies infinite eddy energy density at zero frequency and is physically unacceptable. Even with these difficulties, Sutton's model has been adapted in practice and has some acceptance through usage.

It should be noted that the statistical approach is based on the Lagrangian properties of diffusing particles. Such properties are very difficult to measure, if not impossible. In fact, most experimental data have been collected in the Eulerian coordinate system. Taylor's hypothesis, i.e., $x = Ut$, is usually used to change the Lagrangian coordinate system to the Eulerian coordinate system and vice versa. This should be examined carefully before use, especially for flows where intensive mixing occurs.

2.2 Numerical Solutions to the Diffusion Equation

It has been emphasized in previous sections that analytical solutions to the diffusion equation with prescribed boundary conditions exist only for a few standard functional forms of mean velocity and diffusivities. The numerical values of the velocity and diffusivities thus obtained usually do not correlate well with measurements. At present, reasonably accurate measurements of velocities can be made with a pitot-static probe or a hot-wire anemometer. However, accurate measurements of mass diffusivities are not as yet easily available. The diffusivities can be derived based partially on the assumption of Reynolds analogy and partially on physical grounds.

The diffusion equation can be solved numerically if general functional forms of mean velocity and diffusivities are used. Finite differences have been used extensively to approximate the partial differential equation. The investigations in the studies reviewed below used these techniques.

Yotsukura and Fiering (1964) solved numerically the unsteady diffusion equation in a two-dimensional open channel flow by assuming a logarithmic velocity profile and

$$K = \frac{\tau}{\rho \frac{du}{dz}} \tag{2-26}$$

where τ, the local shear stress, was assumed to vary linearly with depth. The solutions thus obtained indicated that the longitudinal distribution of solute concentration is highly skewed at intermediate time stages but gradually approaches a Gaussian distribution at distances of several hundred times the depth. Sayre (1968) transformed the diffusion equation using the Aris' moment method and then solved the transformed equation numerically. For calculation of the moments of the concentration distribution, Sayre's approach has advantages over that of Yotsukura and Fiering (1964) who solved the diffusion equation directly.

Hino (1968) used a two-layer model for flow over a complicated topography. The diffusivities used in the numerical solution were written as

$$K_z = \begin{cases} A_1 \zeta'^m \sqrt{\overline{q^2}} & \text{for } 0 \le \zeta' \le \zeta'_\star \\ A_1 \zeta_\star'^m \sqrt{\overline{q^2}} & \text{for } \zeta'_\star < \zeta' \end{cases}$$

and (2-27)

$$K_y = \begin{cases} B_1 (x-x_s)^{n_1} \sqrt{\overline{q^2}} & \text{for } 0 \le \zeta' \le \zeta'_\star \\ B_2 (x-x_s)^{n_2} \sqrt{\overline{q^2}} & \text{for } \zeta'_\star < \zeta' \end{cases}$$

where A_1, B_1, B_2, m, n_1 and n_2 are constants, $\sqrt{\overline{q^2}}$ is the root-mean-square of the turbulent kinetic energy, ζ' is the height from the ground surface, and $\zeta'_\star$ denotes the level of an internal boundary where the atmospheric structure changes. The numerical values of these parameters are $A_1 = 0.0495$, $B_1 = B_2 = 0.0075$, $m = 0.85$, $n_1 = n_2 = 1$, and $\zeta'_\star = 200$ meters. A variable grid-size system was designed to improve computational efficiency. Comparing the numerical solutions to wind tunnel measurements, Hino (1968) found that the predicted lateral spread was much greater than the observed data and concluded that the smaller lateral spread of wind tunnel measurements was caused by the restriction of lateral movement by the side walls. Hino (1968) extended the numerical solution for a point source to the case of multiple sources in a thermally stratified atmospheric surface layer.

Rao et al. (1971) related the mass diffusivities to the momentum diffusivity by constant Schmidt numbers and solved the diffusion equation for an infinite line source at ground level in a thermally stratified boundary layer. The calculated data for the neutrally stable case agree reasonably well with the experimental data by Poreh (1961).

Ito (1971) made use of a multiple-layered model to solve numerically the diffusion equation for steady line source in a thermally stratified surface layer. The functional forms for the velocity and diffusivities were derived from similarity theory [Monin and Obukhov (1954) and Yamamoto (1959)] with

$$U = \frac{u_*}{\kappa} f(\zeta) \tag{2-28}$$

and

$$K_z = \kappa z u_* / [\zeta f(\zeta)] \tag{2-20}$$

where $\zeta = z/L$ (L is the Monin-Obukhov stability length), u_* is the friction velocity, κ is the Kármán's constant, and $f(\zeta)$ is a universal function which takes different forms in different stability layers. The numerical solutions agree qualitatively with field observations of Project Green Glow*.

2.3 Diffusion Experiments

2.3.1 Field Measurements

Many recent field experiments have been summarized by Slade (1968). The purposes of the experiments varied. Some experiments were designed to relate diffusion to a number of atmospheric states which might be difficult to duplicate in laboratory studies. Some were designed to evaluate the effect of a particular pollutant-releasing process. Because atmospheric conditions are subject to change and

---

*The Green Glow Diffusion Program, Geophysical Research Papers, No. 73, Air Force Cambridge Research Laboratories, 1962.

atmospheric diffusion processes are affected by a number of complex factors, it is difficult to single out the effects of individual factors from the field observations. Therefore, it is often desirable to conduct laboratory experiments under controlled conditions. The field measurements, however, usually provide the constraints for the laboratory experiments.

2.3.2 Wind Tunnel Experiments

A considerable proportion of experimental mass diffusion studies have been conducted at the Fluid Dynamics and Diffusion Laboratory of Colorado State University. The reliability of modeling atmospheric shear flows in a wind tunnel has been confirmed by Malhotra and Cermak (1963), Plate and Liu (1966), and others. A summary of diffusion wind tunnel experiments conducted at Colorado State University was given by Chaudhry (1969).

A number of evaporation studies from a water surface in the presence of wind waves have been carried out [see for example Lai (1968)] and the present study involves mass diffusion from a point source over wind waves.

2.4 Wind Wave Theory

There is net kinetic energy transfer from air to water as the air flows over a water surface due to the deformability of the latter. Energy extracted from the air is reflected in the generation of surface waves and drift currents. It is expected that the surface waves, forming a rough surface in most cases, not only affect the mean air velocity but also induce additional fluctuations in the air flow near the water surface. Because the wind velocity and turbulent fluctuations are dominant factors governing the diffusion of mass transfer, some understanding of the complex interaction between surface waves and these two factors is necessary.

2.4.1 Mean Velocity Profiles over Water Waves

To a first approximation, the characteristics of air flow over water waves may be compared to those over solid boundaries. For example, a logarithmic velocity profile (U vs. log z) was used by Miles (1957, 1959) to study the underlying mechanism of energy transfer from the wind to the waves. In atmospheric studies, the logarithmic profile has been used to describe air flow over the ocean [Hay (1955)]. In laboratory studies also, many investigators [Hidy and Plate (1966), Plate and Hidy (1967), Shemdin and Hsu (1966), Karaki and Hsu (1969), and Wu (1968)] found the mean wind velocity profile to be logarithmic except very near the water surface (about 2 to 3 wave amplitudes above the mean water level). Chang (1968), with an oscillating probe, was able to make measurements closer to the surface. He found that although velocity profiles at various phase points on the wave differ near the water surface, in the mean, they tended to be logarithmic.

The logarithmic velocity profile over water waves is commonly given in the form

$$\frac{U}{u_*} = \frac{1}{\kappa} \ell n \frac{z}{z_0} \tag{2-30}$$

where u_* is the friction velocity ($u_*^2 = \tau_0/\rho$, τ_0 is the wall shear stress), z_0 is the "aerodynamic roughness" of the wavy surface, z is the distance measured from the mean water level, and κ is the von Kármán's constant, assumed to be about 0.4. Investigators [Bole and Hsu (1967), Sutherland (1967) and Wu (1968)] found that Eq. (2-30), "the law of the wall," fitted a region of z/δ of about 0.7 to very near the water surface. The lower region of applicability is believed to extend to a distance about two or three wave amplitudes above the mean water level [Chang (1968)]. Recent measurements by Chambers et al. (1970) indicated that the fitted region is approximately $0.15<z/\delta<0.6$.

Alternatively, a power-law profile similar to Eq. (2-9) has been used to describe the mean velocity profile in air flow over solid boundaries [Schlichting (1968)]. In analytical studies, the power law is often used because the logarithmic profile presents a singularity at $z = 0$ and cannot describe the flow at the outer limits of the boundary layer. The power law may be written as

$$\frac{U}{U_\infty} = \left(\frac{z}{\delta}\right)^{1/n} \qquad (2\text{-}31)$$

where U_∞ is the free stream velocity, δ is the boundary layer thickness defined as the height at which the local velocity $U = 0.99U_\infty$, and n is a parameter depending on Reynolds number. Schlichting (1968) indicated that a relationship between momentum thickness δ_2, boundary layer thickness δ, and n could be

$$\frac{\delta_2}{\delta} = \frac{n}{(n+1)(n+2)} \ . \qquad (2\text{-}32)$$

The measurements of Karaki and Hsu (1968) and Chambers et al. (1970) indicated that the value of n was not unique. However, the power-law profile is preferred in this study, principally for computational reasons and because the power-law profile with variable n more correctly describes the velocity profile throughout the majority of air flow field above the waves.

2.4.2 Wave Induced Turbulent Fluctuations

Karaki and Hsu (1968) concluded that the wave induced fluctuations seem to be confined to small region of $kz < 3$ over wind waves, ($k = 2\pi/L$, L is the wave length). This finding seems to be equally true for the case of mechanically-generated waves as discussed by Chambers et al. (1970) based on Karaki's results. The oscillating probe measurements of Chang (1968) indicated that the longitudinal fluctuations for $z/\delta > 0.2$ are similar to those in equilibrium turbulent boundary layer flows over rough flat plates [Corrsin and Kistler (1954)]. For $z/\delta < 0.15$, however, the fluctuation intensities significantly exceed values found in an equilibrium boundary layer. Chang's results also strongly suggested the possible existence of separation in the lee-side of wave crests. The wave-induced turbulence and turbulence generated by separation in this region ($z/\delta < 0.2$) can cause intensive mixing and plays a most important role in diffusion of mass as well as of heat and momentum.

2.4.3 The Moving and Flexible Boundary

In the last section, the effects introduced by the surface waves to the flow field were discussed. There are other physical aspects which distinguish a water surface from a solid boundary surface:

1. The water surface is flexible and moving, it is fluctuating about a mean level.

2. The roughness heights, which may be related to the root-mean-square of the wave amplitudes, grow with mean velocity and fetch.
3. Energy is extracted from the air flow and is reflected in wave energy growth.

This water surface will be considered, in the mean, as a flat surface, and disturbances induced by the surface will be implicitly incorporated into the diffusivities as functions of the total turbulence fluctuations.

2.5 Optical Technique for Mean and Fluctuating Concentration Measurements

All field measurements of mass diffusion summarized by Slade (1968) used either mechanical or chemical sampling methods. More accurate measurements under controlled conditions are needed to understand fully the turbulent diffusion mechanism. In laboratory experiments, radioactive tracers [Chaudhry (1969)] were used to measure mean concentration. However, none of the above methods are able to measure the concentration fluctuations which is one major factor yet to be understood.

In the last decade, a few optical devices to measure mean and fluctuating concentrations have been developed. Basically, they relate concentration to the amount of light absorbed or scattered by particles in the flow.

Lee (1962) developed a light-probe to measure turbulent mixing of a dye in pipe flow. The instrument was used to measure the amount of light absorbed (proportional to concentration) by the dye particles as they passed through the sampling volume of the light-probe. Nye (1966) improved the same device by reducing the size of the sampling volume so that meaningful concentration fluctuations could be measured at higher frequencies. McKelvey (1968) used this improved light-probe to measure turbulent mixing in a reactor.

Rosensweig et al. (1961) first developed a device, which measures the amount of light scattered by small particles presented at the focal volume, to measure concentration fluctuations of a smoke jet into stagnant room air. A schematic drawing of this device is shown in Figure 2-1. Subsequent applications of this technique in free and confined jet mixing were investigated by Becker et al. (1963, 1965, 1967a) and Williams et al. (1966). Instruments which measure scattered light have been used in measurement of turbulent mixing in pipe flow [Becker et al. (1966)], mixing in a well-stirred reactor [Hottel et al. (1967)], and temperature induced concentration fluctuations in a turbulent flame [Gurnitz (1966)]. Becker et al. (1967b, 1967c) provided pertinent theory and measurements essential to indicate the capabilities and limitations of the light-scattering technique.

In Rosensweig's device a high intensity light beam was focused at the point of measurement (focal point) in the flow field. The scattered light from smoke particles convected through the focal point was collected by a lens placed at right angle to the incident beam. The lens focused the scattered light onto a photomultiplier to convert the light energy into an electrical signal. For most photomultipliers the electrical signal is linear with light intensity over a wide range. This optical device operated successfully with dilute smoke concentrations so that secondary scattering and absorption at points along the light path other than at the focal point does not contribute appreciably to the signal. In order to obtain high spatial resolution, the focal volume needs to be small which is not difficult to achieve optically.

In the present study, mean and fluctuating concentrations over water waves in a wind-water flume was to be measured. In air, Lee's device was not sensitive enough to yield a detectable signal for even very highly concentrated tracers. Clearly, large amounts of tracers cannot be used in a laboratory facility because contamination of the flume and even the laboratory would result. Furthermore, a large quantity of colored and neutrally buoyant tracers is difficult to generate at a steady rate. An instrument which measures scattered light from dilute concentrations of aerosols was needed, and such a device was developed during the course of this study and is described in Chapter V.

Chapter III

A MODEL FOR DIFFUSION

3.1 A General Diffusion Model

A mathematical model leading to an analytical solution usually requires some idealized assumptions which may deviate considerably from the real case. This may also be true for a numerical solution although less restrictive assumptions are sometimes possible. A discussion of the assumptions pertinent to the formulation of a general diffusion model follows.

Consider an aerosol plume which is not neutrally buoyant in the atmosphere. Let W_f be the particle fall velocity (positive downward). The diffusion equation, Eq. (2-4), becomes

$$U\frac{\partial C}{\partial x} = \frac{\partial}{\partial y}(K_y\frac{\partial C}{\partial y}) + \frac{\partial}{\partial z}(K_z\frac{\partial C}{\partial z}) + (W_f - W)\frac{\partial C}{\partial z} \tag{3-1}$$

where the net vertical convection is indicated by the last term.

If adsorption of particles by the lower boundary is significant, the boundary conditions take a more general form than that described by Eq. (2-5). Let α be the adsorbency coefficient of a boundary where a completely reflecting boundary is indicated by $\alpha = 0$, while for a completely adsorbing boundary, $\alpha = 1$. For a continuous point source, the corresponding boundary conditions are:

1. $C \to 0$ as $y \to \infty$ or $z \to \infty$
2. $C \to 0$ as $x \to x_s$ for all $z \neq z_s$ or $y \neq y_s$

   but $C \to \infty$ as $x \to x_s$, $z \to z_s$ and $y \to y_s$ (3-2)

and 3. $K_z\frac{\partial C}{\partial z} + (1 - \alpha)(W_f - W)C = 0$ at $z = 0$

   for all y and $x > x_s$.

The corresponding continuity condition is given by

$$Q' = \int_{-\infty}^{\infty}\int_{0}^{\infty} UCdydz = Q - \int_{-\infty}^{\infty}\int_{X_s}^{X} \alpha(W_f - W)C(x',y,o)dx'dy \quad (3\text{-}3)$$

where the cumulative rate of adsorption by the lower boundary is given by the last term.

It is assumed that there is no deposition of particles on the lower boundary except those adsorbed by it. This assumption is satisfactory for a water surface or grassland as the lower boundary. For other cases, temporal deposition and entrainment of particles may be important. For example, diffusion of suspended matter in an open channel involve such processes.

With consideration of the above general diffusion model, several salient features concerning the present study will be discussed in the next few sections. The results of the discussion will lead to the formulation of a "working" equation amenable for a numerical calculation.

3.2 Net Vertical Mean Velocity

The net vertical mean velocity which appears in the last term of Eq. (3-1) is usually much smaller than the mean wind speed. The effect on the diffusion process by the net vertical mean velocity, nevertheless, may be significant at locations where the vertical concentration gradients are large. The net vertical mean velocity in a wind tunnel is composed of three components: the particle fall velocity, the vertical velocities induced by the displacement of streamlines in the developing boundary layer, and by the existence of secondary flow.

In the present study, the size of the DOP particles generated by the atomizer is of the order of a few microns [Green (1964)]. For a 10μ water particle, the terminal fall velocity in still air is about

0.1 in./sec [McDonald (1960)]. With a mean wind speed of 10 ft/sec, the total diffusion time for particles traveling through say a 20-foot test section of a wind-water tunnel would be less than 2 seconds. The maximum fall distance of the DOP particles, which are lighter than water particles, is less than 0.2 in. On the other hand, the diffusion experiments were conducted in a developing boundary layer flow. The displacement of streamlines in the developing boundary layer produces a positive vertical mean velocity which is opposite in direction to the particle fall velocity. Furthermore, a secondary flow, which is a special characteristic of flows in a wind tunnel, induces a complicated flow pattern in the tunnel. Either a positive or a negative vertical mean velocity may result in a vertical plane along the centerline of the tunnel depending on the cell structure of the secondary flow. A positive vertical mean velocity will result in a velocity defect in the lateral mean wind speed profile at the centerline of the tunnel, while a negative velocity will produce a velocity excess in the profile. The maximum value of the vertical mean velocity induced by the secondary flow over a flat plate in a wind tunnel has been found to be less than 2 percent of the freestream mean wind speed [Veenhuizen (1969)].

As a first approximation, it is therefore reasonable to assume the net vertical mean velocity equal to zero because the individual components are all small quantities. However, for more refined calculations, corrections may be provided. Necessity of introducing a correction may be judged from comparisons between the experimental data and the numerical solution.

3.3 Boundary Conditions

3.3.1 Initial Condition

Mathematically, a continuous point source presents a singularity at the point of release as depicted in Eq. (2-5). The concentration distribution may be described by a Kronecker delta function at that point. However, it is sufficient to describe the concentration distribution by a Gaussian distribution function at a short distance downwind from the point of release and the actual point source may be omitted from the domain of computation. This argument is based on the fact that the diffusion plume is confined to a small cone in which the velocities and diffusivities may be considered constant. The three dimensional Gaussian distribution function is given by

$$C(x\ ,y,z) = \frac{Q\exp\left(-\dfrac{(y-y_s)^2}{2\overline{Y^2(x)}}\right)}{2\pi U(x_s,y_s,z_s)\left(\overline{Y^2(x)}\cdot\overline{Z^2(x)}\right)^{\frac{1}{2}}} \cdot\left[\exp\left\{-\frac{(z-z_s)^2}{2\overline{Z^2(x)}}\right\} + \exp\left\{-\frac{(z+z_s)^2}{2\overline{Z^2(x)}}\right\}\right] \qquad (3\text{-}4)$$

where

$$\overline{Y^2(x)} = 2K_y(x_s,y_s,z_s)(x-x_s)/U(x_s,y_s,z_s)$$

$$\overline{Z^2(x)} = 2K_z(x_s,y_s,z_s)(x-x_s)/U(x_s,y_s,z_s)\ .$$

The initial condition will be computed from Eq. (3-4) at a short distance from the point of release. It is recommended that this distance, x_0-x_s , should be short enough that a Gaussian representation of the concentration distribution is satisfactory. On the other hand, it should be large enough to avoid regions of extremely large concentration gradients which may cause appreciable errors in the numerical calculation.

3.3.2 Boundary Conditions

(a) Condition on the air-water interface - As discussed in Section 2.4.3, the air-water interface may be viewed, in the mean, as a flat surface. Because the total particle diffusion time is less than 2 seconds, adsorption of DOP particles by the lower boundary may be neglected (α=0), especially for an elevated source. The assumptions of zero net vertical mean velocity and zero adsorbency coefficient lead to a reflecting boundary described by the last expression of Eq. (2-5).

(b) Symmetric condition - In a two-dimensional flow field, the diffusing plume is symmetric to the x-z plane through $y=y_s$. The symmetric condition takes a simple form

$$\frac{\partial C}{\partial y} = 0 \quad \text{at } y = y_s \; .$$

This condition allows Eq. (3-1) to be solved in the spatial domain from $(x_s, y_s, 0)$ to (∞,∞,∞).

(c) Free boundary conditions - The spatial domain of Eq. (3-1) spans a quadrant of the entire space, that is, from $(x_s, -\infty, 0)$ to (∞,∞,∞). In the numerical calculation, a finite domain must be used due to the finite capacity of a digital computer. The domain has been limited to regions where concentrations are negligibly small. The boundaries of the domain for the numerical calculation, both y- and z-directions thus form free boundaries on which the concentrations cannot be solved directly in the progressive x-direction. These boundary values must be extrapolated from calculated values adjacent to the free boundary.

Hino (1968) assumed the concentration gradients to be equal to zero on the free boundary which is not compatible with the boundary condition given in Eq. (2-5). In a strict sense, the concentration gradients vanish as y or z approach infinity. To correct this deficiency, the free boundary values should be extrapolated from the calculated values adjacent to the free boundary inside the domain of computation. The analytical solutions, Eqs. (2-7) and (2-12), both show that the concentrations are exponential functions of y and z. In fact, for large y and z, the solutions indicate that log C varies almost linearly with y for fixed values of z and with z for fixed y. It is found that second degree polynomials in y or z enable extrapolations to the free boundary values from the calculated values. The polynomials take the forms

$$\log C(x,y_{max},z) = a_1(x,z)+b_1(x,z)y_{max}+c_1(x,z)y_{max}^2$$

and

$$\log C(x,y,z_{max}) = a_2(x,y)+b_2(x,y)z_{max}+c_2(x,z)z_{max}^2 \quad (3\text{-}6)$$

where (x,y_{max},z) or (x,y,z_{max}) is the coordinate of the free boundary.

3.3.3 Mass Diffusivities

It is observed that the diffusivities expressed in Eq. (2-27) do not have the proper dimensions except when $m = n_1 = n_2 = 1$. The parameters A_1, B_1, and B_2 are therefore not dimensionless which pose certain disadvantages to the diffusivity model. One of the major disadvantages is that characteristics of a particular wind tunnel and other apparatus are included in these parameters which detracts from the universality of Eq. (2-27). Furthermore, preliminary numerical calculations indicated that the calculated concentrations were always underestimated with the use of a lateral diffusivity independent of height explicitly as given by Eq. (2-27). Revised diffusivity models are therefore required to describe the diffusion process more accurately.

Based on dimensional arguments and results of preliminary calculations, the following diffusivity models are proposed:

$$K_z = \begin{cases} A_2 z^{n_1} \delta^{1-n_1} \sqrt{\overline{q^2}} & \text{for } 0 \le z \le z_* \\ A_2 z_*^{n_1} \delta^{1-n_1} \sqrt{\overline{q^2}} & \text{for } z_* < z \end{cases}$$

and (3-7)

$$K_y = \begin{cases} B_3 z^m \delta^{-m} (x - x_s) \sqrt{\overline{q^2}} & \text{for } 0 \le z \le z_* \\ B_3 z_*^m \delta^{-m} (x - x_s) \sqrt{\overline{q^2}} & \text{for } z_* < z \end{cases}$$

where A_2, B_3, n_1 and m are dimensionless constants. These revised models for the diffusivities have the correct dimensions and include dependency of height in the lateral diffusivity. It also introduces "locality" to the vertical diffusivity by incorporating the boundary thickness δ into the equation. The effect of "locality" becomes important in a developing boundary layer but diminishes in importance in the fully developed zone.

Values of the parameters which appear in the diffusivity models will initially be assumed. The final values will be determined by comparing the numerical solutions with corresponding experimental data. To account for the restriction of lateral movement by the side walls of the wind tunnel, it was assumed that $x - x_s$ has an upper bound. The actual value of the upper bound will also be determined by the above comparison. In application to atmospheric diffusion, judgment should be made to determine the proper upper bound for $x - x_s$ according to local topography.

3.4 Descriptions of the Diffusion Field

Poreh (1961) classified the diffusion field for an infinite line source at ground level into four zones based on the values of λ/δ, where λ is the height of the plume at which $C/C_{max} = 0.5$. Qualitatively, the diffusion field for an elevated continuous point source may also be classified into four zones but based on different criteria. These four zones are explained graphically in Figure 3-1.

3.4.1 Initial Zone

The initial zone is the diffusion field next to the point source. Extremely large values of concentration and its gradient prevent accurate measurements of concentration distribution in this zone. In numerical calculations, the initial condition was specified at 0.3 ft downstream from the point of release with a Gaussian distribution function. Therefore, no diffusion calculations were made in the initial zone.

3.4.2 Intermediate Zone

The diffusion field close to the point source, where the vertical spread of the diffusing plume is comparatively smaller than the boundary layer thickness, is called the intermediate zone. The vertical concentration distribution does not deviate significantly from a Gaussian distribution function even in the presence of wind shear. The intermediate zone terminates as the size of the diffusing plume becomes large enough that the concentration distribution shows the influences by the wind shear and boundary conditions. Measurements of concentration distribution in the experimental flume was first taken at 1.83 ft downstream from the source which is in the intermediate zone.

3.4.3 Transition Zone

Next to the intermediate zone, there exists a transition zone in which the influences of wind shear, ground conditions and other flow characteristics dominate the diffusion process. In this zone, the vertical concentration distribution deviates significantly from a Gaussian distribution function. The maximum concentration is shifted slowly toward the lower boundary where convection and turbulent diffusion are minima.

3.4.4 Final Zone

The final zone is the region of the diffusion field where the plume is fully developed both in the vertical and lateral directions. The prolonged influences of the wind shear and boundary conditions eventually shift the maximum concentration to the ground level. The vertical and lateral concentration gradients are very small in the final zone.

Chapter IV

NUMERICAL SOLUTION OF THE DIFFUSION EQUATION

4.1 Finite-Difference Techniques

The finite-difference method of solution was chosen to solve the the diffusion equation, Eq. (3-1). There are a number of schemes to represent a partial differential equation by a set of finite-difference equations. The choice of an appropriate scheme depends on the type of equation and the associated boundary and initial conditions. The criteria of stability, truncation errors, rate of convergence, and computation time are also important factors to be considered [Smith (1965) and Richtmyer (1967)].

Consider a partial differential equation with constant coefficients, for example,

$$\frac{\partial T}{\partial x} = \sigma \frac{\partial^2 T}{\partial y^2} . \tag{4-1}$$

Let i , j , and k be the indices of the mesh system in a general three dimensional space domain and Δx , Δy , and Δz be the increments of the variables x , y , and z , respectively, where $x = i\Delta x$, $y = j\Delta y$, and $z = k\Delta z$. By using forward-differencing on the left-hand-side and central-differencing on the right-hand-side of Eq. (4-1), the finite-difference representation of Eq. (4-1) takes the form

$$T_{i+1,j} = T_{i,j} + \frac{\sigma\Delta x}{\Delta y^2} \{\theta[\delta_j^2 T]_{i+1,j} + (1-\theta)[\delta_j^2 T]_{i,j}\} \tag{4-2}$$

where δ_j is the central-differencing operator defined as

$$[\delta_j T]_{i,j} = \frac{T_{i,j+\frac{1}{2}} - T_{i,j-\frac{1}{2}}}{\Delta y} \tag{4-3a}$$

and

$$[\delta_j^2 T]_{i,j} = \frac{T_{i,j+1} - 2T_{i,j} + T_{i,j-1}}{\Delta y^2} \tag{4-3b}$$

It should be noticed that $\theta = 0$ implies the explicit scheme and $\theta = 1$ implies the fully implicit scheme. For stability, Smith (1965) showed that

$$S = \frac{\sigma\Delta x}{\Delta y^2} \le \frac{1}{2-4\theta} \quad \text{if} \quad 0 \le \theta < \frac{1}{2}$$

$$\text{no restriction if } \frac{1}{2} \le \theta < 1. \tag{4-4}$$

For small truncation errors, the following condition should be established:

$$\frac{\sigma\Delta x}{\Delta y^2} = \frac{1}{6} . \tag{4-5}$$

The stability analysis may be generalized to partial differential equations of more than two variables [Richtmyer (1967)]. For example, the stability criteria corresponding to the equation

$$\frac{\partial T}{\partial x} = \sigma_1\frac{\partial^2 T}{\partial y^2} + \sigma_2\frac{\partial^2 T}{\partial y\partial z} + \sigma_3\frac{\partial^2 T}{\partial z^2} \tag{4-6}$$

are exactly the same as given by Eq. (4-4) except that

$$S = \frac{\sigma_1\Delta x}{\Delta y^2} + \frac{\sigma_3\Delta x}{\Delta z^2} . \tag{4-7}$$

If the mesh sizes are not constant, S may exceed 1/2 for $\theta = 0$ at certain locations. In fact, for boundary layer calculations, the vertical increments have to be small enough to avoid distortion of the important information near the boundary surface. In such a case, it is expected $S << \frac{1}{2}$ near the surface and an implicit scheme should be used to ensure stability.

In some cases, however, the use of an implicit scheme is time consuming for $S << \frac{1}{2}$. For the sake of generality, therefore, a mixed scheme incorporating both explicit and implicit schemes seems more practical. The mixed scheme was successfully adopted by Hino (1968) for the solution of the diffusion equation. In the present study, a revised scheme was developed and is described in Appendix A.

The finite-difference representation of the diffusion equation, Eq. (3-1), is also discussed in Appendix A. The set of finite-difference equations, Eq. (A-8), can be solved iteratively. The calculated values of the last step, multiplied by a correction factor, if desired, is an adequate choice for the initial approximation for the new step. The formulations of the iterative scheme are also described in Appendix A.

4.2 Discrete Mesh System

To improve calculation efficiency, Eq. (A-8) was solved iteratively with variable mesh sizes. The mesh size at each location was chosen such that the discrete coordinate system was sufficient to represent the continuous coordinate system. Detailed information at any location must not be distorted by the introduction of a discrete system. A general guideline for choosing appropriate mesh sizes for the discrete system is that they must be small wherever the gradient of either the velocity or the concentration is large. In this study, the stability criteria of the explicit scheme was not satisfied near the water surface. Therefore, an implicit scheme was used throughout the entire numerical calculation.

The diffusing plume spreads as it is being convected downwind. The mesh system was therefore designed to expand with the spreading of the plume (see Figure 4-1). There were 52 and 85 mesh points in the lateral and vertical directions, respectively.

Near the point of release, small mesh sizes were used. Once the mesh sizes were determined, the number of mesh points used in the calculation, which could be less than the maximum value (52 x 85), depended on the height and width of the plume. At each station, the mesh system was broadened by adding one grid point to both y- and z-directions, if any free boundary values exceed a predescribed fraction of the local maximum. The concentration at each newly added grid points was extrapolated according to Eq. (3-6). Until the maximum number of mesh points was reached, the mesh system was expanded by retaining only every other grid point (see Figure 4-1). As a result, the number of mesh points was reduced to 26 x 42 while covering the same area (width x height) as before. Therefore, the cross-sectional area increased with the spreading of the plume as the numerical calculation progressed from one station to another. In order to optimize the computational procedure, the x-increments also increased with x. This was one of the major revisions to Hino's scheme in which only the lateral mesh was expanded by a sudden doubling of the mesh size. This sudden doubling of the mesh size left the concentrations at the newly expanded grid points undefined.

4.3 Test of the Present Finite-Difference Scheme

A computer program, written in Fortran IV, was developed to solve the diffusion equation from a continuous point source into a turbulent boundary layer corresponding to the present finite-difference scheme. The complete computer program is listed in Appendix B. Figure 4-2 shows the corresponding flow chart for the program.

Two diffusion equations, as test problems with known analytical solutions, were solved numerically by using the present finite-difference scheme. Comparisons between the numerical and analytical solutions enabled the accuracy of the computational scheme to be examined. In test problem I, Eq. (2-4) and Eq. (2-5) were solved with uniform mean velocity and diffusivity. The numerical values of the physical variables are listed in Table 4-1a. The numerical solution and the analytical solution given by Eq. (2-7) agree satisfactorily as shown in Figure 4-3. The agreement is better than that obtained by using Hino's scheme [Hino (1967)].

In a shear flow where large gradients of both velocity and diffusivities are present near the boundary, the mesh sizes for numerical calculation must be chosen with great care. In order to test the general applicability of the present scheme, Eqs. (2-4) and (2-5) were again solved numerically but with the velocity and diffusivities following the power laws according to Eqs. (2-9), (2-10) and (2-11). Pertinent numerical values of the physical variables are listed in Table 4-1b. It was found that the mesh sizes could be chosen quite arbitrarily, provided the requirements discussed in Section 4.2 were satisfied. Again, the numerical solution and the analytical solution given by Eq. (2-12) show satisfactory agreement as depicted by Figure 4-4.

4.4 Physical Variables for Numerical Calculation of Particle Diffusion over Wind Waves

4.4.1 Mean Velocities

The mean velocity profiles were measured with a pitot-static probe (described in Chapter V). The boundary thickness was directly calculated from individual velocity profiles by linear interpolation. Taking the logarithmic values on both sides of Eq. (2-31), the exponent 1/n was fitted with linear least-square technique. The parameter n, the boundary layer thickness δ, and the freestream velocity which are functions of x were then approximated by third degree polynomials. Normalized mean velocity profiles, U/U_∞ with z/δ, are shown in Figure 4-5.

4.4.2 Mass Diffusivities

The numerical values of the parameters used in the diffusivity models of Eq. (3-7) are $A_2 = 0.058$, $B_3 = 0.017$, $n_1 = 0.85$, $m = 0.5$, and $z_\star = 0.8\delta$. The upper bound for $x - x_s$ was determined to be 3.2 ft. In the present study, only the longitudinal and vertical velocity fluctuations were measured. A near universal behavior was observed for $\sqrt{\overline{u'^2}}/U_\infty$ and $\sqrt{\overline{w'^2}}/U_\infty$ in z/δ for all downwind stations as shown in Figure 4-6. Seventh degree polynomials in z/δ were chosen to approximate the vertical distribution of $\sqrt{\overline{u'^2}}/U_\infty$ and $\sqrt{\overline{w'^2}}/U_\infty$.

Experimental investigations [Klebanoff (1954) and Corrsin et al. (1954)] showed that in a two-dimensional boundary layer flow over smooth or rough surface

$$\frac{\sqrt{\overline{v'^2}}}{U_\infty} \approx \frac{1}{2}\left(\frac{\sqrt{\overline{u'^2}}}{U_\infty} + \frac{\sqrt{\overline{w'^2}}}{U_\infty}\right) . \tag{4-8}$$

Therefore, a "recovered" total kinetic energy may be defined as

$$\begin{aligned}\sqrt{\overline{q^2}} &= [\overline{u'^2} + 0.25(\sqrt{\overline{u'^2}} + \sqrt{\overline{w'^2}})^2 + \overline{w'^2}]^{\frac{1}{2}} \\ &= [1.25(\overline{u'^2} + \overline{w'^2}) + 0.5\sqrt{\overline{u'^2}}\sqrt{\overline{w'^2}}]^{\frac{1}{2}} \qquad (4\text{-}9) \\ &\approx \sqrt{\overline{u'^2} + \overline{v'^2} + \overline{w'^2}} .\end{aligned}$$

The numerical values of $\sqrt{q^2}$ and thus the mass diffusivities were computed in accordance with the values given above.

4.4.3 Initial Mesh Sizes

As discussed in Section 4.2, the present mesh system was so designed to broaden and expand with the spreading diffusing plume. Therefore, it was necessary to define only the initial mesh sizes. Furthermore, the results of the test problems indicated that the mesh sizes could be chosen quite arbitrarily provided the requirements discussed in Section 4.2 are satisfied.

4.5 Computational Procedures

The computational procedures which have been discussed in previous sections are summarized below:

1. Input original mesh sizes Δx, Δy, and Δz and other flow conditions.
2. Compute velocities and diffusivities from measured data with the approximate polynomials.
3. Compute concentration by Eq. (A-8) and the associated boundary conditions; for the initial condition, use Eq. (3-10).
4. Extrapolate concentration on the free boundary surface according to Eq. (3-13).
5. Check continuity and smooth result, if necessary.
6. Output results.
7. Broaden or expand mesh system, if necessary, and repeat steps 2 to 6 until the prescribed distance is reached.

Chapter V

INSTRUMENTATION AND EXPERIMENTAL PROCEDURE

Detailed descriptions of the facility and pertinent instrumentation, calibration techniques, and experimental procedures are presented in this chapter. The experiments were performed in the wind-water tunnel at the Fluid Dynamics and Diffusion Laboratory at Colorado State University. The equipment consisted of the wind-water tunnel, devices for measuring concentration, velocities, and the wave heights, and the carriage.

5.1 The Wind-Water Tunnel

The wind-water tunnel shown in Figure 5-1 has been described in detail by Plate (1965). A plunger-type mechanical wave generator has been installed recently [Veenhuizen (1972)]. The tunnel consists essentially of a water tunnel above which a wind tunnel is constructed so that the air flows tangentially over the water surface. It is 2 ft wide by 2.5 ft high, and has a 40-ft plexiglass test section. Sloping beaches made of aluminum honeycomb are installed at both ends to reduce wave reflection. Two pieces of 1/8-in. aluminum honeycombs (1.5-in. thick) separated by approximately 1 in. were installed vertically behind the mechanical wave generator to straighten the wind direction and to ensure stable turbulence level. An axial fan controls the air discharge through the tunnel. The water depth was always maintained at 6 in. and the tunnel was adjusted to a horizontal position (no longitudinal slope).

Water was placed in the tunnel several days before a run to eliminate the existence of temperature gradients between water and room air. Water was not circulated during the experiments. Fresh water was added between runs to replenish the minor loss due to evaporation. The temperature gradients caused by latent heat of vaporization was believed to be small. Therefore, the assumption of a neutrally stable boundary layer was satisfactory.

5.1.1 Special Arrangement

Aluminum plates and plywood boards, covered with #1½E floor sandpapers made by Norton - 40 grains/in., were suspended in the wind-water tunnel at an equivalent level to a water surface to constitute a flat surface. The suspended flat surface spanned the entire length of the tunnel. The special arrangement enabled comparison of measurements of mass diffusion process and flow characteristics in the same facility for air flow over a water surface and the flat plate. In this way, the overall influences of the facility, such as entrance conditions and secondary flow, could be minimized in the comparisons.

5.2 Measurements of Water-Wave Heights

The displacement of the water surface was measured with a capacitance gauge (Figure 5-2). Detailed information of the gauge and the associated circuitry have been described by Chang (1968). The gauge consists essentially of a 32-gauge Nyclad insulated magnetic wire which is stretched vertically in the wind-water tunnel. The copper wire and the water act as two dielectric media. The gauge measures the changes in wire capacitance responsive to the changes in immersion depth. The wave gauge was calibrated before and after each series of experiments. Calibration was made by lowering and raising the gauge in a still water tank with a point gauge. Slight shift in the output DC voltage due to temperature change and the wetting effect of the wire was observed, but the slope of the calibration curves remained unchanged. Typical calibration curves of the wave gauge is shown in Figure 5-3. Output voltage has been found to be linear with immersion depth. The output signal was recorded by an Ampex FM tape recorder (Model FR-1300) for later analysis.

5.3 Measurements of Drift Velocities on the Water Surface

The drag of the wind shear generates a drift current on the water surface. Floating polyethylene balls (0.125-in. O.D.) dropped one at a time on the water surface were used to measure the drift velocity. The travel time of individual balls for every 4-ft span was recorded. The average drift velocity equals the travel distance divided by the mean time. It was observed that the polyethylene balls did not follow straight courses. Lateral movements were caused by the secondary flow developed in the water body. The average drift velocity was approximately 2% of the freestream velocity which corresponds to recent measurements by Chambers et al. (1970).

5.4 Measurements of Mean and Fluctuating Velocities

The mean air velocity was measured with a 1/6-in. O.D. pitot-static probe made by United Sensors and Control Corporation (Model PBA-12-F-11-KL) together with a pressure transducer made by Tran Sonic, Inc. (Type 120). The pressure transducer was calibrated against a Meriam 34FB2 TM micromanometer accurate to .001 in. of H_2O. The calibration curves are shown in Figure 5-4. The pitot-static probe was mounted on a carriage which could be positioned anywhere in the tunnel. A motorized mechanism was provided for vertical movement of the mounted probe. A counter displaced on the control panel registered the number of turns made by the driving motor. Each turn of the motor was equivalent to a vertical distance of .0252 in. Point by point velocity measurements were made with reference to the mean water level. Output voltage from the pressure transducer was recorded on an X-Y recorder (Moseley, Model 136A) with a record length of 90 seconds.

The longitudinal and vertical fluctuating velocities were measured with a two-channel constant temperature hot-wire anemometer (Thermo-System, Inc., Model 1050). The sensing elements (Thermo-Systems, Inc., Model 1241) were two .00015-in. O.D. tungsten wires arranged in an x-configuration with their axes parallel to the y-direction. The hot-wire probe was calibrated against the pitot-static probe in the free-stream at several mean velocities within the range of interest. A calibration was made every two hours. The pitot-static probe and the hot-wire probe were mounted side by side in the wind-water tunnel with sufficient separation to avoid interference of the flow pattern by either probe. The calibration data were fitted with the King's law with variable powers. Figure 5-5 shows a set of typical calibration curves.

The DC signals from the anemometer were recroded on X-Y recorder and the AC signals were recorded on analog tapes. A sum and difference circuitry was used to analyze the turbulence signals. Root-mean-square values were determined with a true RMS meter (Disa, Type 55D35). The turbulence intensities of velocity fluctuations u' and w' were calculated by formulas given by Klatt (1968).

5.5 Measurements of Mean and Fluctuating Concentration

An optical device to measure mean and fluctuating concentration was developed. This new device enables a photomultiplier (PM) tube, which converts light signals into electrical signals, to operate essentially in a dark field. It measures the forward-scattered light from aerosol particles rather than lateral-scattered light as in Rosensweig's device. This feature increases the signal-to-noise ratio because the forward-scattered light intensity is stronger than the lateral-scattered light intensity. The optical path of the new device has been significantly shortened. Less effect due to secondary scattering and absorption is expected. The frequency response of the optical device has been found to be comparable to that of a hot-wire anemometer, which enables equally accurate measurements of velocity and concentration fluctuations to be made. The space resolution of the optical-probe has also been found to be small enough to retain information at high wave numbers.

The optical device is composed of three main portions: the light source, the optical probe, and the photomultiplier (PM) tube. The principle of operation is relatively simple. Light scattered from aerosol particles at the sampling volume is sensed by the PM tube which converts the scattered light into electrical currents. After a few stages of amplification in the PM tube, the light intensity is output in the form of voltage. The output voltage is proportional to the scattered light intensity and thus is proportional to the number of particles in the sampling volume.

5.5.1 The Light Source

A Sylvania CAZ projector light bulb (750 watts, 120 volts) with a DC power supply (Technique Power LA-160V-6Amp) was used as the light source. After a sufficient warm-up period of 1½ to 2 hours, the light source yields a very steady yellowish-white light, within ±1.5 percent shifting in light intensity, in a duration of one hour or longer.

5.5.2 The Optical-Probe

The optical-probe is comprised of two 6-foot fiber optics leads (Dolan-Jenner Industries, Inc., BXL 672 and 872), transmitting and receiving lens housings, and mounting units (see Figure 5-6). Light transmitted through the transmitting fiber-optics lead and lenses is focused at the midpoint of the probe gap. The center areas of the transmitting lenses are coated with 3M 101-C10 non-reflective black paint. Conical dark regions are thus formed in the probe gap as shown in Figure 5-6b. A tapered dowel (painted black) glued on lens 1 reduces leakage of light into the dark regions. The sensing aperture (0.02-in. diameter pin hole) of the receiving housing is completely immersed in the dark zone. Therefore, the PM tube is essentially operated in a dark field. Noise from the incident light beam is eliminated except through leakage.

The scattered light from aerosol particles at the focal volume is picked up by the receiving lens through the aperture and hence detected by the PM tube. The output voltage from the PM tube is directly proportional to the light intensity over a wide range. The scattered light intensity is also linearly proportional to the number of particles at the focal volume provided the concentration is small such that both secondary scattering and absorption effects are insignificant. In these experiments measurements of aerosol concentrations were derived at a distance of 15 to 20 feet downwind from the source with maximum wind speed of about 30 ft/sec. This required a comparatively large particle discharge rate so that the concentration at sections near a point source might be sufficiently large that the secondary scattering and absorption effects might no longer be negligible. Also, the physical configuration of the optical probe could not be allowed to disturb the velocity field at the sampling volume. A calibration of the optical system was thus needed to relate instrument output to concentration. The calibration technique which treated the optical system as a black box will be described in a later section.

5.5.3 The Photomultiplier Tube

An RCA 7265 12-stage photomultiplier tube with S-20 response characteristics (see Figure 5-7a) was chosen. Figure 5-7b shows the associated circuitry. The PM tube is magnetically shielded with a Miller No. 80802E shield. Proper grounding is required to prevent buildup of static charge on the chassis. A Hewlett Packard 6516A power supply with 3000 VDC maximum output was used to operate the PM tube. The PM tube was normally operated at 2800 VDC. The stability was found to be excellent under the predescribed conditions.

5.5.4 The Aerosol Generator (Atomizer)

The atomized liquid in this study was Dioctyl Phthalate (DOP). The discharge rate was proportional to the pressure applied to the atomizer. In the present study, the range of pressure applied to the atomizer was below 20 psi. A two-stage air flow regulator was attached to a compressed air tank outlet to ensure a constant pressure output. The discharge rate was found to be independent of the amount of DOP in the atomizer. Figure 5-8 shows a picture of the atomizer. Between the atomizer and the source nozzle, a 3-ft 10-in. expanded aluminum section (2-3/4-in. I.D.) was inserted so that large aerosol particles could settle out of the flow. The atomizer generated fairly uniformly distributed and constant concentration of aerosol particles with sizes of a few microns in diameter [Green (1964)]. According to Becker (1967b) slip velocity between particles of this size and the velocity field may be safely neglected. The atomized DOP particles have small tendency to evaporate, sublime, coagulate, or react chemically. The fall velocity of the aerosol particles may also be neglected (see Section 3.2). In fact, only a small amount of DOP deposit was observed on the water surface after a few hours of testing in the wind-water tunnel. In the early development stage, it was found that DOP particles tended to collect on the receiving lens of the optical-probe, thus affecting the optical transmissivity. This problem was eventually overcome by covering the lens with a small cap as shown in Figure 5-6b.

A block diagram of the instrumentation for concentration measurements is shown in Figure 5-9. The output voltage from the PM tube was recorded on magnetic tape for later analysis.

5.5.5 Calibration of the Optical System

A linear relationship between the PM voltage output and the concentration was assumed by Rosensweig et al. (1961) and their successors Becker et al. (1963, 1965, 1967a) and Williams et al. (1966).

If the concentration is dilute so that both secondary scattering and absorption effects are insignificant, and the sizes of the particles are truly uniform, the linear relationship is justified. To examine this point, a method to calibrate the optical system was developed and is described below.

It is difficult to measure the absolute concentration of an aerosol cloud, but in most experimental work knowledge of only the relative concentration is needed. A 5-3/4-in. I.D. cast iron pipe 45 ft long with a blower at one end and the optical system at the other was set up as shown in Figure 5-10. The aerosol source was introduced to the pipe flow system through a 1/4-in. I.D. brass tubing. The aerosol was released upstream of the blower to ensure thorough mixing before reaching the outlet where the optical-probe was located. A uniform concentration distribution across the pipe was thus expected at the outlet for a constant aerosol discharge rate. The discharge rate may be expressed by

$$Q = \int_S CUdS = C\int_S UdS = C\overline{U} = \text{constant} \qquad (5\text{-}1)$$

where $$\overline{U} = \int_S UdS = 2\pi\int_0^R rUdr \ .$$

A linear relationship was found between the average and maximum pipe velocities. In the range from 10 to 40 ft/sec, the least square best fit line is expressed by

$$\overline{U} = 0.821\ U_{max} - 0.404\ . \qquad (5\text{-}2)$$

The measured data of U_{max} and $\overline{U}$ along with the best fit line are shown in Figure 5-11. The velocities were measured with a 1/16-in. O.D. pitot-static probe and pressure meter (Tran Sonic, Inc., Type 120).

Three concentration profiles are shown in Figure 5-12 corresponding to three different pressures applied to the atomizer across the pipe outlet. The concentration distribution was practically uniform within ±2% error. This error is partially introduced by the entrainment effect near the outside edges of the jet beyond the pipe exit where the concentration is slightly higher.

With a fixed aerosol discharge rate, the concentration was measured by varying the wind speed in the pipe. Should the linear relationship between the PM voltage V_p and the concentration be established, the product of V_p and the average wind speed $\overline{U}$ must be independent of $\overline{U}$. Originally, it was observed that $V_p\overline{U}$ decreases with increasing $\overline{U}$. The amount of decrease is proportional to the discharge rate or the pressure applied to the atomizer. A closer investigation revealed that such decrease was caused by the adsorption of aerosol particles on the fan and honeycombs. The larger the wind speed, the faster the fan revolved and thus more particles impinged on the fan. Therefore, the linear relationship between the PM voltage and the concentration should be used within the limit of experimental errors for the range of discharge rate used in this investigation.

5.5.6 Characteristics of the Optical System

(a) Frequency response - The anode pulse rise time of the PM tube is 2.7×10^{-9} sec at 3000 VDC which is much higher than the frequency of the air turbulence whose energy is concentrated in frequencies below 10 KHz. The frequency response is therefore limited by that of the associated circuitry and by the noise level.

A stroboscope with frequency range from 100 to 25,000 rpm was used to determine the frequency response of the optical system. Oscillograms corresponding to the frequency response of the optical system to a strobe light of known frequency were photographed. The time constant, defined as the time required from peak rolling to 3 db of the peak value, may then be measured. Figure 5-13 shows two sample oscillograms corresponding to strobe lights of 417 and 300 cps. The time constant, t, is found to be 9×10^{-6} second. The frequency at which the amplitude is 3 db down is

$$f = \frac{1}{1.5t} = 7.4 \times 10^{4} \text{ Hz.}$$

The above calculation is based on the assumption that the stroboscope generates a square wave light signal. Hence, the actual value should be higher than the calculated one. It should be noted that the frequency response thus determined represents that of the optical system as a whole unit.

(b) <u>Attenuation with frequency</u> - The light intensity of the stroboscope decreases with frequency. To measure signal attenuation with frequency, a special technique was developed. A disc with 100 holes (.04-in. dia) at .08 in. center-to-center around the perifery was attached to a 9800 rpm DC motor. The transmitting tip was partially covered so that a light beam of diameter less than 0.04 in. was emitted. The disc was then rotated between the two probe tips with the light beam, the hole centers and the sensing aperture in perfect alignment. As the disc rotated, the PM tube sensed a nearly square wave light signal. It can be seen from Figure 5-14 that there was only 2 percent drop up to 7 KHz. If desired, the measured data may be corrected according to Figure 5-14.

(c) Space resolution - The focal volume of the optical-probe is of order 6.0×10^{-5} in.^{3}. The effective focal volume which contributes 80 percent or more of the total response is about 4.8×10^{-5} in.^{3}. To simulate the effect of light scattering from small particles, a thin wire painted black and with a white pointer was made. As it was moved along a certain path (axially or radially) in the probe gap, the PM output corresponding to the intensity of scattered light from the white point along that path was recorded. The envelope of all the output curves, as shown in Figure 5-15, may be then used to determine approximately the size of the focal volume. Figure 5-16 shows the size of the focal volume versus the normalized signal strength. The effective focal volume is actually about 2/3 of the calculated value because the latter includes part of the dark region which makes no contribution to the signal. Furthermore, the actual size of the focal volume should be smaller because the size of the white point on the wire was comparable to that of the focal volume.

(d) Velocity disturbance due to the optical-probe - It is expected that the optical-probe tips may introduce a velocity disturbance at the sampling or focal volume where the concentration is measured. The amount of disturbance must be small in order to obtain meaningful results. A sub-miniature hot-wire probe made by Thermo Systems, Inc. (Model 1276) was used to measure velocities at a point with and without the optical-probe in position. There was approximately 10 to 15 percent increase in mean velocity (at a speed of 35 ft/sec) due to the optical-probe. However, this increase does not necessarily represent the disturbance due to the optical-probe tips, because the hot-wire probe itself introduces additional disturbance which would be significant. The uniformity of the concentration profile measured with the calibration pipe indicates that the velocity disturbance at the focal volume was not significant.

Chapter VI

DISCUSSION OF RESULTS

In this chapter, the results of the present study are discussed. The measured and calculated concentration distributions over a water surface with and without mechanical waves, and over a flat plate are presented. The concentration fluctuations are also examined. In order to examine the validity of the present diffusion model and to determine the accuracy of the finite-difference scheme in the numerical solution, comparisons between numerical results and corresponding experimental data are provided. Possible influences of certain characteristics of the wind-water tunnel on the experimental data are investigated to seek refinement in the numerical solutions. A summary of experimental conditions is tabulated in Table 6-1.

The accuracy of turbulent intensity measurements with a hot-wire anemometer was about ±10%, especially in regions near the lower boundary where velocity gradient is steep and turbulent fluctuations are large. In the same regions, the measurements of mean velocity with a pitot-static probe are also affected. Its accuracy, however, was estimated to be ±3%. The deviation between a standard pitot-static probe, which was calibrated with a rotating arm [Kung (1967)], and the present probe was found to be less than ±2%. The measurements of mean and fluctuating velocities were considered to be standard laboratory procedures. Detailed information and discussions on possible errors introduced in these measurements may be found elsewhere [See for example Kung (1970)]. Errors in sampling probe placement in x, y and z directions were within ±0.003, ±0.004, ±0.005 ft, respectively. An overall accuracy of ±8% for concentration measurements were estimated. An uncertainty analysis using random simulation technique to evaluate experimental errors is provided in Appendix C.

6.1 Flow Conditions

6.1.1 Mean Velocity Distributions

The normalized mean velocity profile U/U_∞ versus z/δ at successive stations were shown in Figure 4-5. For $U_\infty \simeq 10$ fps, the velocity profile over a wind-disturbed water surface, on which capillary waves predominated, was similar to that over a flat plate for $U_\infty \simeq 10$ and 20 fps. As the wind speed was increased beyond 10 fps, gravity waves developed. With the advent of gravity waves, there was no longer similarity of profiles to that over a flat plate. At a given height above the mean water level, U/U_∞ decreased with increasing wave heights. This indicated that momentum was transferred from the air flow to the water waves and caused the waves to increase in height with fetch and with wind speeds. However, for flow over mechanical waves with a frequency of 2.5 Hz, U/U_∞ was greater than that over wind waves with the same wind speed ($\simeq$ 20 fps) at the same height above the mean water level. Thus it would seem that there was less net momentum transfer from the air flow to the mechanical waves. The rms wave amplitudes for flows over wind waves and mechanical waves are shown in Figure 6-1. It should be noted that linear growth of wave heights with fetch was observed for all cases. The foregoing results for mean velocity distributions were reflected in the values of n in the power-law profile, Eq. (2-31). For flow over wind waves, the value of n decreased with increasing wind speeds which conform to recent measurements by Chambers et al. (1970).

6.1.2 Turbulent Intensities

The relative turbulent intensities $\sqrt{\overline{u'^2}}/U_\infty$ and $\sqrt{\overline{w'^2}}/U_\infty$ over wind waves, and thus the "recovered" turbulent kinetic energy defined in Eq. (4-9), increased with increasing wind speeds. This can be observed in Figure 4-6. Energy extracted from the mean air flow was therefore partially returned in the form of increased turbulence. At $U_\infty \simeq 10$ fps, the relative turbulent intensities over wind waves were distributed similarly to those over a flat plate at $U_\infty \simeq 10$ and 20 fps. For flow over mechanical waves, however, the distributions of $\sqrt{\overline{u'^2}}/U_\infty$ and $\sqrt{\overline{w'^2}}/U_\infty$ in z/δ showed marked differences between those over wind waves. The comparatively large vertical gradients of $\sqrt{\overline{u'^2}}/U_\infty$ and $\sqrt{\overline{w'^2}}/U_\infty$ characterized the flow over mechanical waves. Although data are scattered, a near universal behavior of $\sqrt{\overline{u'^2}}/U_\infty$ and $\sqrt{\overline{w'^2}}/U_\infty$ in z/δ was observed at successive stations. The scatter of these data was caused by the limitation of measuring turbulent intensities accurately with a hot-wire anemometer as discussed earlier in this chapter.

6.2 Concentration Distributions

6.2.1 Experimental Results

6.2.1.1 Mean Concentration Distributions

The measured mean concentration distributions over a water surface with and without mechanical waves are shown in Figures 6-2 to 6-5. The mean concentrations were normalized by the maximum concentration at $x - x_s = 1.83$ ft of individual cases. Corresponding numerical solutions discussed in later sections are also shown on these figures. At a given station, the vertical and lateral spread of the diffusing plume increased with increasing relative turbulent intensities of the flow as expected. For flow over wind waves, the relative turbulent intensities have been found to be proportional to the wind speed and thus to the wave height. The direct influence of the wind waves on mass diffusion is therefore to increase the spread of a diffusing plume through turbulent diffusion. A larger spread of the plume at a given station results in smaller local maximum concentration.

The lateral mean concentrations in a horizontal plane 2 in. above the mean water level displayed essentially symmetric distributions through $y = y_s$. Slight skewness to one side was observed occasionally. The vertical mean concentration distributions over wind waves show a weak trend of higher concentrations at the water level in the transition zone for flows of lower relative turbulent intensities. Figure 6-5 shows the mean concentration distributions over mechanical waves. The period of the mechanical waves was 2.5 Hz and the root-mean-square wave amplitudes at successive stations are shown in Figure 6-1. The vertical mean concentration distributions over mechanical waves deviated significantly from those over wind waves. There are comparatively larger concentrations near the interface with the presence of mechanical waves. The large vertical gradients of $\sqrt{\overline{u'^2}}/U_\infty$ and $\sqrt{\overline{w'^2}}/U_\infty$ for flow over mechanical waves apparently cause larger downward flux of particles where convection is smaller and contributes to larger concentration accumulation. Neither flow over a flat plate for $U_\infty \simeq 20$ fps (Figure 6-6a) nor flow over wind waves displays this characteristic in the vertical mean concentration distributions.

As it can be seen in comparing Figures 6-2a and 6-6a, there is similarity in the vertical mean concentration distributions between flows over a flat plate for $U_\infty \approx 20$ fps and over wind waves for $U_\infty \approx 10$ fps where the flow conditions in dimensionless forms are similar.

6.2.1.2 Concentration Fluctuations

Vertical and lateral distributions of concentration fluctuations, normalized by local maximum concentrations, are shown in Figures 6-6b to 6-10. The lateral distributions were measured in a horizontal plane 2 in. above the mean water level. It can be observed distinctly that the maximum concentration fluctuations, which occurred along the centerline of the diffusing plume close to the point source, were shifted upward and laterally as the plume was convected downwind. The trajectory of these maxima is interpreted to define the region of the diffusing plume at which concentration fluctuations are highly intermittent. The spread of the plume, which may be designated by this trajectory, is directly proportional to the relative turbulent intensity of a flow field. A similar feature is observable, although less distinct in the mean concentration distributions as discussed in Sec. 6.2.1.1. Figure 6-11 shows such trajectories of individual cases measured on the x - z plane through $y = y_s$. Near the water surface where intensive turbulent mixing occurs, the concentration fluctuations are limited to high frequency components which have insignificant contribution to the rms concentration. On the other hand, in the upper portion of the plume where turbulent intensity is diminished, comparatively low frequency fluctuations predominate due to certain large scale motions such as the meandering of the plume. At the outer edge of the plume, which corresponds to the locations of the above trajectories, low frequency mixing due to entrainment results in formation of an irregular interface with intermittent regions of clean and contaminated air. This comparatively low frequency fluctuation of large amplitude is responsible for the high rms concentration fluctuations.

An important feature follows immediately from these results. The close resemblance of flow conditions in dimensionless forms between flows over a wind-disturbed water surface for $U_\infty \approx 10$ fps and those over a flat plate for $U_\infty \approx 10$ and 20 fps resulted in similar concentration distributions at successive stations. This suggested that the mass diffusion process could be better described if the diffusivities which govern the diffusion mechanism are properly related to these flow conditions with appropriate scale factors. The present diffusivity models, Eq. (2-31), were expressed in accordance with this observation. The numerical solutions, which considered the water surface, in the mean, as a flat surface but incorporated implicitly the influences of the wavy surface into the diffusivity models, are discussed in the following sections.

6.2.2 Numerical Solutions

The computer program for the numerical solutions is described in Appendix B for a CDC 7600 at the National Center for Atmospheric Research, Boulder, Colorado. The measured mean velocity profiles, turbulent intensities and corresponding physical variables of individual cases were best fitted with appropriate polynomials as described in Sec. 4.4 and the polynomial coefficients were input to the computer program. The computational time, which varied from one case to another, was from 35 seconds for $U_\infty \approx 30$ fps to 48 seconds for $U_\infty \approx 10$ fps over wind waves.

The numerical solutions designated by dotted lines for $W - W_f = 0$ and by solid lines for $W - W_f \neq 0$, are shown in Figures 6-2 to 6-6. A simple correction to account for the net vertical mean velocity, which will be discussed in later sections, is given by

$$W - W_f = \begin{cases} a_o(1 - \frac{z}{\delta}) & \text{for } z < \delta \\ 0 & \delta < z \end{cases} \tag{6-1}$$

The values of a_o were adjusted for individual cases to obtain the best possible fit between numerical solutions and corresponding experimental data. The maximum correction required for $W - W_f$ was 0.9% of the local freestream velocity. With $W - W_f = 0$, the numerical solutions did not agree with corresponding experimental data near the lower boundary. With proper corrections to $W - W_f$, the agreements were improved substantially; in fact, a general agreement was observed for all cases.

To account for the finite size of the source tubing in the experiments, which was 0.25 in. in diameter, the origin of the point source for numerical solutions was shifted to $x_s = -0.02$ ft upstream from the actual point of release. For flow over mechanical waves, it was found that the low frequency oscillation (2.5 Hz) in the air stream induced by the mechanical waves increased the effective size of the source and the correction to x_s of -0.20 ft was made.

The general agreement between numerical solutions and corresonding experimental data indicated that, for engineering purposes, the present diffusion model was adequate to describe the mass diffusion process over wind waves. Even for flow over mechanical waves with amplitudes appreciably greater than those of wind waves, the numerical prediction followed the same trend as those of the experimental data. It should also be noted that the deletion of the longitudinal diffusivity from the diffusion equation did not cause significant errors.

Typical vertical diffusivities of the present models together with other momentum diffusion models are shown in Figure 6-12. The maxima of these vertical diffusivities occur at about 0.6δ whereas those of other models occur at 0.5δ or lower. It was believed that the difference was caused by the comparatively high residual turbulent intensities in the freestream induced by the honeycombs installed at the tunnel entrance. Rao et al. (1971), who assumed a constant Schmidt number in the numerical solution of the diffusion equation using a line source, modified the model of Nee and Kovasznay (1967) to accommodate the turbulent measurements of the diffusion experiment by Poreh (1961). Poreh's measurements indicated that $\sqrt{\overline{u'^2}}$ approached zero at $y \simeq 1.7\delta$ which conforms to the present measurements. The vertical diffusivity profile of Rao's modified model (Figure 3 of the cited reference) which has a maximum at 0.63δ conforms to the present models although the formulations are different. This coincidence confidently suggested that a constant Schmidt number was valid for the vertical mass diffusion in a neutrally stable boundary layer.

The present lateral diffusivity model displayed a stronger dependency on z than that given by Hino (1968). Without the explicit dependency on z as given by Eq. (2-31), the lateral diffusion at ground level is consistently too large.

The dependency on z and x of the diffusivity models may be best interpreted by the idea of "effective eddies." Consider a turbulent flow field which contains eddies of different sizes. Only eddies comparable to the plume dimensions are effective in spreading the plume. The eddies in the flow field that are larger than plume dimensions tend to transport the entire plume whereas those that are smaller tend to diffuse the plume. Near the point source, the particles are closely spaced, the large scale eddies have little influence on the spread of the plume. As the plume reaches farther downstream and grows in size, the large scale eddies become more effective and small eddies become less effective. In a wind tunnel, eddy size is limited because of the restriction of the side walls. To account for this restriction which also limits the largest size of the eddies, it seems reasonable to impose an upper bound on the values of $x - x_s$ which is included in Eq. (3-7). The side walls of the wind-water tunnel were two feet apart. The optimum value of the upper bound was found to be $x - x_s \leq 3.2$ ft. Without this upper bound imposed on the lateral diffusivity, Hino (1968) observed that the numerical solutions predicted a much wider lateral spread than those measured in wind tunnel experiments.

It should be pointed out that measurements of mean and fluctuating velocities as well as concentrations were made down to a level about 0.2 in. above the highest wave crests at each station. In general, the accuracy of velocity measurements was comparatively poor near the interface due to the limitations of instrumentation. For numerical calculations, the values of velocities and turbulence intensities were extrapolated to the mean water level. These extrapolated values significantly affect the numerical solutions. For example, if the turbulent intensities are overestimated, the numerical solutions predict large lateral spread and thus small concentrations at the lower boundary and vice versa. In the present analysis, the correction on $W - W_f$ [Eq. (6-1)] also compensated for the extrapolation of measurements to the mean water level.

It is necessary to provide better estimation of the turbulent intensities near the water surface in order to refine the numerical solutions. Kendall (1970), who investigated experimentally the turbulent structure over a rigid wall with progressive surface waves, observed that, next to the wall, the wave induced vertical fluctuation $\tilde{v}$ is more sinusoidal than is the corresponding longitudinal fluctuation $\tilde{u}$. Furthermore, the amplitude of $\tilde{u}$ was everywhere small compared to that of the turbulent fluctuation u' where u' is the sum of $\tilde{u}$ and a random component u_t' . The oscillating probe measurement of Chang (1968) also indicated that next to the water surface $\sqrt{\overline{u'^2}}$ varied considerably at different phase positions along a dominant wave.

At the water surface $z = \eta$, where $\overline{\eta} = 0$, the vertical rms velocity may be written as

$$\sqrt{\overline{w'^2}}\bigg|_{z=\eta} = \sqrt{\overline{\left(\frac{d\eta}{dt} + w_t'\right)^2}}\bigg|_{z=\eta} = \sqrt{\overline{\left(\frac{d\eta}{dt}\right)^2}} \qquad (6\text{-}2)$$

where w_t' is a random component which vanishes at $z = \eta$. The vertical fluctuating velocity at mean water level, therefore, may be considered as the oscillating velocity of the surface waves. The random longitudinal fluctuations very close to the water surface may be better estimated from data measured with an oscillating probe [Chang (1968)].

6.3 Possible Influences of Wind Tunnel Characteristics on Mass Diffusion

Favorable pressure gradients and the secondary flow have been two major concerns in modeling atmospheric flows in a wind tunnel. Their possible influences on mass diffusion are discussed below.

6.3.1 Influence of Pressure Gradient

The pressure gradient is considered to be mild if the absolute value of $\frac{\nu}{U_\infty^2}\frac{\partial U_\infty}{\partial x}$ is less than 0.5×10^{-6} as described by Schraub and Kline (1965). In the present study, a favorable pressure gradient existed in the wind-water tunnel. The value of $\frac{\nu}{U_\infty^2}\frac{\partial U_\infty}{\partial x}$, however, did not exceed 0.9×10^{-9} for any case. Therefore, the influence on mass diffusion because of a mild favorable pressure gradient was expected to be insignificant. In any event, the effects of the pressure gradient was implicitly accounted for in the numerical calculations because the velocity profiles and turbulence intensities of measured quantities were used.

6.3.2 Influence of Secondary Flow

Due to the corner effect of a noncircular wind tunnel, a complicated secondary flow pattern is induced and superimposed on the main flow. This secondary flow disturbs the mean velocity distribution and thus the two-dimensionality of the main flow, especially within the boundary layer. The maximum velocity of the secondary flow has been found to be less than two percent of the freestream velocity

[Veenhuizen (1969)]. In most boundary layer analysis, the effects of three-dimensionality induced by the secondary flow in a wind tunnel have been neglected.

In the present analysis, the correction given in Eq. (6-1) was designed to provide an integrated value to account for possible errors due to inaccurate measurements of flow conditions near the water surface as well as for the influence of secondary flows. Although the correction is simple, it served to improve the comparison of the numerical solution to experimental data. A qualitative justification for the use of the above correction is given below.

As depicted in the diffusion equation, Eq. (3-1), the vertical mean convection is important only at locations where the vertical concentration gradients are large. For an elevated point source, the maximum concentration gradient occurs along the centerline of the diffusing plume. Although there is no y-dependency in Eq. (6-1), the amount of correction provided diminishes as the vertical concentration gradients decrease with increasing $y - y_s$. Therefore, the errors introduced by incorrect estimation of $W - W_f$ at large $y - y_s$ is insignificant.

Measurements of lateral mean wind distributions in the boundary layer over wind waves displayed a slight velocity excess near the centerline at $U_\infty \approx 10$ and 20 fps and a slight velocity defect at $U_\infty \approx 30$ fps. This indicated that the vertical mean velocity was negative at low wind speed, which tended to decrease with increasing wind speed, and eventually changed direction. That is, the cellular structure of the secondary flow seemed to change with wind speed over wind waves. The corrections required on $W - W_f$ according to Eq. (6-1) conformed to this observation.

Chapter VII

CONCLUSIONS AND RECOMMENDATIONS

7.1 Conclusions

The objective of the present study was to investigate experimentally and numerically the mass diffusion process over a water surface from an elevated point source. To obtain experimental data of the fluctuating particle concentration, an optical device was developed and its performance was proven to be satisfactory. The frequency response of the optical device at 3db down was 7.4×10^4 Hz and the focal volume of the optical-probe was approximately 6.0×10^{-5} in.^{3}. These features were comparable to those of a hot-wire anemometer, which enabled comparable measurements of velocity and concentration fluctuations to be made. Results of the calibration of the optical device confirmed the linear relationship between the photomultiplier voltage output and particle concentration at the focal volume which was assumed by other investigators [Rosensweig et al. (1960)].

For low wind speeds for $U_\infty \simeq 10$ fps, the flow conditions and thus the mean concentration distributions over a water surface, on which capillary waves predominated, were found to be similar to those over a flat plate for $U_\infty \simeq 10$ and 20 fps. For wind speed higher than 10 fps, however, similarity no longer existed between the flat plate and the wavy water surface. In such cases, the gravity waves developed on the water surface introduced additional turbulence to the air stream near the interface, thus influencing the mass diffusion process. For flow over wind waves, net momentum was transferred from the air stream to water waves. The amount transferred was proportional to the wave height and thus the wind speed. For flow over mechanical waves, however, there was less net momentum transfer from the air stream to the waves.

The relative turbulent intensities in the air near the interface, which relate directly to the wave height at a given station, increased with increasing wind speed over wind waves. Measurements of mean and fluctuating concentrations demonstrated that the vertical and lateral spreads of a diffusing plume increased with increasing "recovered" relative turbulent kinetic energy as defined in Eq. (4-9). The comparatively large vertical gradients of $\sqrt{\overline{u'^2}}/U_\infty$ and $\sqrt{\overline{w'^2}}/U_\infty$ characterized the flow over mechanical waves which resulted in large concentration accumulation at ground level.

The influences of wind shear, surface reflection, and turbulent diffusion caused the maximum concentration to be shifted toward the lower boundary while turbulent diffusion caused the maximum concentration fluctuations to be shifted upward and laterally. In fact, the spread of a diffusing plume in a turbulent flow field can be observed more distinctly from fluctuating concentration distributions rather than from mean concentration distributions. It would seem appropriate to adopt the trajectory of the maximum fluctuating concentrations at successive stations as an alternate definition of the outer edge of a diffusing plume.

Several improvements were incorporated into a finite-difference scheme for computational efficiency. The grid system was designed to expand with the spread of the diffusing plume. Small grid-sizes were used at locations where concentration gradients or velocity gradients were expected to be large. The free boundary values were extrapolated from calculated concentration adjacent to the free surface within the domain of calculation.

The present diffusivity models introduced local conditions to the diffusivities by including dependency on the boundary layer thickness. The lateral diffusivity depends on the scale of the phenomenon by imposing an upper bound on the dependency of $x - x_s$. The vertical diffusivity agreed with that of Rao et al. (1971) who assumed a constant Schmidt number of 0.9. This agreement indicated that the Schmidt number is very close to a constant with its value somewhat greater than 0.9 but smaller than unity.

With proper correction to $W - W_f$, numerical solutions based on the present diffusivity model agreed reasonably well with corresponding experimental data with few exceptions. An integrated correction given in Eq. (6-1) was provided to account for the influences of wind tunnel characteristics and for possible errors introduced by inaccurate measurements and extrapolations of flow conditions adjacent to the water surface. The maximum correction required on $W - W_f$ was 0.9% of the freestream velocity. The corrected $W - W_f$ conformed properly in direction to the secondary flow along the geometric center of the wind-water tunnel as depicted from the measured lateral mean wind profile in the boundary layer.

There was general agreement between numerical solutions and corresponding experimental data. The influences of the wavy surface were implicitly incorporated into the "recovered" turbulent kinetic energy which is one of the variables in determining diffusivities.

7.2 Recommendations for Future Research

Although the mass diffusivity models derived in the present study provide reasonable predictions of mean concentration distributions, the method of derivation is indirect and the models are empirical. A direct and accurate method to derive the exact diffusivity models is to measure the covariance $\overline{c'u'}$. The comparatively large size of the optical-probe prevented accurate measurements of $\overline{c'u'}$ to be made due to appreciable velocity disturbances by the probe tips. It may be possible to reduce the size of the optical-probe, hence its disturbance to the flow by using a laser light source and improved optics.

The present grid system for numerical solutions, which was designed to expand with the spread of the diffusing plume, may be applied to other calculations such as that for general solution to boundary layer flows. Calculation efficiency and accuracy will be improved especially in the region near the leading edge where the velocity gradient is large and small grid sizes are required.

The influences of secondary flow on mass diffusion from an elevated point source, which was found to be important, should be further investigated. The results of such investigation will provide a better understanding of the secondary flow and its influences which is understood only qualitatively at present.

The present diffusion model may be extended to predict concentration distributions downwind from multiple point sources or from an area source such as from a heavily industrialized district. Further investigation should be extended to investigate the mass diffusion process in a thermally stratified surface layer in the atmosphere.

Multiple-layered models may be used to describe the momentum and mass diffusivities to account for the influences of thermal stratification.

REFERENCES

Anyiwo, J. C. and R. N. Meroney (1971) An effective-viscosity model for turbulent wall boundary layers. Project THEMIS Technical Report No. 10, Fluid Dynamics and Diffusion Laboratory, College of Engineering, Colorado State University, Fort Collins.

Aris, R. (1956) On dispersion of a solute in a fluid flowing through a tube. Proceedings Royal Society, Vol. A 235, pp. 67-77.

Atesman, K. M. (1970) The dispersion of matter in turbulent shear flows. Ph.D. Dissertation, Department of Mechanical Engineering, Colorado State University, Fort Collins.

Becker, H. A., H. C. Hottel and G. C. Williams (1963) Mixing and flow on ducted turbulent jets. Ninth International Symposium on Combustion, pp. 7-20.

Becker, H. A., H. C. Hottel and G. C. Williams (1965) Concentration intermittency in jets. Tenth International Symposium on Combustion, p. 1253.

Becker, H. A., R. E. Rosensweig and J. R. Gwozdz (1966) Turbulent dispersion in a pipe flow. A.I.Ch.E. Journal, Vol. 12, pp. 964-972.

Becker, H. A., H. C. Hottel and G. C. Williams (1967a) Concentration fluctuations in ducted turbulent jets. Eleventh International Symposium on Combustion, p. 791-798.

Becker, H. A., H. C. Hottel and G. C. Williams (1967b) On the light-scatter technique for the study of turbulence and mixing. Journal of Fluid Mechanics, Vol. 30, Part 2, pp. 259-284.

Becker, H. A., H. C. Hottel and G. C. Williams (1967c) The nozzle-fluid concentration field of the round, turbulent, free jet. Journal of Fluid Mechanics, Vol. 30, Part 2, pp. 285-303.

Bole, J. B. and E. Y. Hsu (1967) Response of gravity water waves to wind excitation. Department of Civil Engineering, Technical Report No. 79, Stanford, University, Stanford.

Bosanquet, C. H. and J. L. Pearson (1936) The spread of smoke and gases from chimneys. Trans. Faraday Soc., 32, pp. 1249-1264.

Calder, K. L. (1949) Eddy diffusion and evaporation in flow over aerodynamically smooth and rough surfaces. Quarterly Journal of Mechanics and Applied Mathematics, Vol. 2, pp. 153-176.

Chang, P. C. (1968) Laboratory measurements of air flow over wind waves following the moving water surface. Ph.D. Dissertation, Department of Civil Engineering, Colorado State University, Fort Collins.

Chatwin, P. C. (1968) The dispersion of a puff of passive contaminant in the constant stress region. Quarterly Journal of Royal Meterological Society, Vol. 94, pp. 401-411.

Chaudhry, F. H. (1969) Turbulent diffusion in a stably stratified shear layer. Ph.D. Dissertation, Department of Civil Engineering, Colorado State University, Fort Collins.

Corrsin, S. and A. L. Kistler (1954) Free stream boundaries of turbulent flow. Natl. Adv. Comm. Aero., Tech. Note 3133.

Davies, D. R. (1950a) Three dimensional turbulence and evaporation in lower atmosphere I. Quarterly Journal of Mechanics and Applied Mathematics, Vol. 3, pp. 51-63.

Davies, D. R. (1950b) Three dimensional turbulence and evaporation in lower atmosphere II. Quarterly Journal of Mechanics and Applied Mathematics, Vol. 3, pp. 64-73.

Davies, D. R. (1952) On diffusion from a continuous point source at ground level into a turbulent atmosphere. Quarterly Journal of Mechanics and Applied Mathematics, Vol. 5, pp. 168-178.

Fischer, H. B. (1964) Longitudinal dispersion by velocity gradients in open channel flow. Technical Memorandum 64-4, W. M. Keck Laboratory, California Institute of Technology.

Frankeil, F. N. (1953) Turbulent diffusion. Advances in Applied Mechanics, Vol. 3, pp. 61-107.

Green, H. L. (1964) Particulate Clouds: Dusts, Smokes, and Mists. D. Van Nostrand Company, Ltd., New Jersey.

Gurnitz, R. N. (1966) Development and application of light scattering technique for the study of premixed turbulent flame. Sci. D. Thesis, Department of Chemical Engineering, Massachusetts Institute of Technology, Cambridge.

Hay, J. S. (1955) Some observations of air flow over the sea. Quarterly Journal of the Royal Meteorological Society, Vol. 81, No. 349, pp. 307-319.

Hidy, G. M. and E. J. Plate (1966) Wind action on water standing in a laboratory channel. Journal of Fluid Mechanics, Vol. 26, Part 4, pp. 651-687.

Himus, G. (1929) The evaporation of water in open pans. Presented at Conference on Vapor Absorption and Adsorption sponsored by Inst. of Chem. Engr., London.

Hine, T. B. (1924) Rate of evaporation of liquids in a current of air. Physical Review, Vol. 24, pp. 79-91.

Hino, M. (1967) Numerical analysis of smoke diffusion considering the effects of topography. Cent. Res. Inst. Elec. Power Ind., Report No. 66063, Part 2 (in Japanese).

Hino, M. (1968) Computer experiment on smoke diffusion over a complicated topography. Atmospheric Environment, Pergamon Press, Vol. 2, pp. 541-558.

Hottel, H. C., G. C. Williams and G. A. Miles (1967) Mixedness in the well-stirred reactor. Eleventh International Symposium on Combustion, p. 771.

Ito, S. (1971) A mechanism of turbulent diffusion in the atmospheric surface layer. Meteorology and Geophysics, Vol. 21, No. 2, pp. 141-241.

Karaki, S. and E. Y. Hsu (1968) An experimental investigation of the structure of a turbulent wind over water waves. Department of Civil Engineering, Technical Report No. 88, Stanford University, Stanford.

Kendall, J. M. (1970) The turbulent boundary layer over a wall with progressive surface waves. Journal of Fluid Mechanics, Vol. 41, Part 2, pp. 259-281.

Klatt, F. (1968) The X hot-wire probe in a plane flow field. DISA Information, No. 8, pp. 3-12.

Kung, R. J. and G. J. Binder (1967) Ultra low-speed anemometry. Department of Civil Engineering, Technical Report No. CER66-67-RJK49, Colorado State University, Fort Collins.

Kung, R. J. (1970) Boundary layer development over equally spaced fences. Ph.D. Dissertation, Department of Civil Engineering, Colorado State University, Fort Collins.

Lai, J. R. (1969) Evaporation from small wind waves. Ph.D. Dissertation, Department of Civil Engineering, Colorado State University, Fort Collins.

Lee, J. H. (1962) Turbulent motion and mixing. Ph.D. Dissertation, Chemical Engineering Department, Ohio State University, Columbus.

Malhotra, R. C. and J. E. Cermak (1963) Wind tunnel modelling of atmospheric diffusion. Journal of Geophysical Research, Vol. 68, pp. 2181-2184.

McDonald, J. E. (1960) An aid to computation of terminal fall velocities of spheres. Journal of Meteorology, 17, pp. 463-465.

McKelvey, K. N. (1968) Turbulent mixing with chemical reaction. Ph.D. Dissertation, Chemical Engineering Department, Ohio State University, Columbus.

Mellor, G. L. and H. J. Herring (1968) Two methods of calculating turbulent boundary layer behavior based on numerical solutions of the equations of motion. Proc. Computation of Turbulent Boundary Layers, AFOSR-IFP-Stanford Conference, Vol. I, pp. 331-345.

Miles, J. W. (1957) On the generation of surface waves by shear flows. Journal of Fluid Mechanics, Vol. 3, pp. 185-204.

Miles, J. W. (1959) On the generation of surface waves by shear flows, Part 2. Journal of Fluid Mechanics, Vol. 6, Part 4, pp. 568-582.

Moffat, R. J., R. J. Lloyd and W. M. Kays (1970) The turbulent boundary layer on a porous plate: An experimental study of the fluid dynamics with strong favorable pressure gradients and blowing. Report No. HWT-13, Stanford University, Stanford.

Monin, A. S. and A. M. Obukhov (1954) Basic relationships for turbulent mixing in the atmospheric ground layer. Transactions Geophysics Institute, Academy of Sciences, U.S.S.R., Vol. 24, pp. 225-259.

Nee, V. W. and L. S. G. Kovasznay (1968) The calculation of the incompressible turbulent boundary layers by a simple theory. Proc. Computations of Turbulent Boundary Layers, AFOSR-IFP-Stanford Conference, Vol. I, pp. 300-319.

Nye, J. O. (1966) Turbulent motion and mixing. M.S. Thesis, Chemical Engineering Department, Ohio State University, Columbus.

Pasquill, F. (1966) Atmospheric Diffusion. D. Van Nostrand Company, Ltd., New York.

Plate, E. J. (1965) A research facility with concurrent air and water flows. La Houille Blanche, Vol. 2, pp. 595-598.

Plate, E. J. and C. R. Goodwin (1965) The influence of wind on open channel flow. Paper Presented at the Special Conference on Coastal Engineering, Santa Barbara, California, pp. 391-423.

Plate, E. J. and C. W. Liu (1966) Investigations of the thermally stratified boundary layer. Fluid Mechanics Paper No. 5, Fluid Dynamics and Diffusion Laboratory, Colorado State University, Fort Collins.

Plate, E. J. and G. M. Hidy (1967) Laboratory study of air flowing over a smooth surface onto small water waves. Journal of Geophysical Research, Vol. 72, pp. 4627-4642.

Poreh, M. (1961) Diffusion from a line source in a turbulent boundary layer. Ph.D. Dissertation, Department of Civil Engineering, Colorado State University, Fort Collins.

Priestley, C. H. B. (1959) Turbulent Transfer in the Lower Atmosphere. The University of Chicago Press, Chicago Press, Chicago.

Rao, K. S., V. W. Nee and K. T. Yang (1971) Mass diffusion in a neutral or thermally stratified atmospheric surface layer. Department of Aerospace and Mechanical Engineering, Technical Report No. 71-28, University of Notre Dame, Notre Dame.

Richtmyer, R. D. and K. W. Morton (1967) Difference Methods for Initial-Value Problems. Interscience Publishers, New York.

Roberts, O. F. T. (1923) The theoretical scattering of smoke in a turbulent atmosphere. Proceedings Royal Society, Series A, 104, pp. 640-654.

Rosensweig, R. E., H. C. Hottel and G. C. Williams (1961) Smoke-scattered light measurement of turbulent concentration fluctuations. Chemical Engineering Science, Vol. 15, p. 111.

Saffman, P. G. (1962) The effect of wind shear on horizontal spread from an instantaneous ground source. Quarterly Journal of Royal Meteorological Society, Vol. 88, pp. 382-393.

Sayre, W. W. (1967) Dispersion of mass in open channel flow. Ph.D. Dissertation, Department of Civil Engineering, Colorado State University, Fort Collins.

Schlichting, H. (1968) Boundary Layer Theory. McGraw-Hill Book Company, Inc., New York.

Shemdin, O. H. and E. Y. Hsu (1966) The dynamics of wind in the vicinity of progressive water waves. Department of Civil Engineering, Technical Report No. 66, Stanford University, Stanford.

Slade, D. H. (1968) Meteorology and atomic energy. U. S. Atomic Energy Commission, Division of Technical Information.

Smith, A. M. O. and D. W. Clutter (1963) Solution of the incompressible laminar boundary layer equations. AIAA Journal, Vol. 1, No. 9, pp. 2062-2071.

Smith, F. B. (1957) The diffusion of smoke from a continuous elevated point source into a turbulent atmosphere. Journal of Fluid Mechanics, Vol. 2, pp. 49-76.

Smith, G. D. (1965) Numerical Solution of Partial Differential Equations. Oxford University Press, New York.

Sutherland, A. J. (1967) Spectral measurements and growth rates of wind-generated water waves. Department of Civil Engineering, Technical Report No. 84, Stanford University, Stanford.

Sutton, O. G. (1934) Wind structure and evaporation in a turbulent atmosphere. Proceedings Royal Society, Series A, 146, pp. 701-722.

Sutton, O. G. (1953) Micrometeorology. McGraw-Hill Book Company, Inc., New York.

Taylor, G. I. (1921) Diffusion by continuous movements. Proceedings London Mathematical Society, Series 2, Vol. 20, pp. 196-202.

Veenhuizen, S. D. (1969) Secondary flow in a boundary layer. M.S. Thesis, Department of Civil Engineering, Colorado State University, Fort Collins.

Veenhuizen, S. D. (1972) Air turbulence over laboratory water waves. Ph.D. Dissertation (to be published), Department of Civil Engineering, Colorado State University, Fort Collins.

Williams, G. C. and H. A. Becker (1963) Ducted jet mixing. Tech. Assoc. of the Pulp and Paper Ind. (Tappi), Vol. 46, No. 8, pp. 153-158.

Wu, J. (1968) Laboratory studies of wind-wave interactions. Journal of Fluid Mechanics, Vol. 34, pp. 91-112.

Yamamoto, G. (1959) Theory of turbulent transfer in non-neutral conditions. Journal of Meteorological Society, Japan, Vol. 37, pp 60-69.

Yotsukura, N. and M. B. Fiering (1964) Numerical solution to a dispersion equation. ASCE Journal of the Hydraulics Division, Vol. 90, pp. 83-104.

APPENDIX A

FORMULATION OF FINITE-DIFFERENCE EQUATIONS

APPENDIX A

FORMULATION OF FINITE-DIFFERENCE EQUATIONS

The Crank-Nicolson implicit scheme ($\theta = \frac{1}{2}$) corresponding to Eq. (3-1) is written as

$$
\begin{aligned}
C_{i+1,j,k} = C_{i,j,k} + \frac{\Delta X_i}{2U_{i,j,k}} \{ & \frac{(K_y)_{i,j+\frac{1}{2},k}}{\Delta y_j \Delta y_{j-\frac{1}{2}}} \cdot \\
& [(C_{i+1,j+1,k} - C_{i+1,j,k}) + (C_{i,j+1,k} - C_{i,j,k})] \\
& - \frac{(K_y)_{i,j-\frac{1}{2},k}}{\Delta y_{j-\frac{1}{2}} \Delta y_{j-1}} [(C_{i+1,j,k} - C_{i+1,j-1,k}) - (C_{i,j,k} \\
& - C_{i,j-1,k})] + \frac{(K_z)_{i,j,k+\frac{1}{2}}}{\Delta z_k \Delta z_{k-\frac{1}{2}}} [(C_{i+1,j,k+1} - C_{i+1,j,k}) \\
& + (C_{i,j,k+1} - C_{i,j,k})] - \frac{(K_z)_{i,j,k-\frac{1}{2}}}{\Delta z_{k-\frac{1}{2}} \Delta z_{k-1}} [(C_{i+1,j,k} \\
& - C_{i+1,j,k-1}) + (C_{i,j,k} - C_{i,j,k-1})] \\
& - \frac{(W_{i,j,k} - W_f)}{(\Delta z_k + \Delta z_{k-1})} [(C_{i+1,j,k+1} - C_{i+1,j,k-1}) \\
& + (C_{i,j,k+1} - C_{i,j,k-1})]\} \qquad \text{(A-1)}
\end{aligned}
$$

where $\Delta y_j = y_j - y_{j-1}$ and $\Delta z_k = z_k - z_{k-1}$.

By introducing a parameter γ either equal to 1 or 0, both explicit ($\gamma = 1$) and the Crank-Nicolson implicit ($\gamma = 0$) schemes may be incorporated into Eq. (A-1). This mixed scheme takes the following form

$$C_{i+1,j,k} = C_{i,j,k} + \frac{\Delta X_i}{2U_{i,j,k}} \{ \frac{(K_y)_{i,j+\frac{1}{2},k}}{\Delta y_j \Delta y_{j-\frac{1}{2}}} (1+\gamma) \cdot$$

$$[(C_{i+1,j+1,k} - C_{i+1,j,k})(1-\gamma) + (C_{i,j+1,k} - C_{i,j,k})]$$

$$- \frac{(K_y)_{i,j-\frac{1}{2},k}}{\Delta y_{j-\frac{1}{2}} \Delta y_{j-1}} (1+\gamma)[(C_{i+1,j,k} - C_{i+1,j-1,k})(1-\gamma)$$

$$+ (C_{i,j,k} - C_{i,j-1,k})] + \frac{(K_z)_{i,j,k+\frac{1}{2}}}{\Delta z_k \Delta z_{k-\frac{1}{2}}} (1+\gamma) \cdot$$

$$[(C_{i+1,j,k+1} - C_{i+1,j,k})(1-\gamma) + (C_{i,j,k+1} - C_{i,j,k})]$$

$$- \frac{(K_z)_{i,j,k-\frac{1}{2}}}{\Delta z_{k-\frac{1}{2}} \Delta z_{k-1}} (1-\gamma)[(C_{i+1,j,k} - C_{i+1,j,k-1})(1-\gamma)$$

$$+ (C_{i,j,k} - C_{i,j,k-1})] - \frac{(W_{i,j,k} - W_f)}{(\Delta z_k + \Delta z_{k-1})} [(C_{i+1,j,k+1}$$

$$- C_{i+1,j,k-1})(1-\gamma) + (C_{i,j,k+1} - C_{i,j,k-1})]\} . \qquad \text{(A-2)}$$

Let

$$\alpha'_{i,j,k} = \frac{\Delta X_i (1+\gamma)}{2U_{i,j,k}}$$

$$(\beta_{y1})_{i,j,k} = \frac{(K_y)_{i,j-\frac{1}{2},k}}{\Delta y_{j-\frac{1}{2}} \Delta y_{j-1}}$$

$$(\beta_{y2})_{i,j,k} = \frac{(K_y)_{i,j+\frac{1}{2},k}}{\Delta y_j \Delta y_{j-\frac{1}{2}}}$$

$$(\beta_{z1})_{i,j,k} = \frac{(K_z)_{i,j,k-\frac{1}{2}}}{\Delta z_{k-\frac{1}{2}} \Delta z_{k-1}}$$

$$(\beta_{z2})_{i,j,k} = \frac{(K_z)_{i,j,k+\frac{1}{2}}}{\Delta z_k \Delta z_{k-\frac{1}{2}}}$$

$$\phi_{i,j,k} = \frac{(W_{i,j,k} - W_f)}{(\Delta z_k + \Delta z_{k-1})} \qquad \text{(A-3)}$$

and $$b_{i,j,k} = C_{i,j,k} + \alpha'_{i,j,k} \{(\beta_{y2})_{i,j,k}(C_{i,j+1,k} - C_{i,j,k})$$
$$- (\beta_{y1})_{i,j,k}(C_{i,j,k} - C_{i,j-1,k}) + (\beta_{z2})_{i,j,k} \cdot$$
$$(C_{i,j,k+1} - C_{i,j,k}) - (\beta_{z1})_{i,j,k}(C_{i,j,k} - C_{i,j,k-1}$$
$$+ \phi_{i,j,k}(C_{i,j,k+1} - C_{i,j,k-1})\} . \qquad \text{(A-4)}$$

The numerical calculation, starting from $x = x_0$ where the concentration distribution is assumed, proceeds in the positive x-direction. As the calculation advances to a new section, $b_{i,j,k}$ is a known quantity. By substituting the above expressions into Eq. (A-2), it reduces to

$$C_{i+1,j,k} = \alpha'_{i,j,k}(1-\gamma)\{(\beta_{y2})_{i,j,k}(C_{i+1,j+1,k} - C_{i+1,j,k})$$
$$- (\beta_{y1})_{i,j,k}(C_{i+1,j,k} - C_{i+1,j-1,k}) + (\beta_{z2})_{i,j,k} \cdot$$
$$(C_{i+1,j,k+1} - C_{i+1,j,k}) - (\beta_{z1})_{i,j,k}(C_{i+1,j,k}$$
$$- C_{i+1,j,k-1}) - \phi_{i,j,k}(C_{i+1,j,k+1} - C_{i+1,j,k-1})\}$$
$$+ b_{i,j,k} \qquad \text{(A-5)}$$

or $$C_{i+1,j,k} = \frac{\alpha'_{i,j,k}(1-\gamma)}{A_{i,j,k}} \{(\beta_{y2})_{i,j,k} C_{i+1,j+1,k}$$
$$+ (\beta_{y1})_{i,j,k} C_{i+1,j-1,k} + [(\beta_{z2})_{i,j,k} - \phi_{i,j,k}] \cdot$$
$$C_{i+1,j,k+1} + [(\beta_{z1})_{i,j,k} - \phi_{i,j,k}] C_{i+1,j,k-1}\}$$
$$+ \frac{b_{i,j,k}}{A_{i,j,k}} \qquad \text{(A-6)}$$

where $$A_{i,j,k} = 1 + \alpha'_{i,j,k}(1-\gamma)[(\beta_{y2})_{i,j,k} + (\beta_{y1})_{i,j,k}$$
$$+ (\beta_{z2})_{i,j,k} + (\beta_{z1})_{i,j,k}] .$$

Let n be the number of iterations. The Jacobi iteration scheme corresponding to Eq. (A-6) is

$$C^{n+1}_{i+1,j,k} = \frac{\alpha'_{i,j,k}(1-\gamma)}{A_{i,j,k}} \{(\beta_{y2})_{i,j,k}\, C^{n}_{i+1,j+1,k} + (\beta_{y1})_{i,j,k}\, C^{n}_{i+1,j-1,k} + [(\beta_{z2})_{i,j,k} - \phi_{i,j,k}] \cdot C^{n}_{i+1,j,k+1} + [(\beta_{z1})_{i,j,k} - \phi_{i,j,k}]\, C^{n}_{i+1,j,k-1}\} + \frac{b_{i,j,k}}{A_{i,j,k}} . \quad \text{(A-7)}$$

Considerable improvement in the rate at which C^{n+1} converges to the final solution can be achieved by using the most recent iterates as soon as they are available, i.e., by replacing C^{n} by C^{n+1} immediately as they have been computed. This leads to the Gauss-Seidel scheme. Based on this scheme and by defining a relaxation factor ω , the successive-over-relaxation (S.O.R.) scheme is derived [Smith (1965)]. Corresponding to Eq. (A-6), the S.O.R. scheme, which further accelerates the rate of convergence, is expressed in the following equation.

$$C^{n+1}_{i+1,j,k} = \frac{\omega\alpha'_{i,j,k}(1-\gamma)}{A_{i,j,k}} \{(\beta_{y2})_{i,j,k}\, C^{n}_{i+1,j+1,k} + (\beta_{y1})_{i,j,k}\, C^{n+1}_{i+1,j-1,k} + [(\beta_{z2})_{i,j,k} - \phi_{i,j,k}] \cdot C^{n}_{i+1,j,k+1} + [(\beta_{z1})_{i,j,k} - \phi_{i,j,k}]\, C^{n+1}_{i+1,j,k-1}\} + \frac{\omega b_{i,j,k}}{A_{i,j,k}} - (\omega-1)\, C^{n}_{i+1,j,k} . \quad \text{(A-8)}$$

The relaxation factor ω lies between 1 and 2 for most linear problems.

APPENDIX B

COMPUTER PROGRAM FOR NUMERICAL CALCULATIONS

Nomenclature

A1,B1,PM,PN	=	CONSTANTS CORRESPONDING TO A_3, B_3, m, AND n OF EQ.(3-7), RESPECTIVELY
A(J,K)	=	EXPRESSION DEFINED IN EQ.(A-6)
ALPHA(K)	=	EXPRESSION DEFINED IN EQ.(A-3)
AU(L),AN(L),AD(L)	=	THIRD-DEGREE POLYNOMIAL COEFFICIENTS FOR THE FREESTREAM VELOCITY, EXPONENT OF THE POWER-LAW PROFILE, AND BOUNDARY LAYER THICKNESS, RESPECTIVELY
AUT(L),AWT(L)	=	SEVENTH-DEGREE POLYNOMIAL COEFFICIENTS FOR THE RELATIVE TURBULENT INTENSITIES IN X AND Z DIRECTIONS, RESPECTIVELY
AV,BV	=	CONSTANT OF PROPORTIONALITY FOR THE CORRECTION OF W(K)-WF
B(J,K)	=	EXPRESSION DEFINED IN EQ.(A-4)
BETAY1(J,K)	=	EXPRESSION DEFINED IN EQ.(A-3)
BETAY2(J,K)	=	EXPRESSION DEFINED IN EQ.(A-3)
BETAZ1(K)	=	EXPRESSION DEFINED IN EQ.(A-3)
BETAZ2(K)	=	EXPRESSION DEFINED IN EQ.(A-3)
CC(J,K)	=	CONCENTRATION CALCULATED WITH A GAUSSIAN DISTRIBUTION FUNCTION FOR THE INITIAL CONDITION OR ESTIMATED VALUES FOR THE INITIAL APPROXIMATION
CNO(J,K)	=	CONCENTRATION CALCULATED AT LAST ITERATION
CN1(1,J,K)	=	CONCENTRATION CALCULATED AT ADJACENT UPSTREAM STATION
CN1(2,J,K)	=	CONCENTRATION TO BE CALCULATED AT PRESENT ITERATION
DMIN	=	MAXIMUM TOLERANCE FOR DISMAX
DISPL	=	COMPONENT OF THE DISPLACEMENT VECTOR
DISMAX	=	MAXIMUM COMPONENT OF THE DISPLACEMENT VECTOR
DX(II),DY(J),DZ(K)	=	INCREMENTS OF X(II), Y(J), AND Z(K), RESPECTIVELY
II,J,K	=	INDICES OF X,Y,AND Z COORDINATES, RESPECTIVELY
IMAX,JMAX,KMAX	=	ABSOLUTE MAXIMUM VALUES OF II, J, AND K, RESPECTIVELY
JMAX1	=	JMAX-2
JMM	=	JMAX1-1

Nomenclature – continued

JMP	=	JMAX-1
KMAX1	=	KMAX-2
KMM	=	KMAX1-1
KMP	=	KMAX-1
KS	=	INDEX OF Z DESIGNATING THE SOURCE HEIGHT, THAT IS, Z(KS)=ZSOUR
N	=	NUMBER OF ITERATIONS
OMEGA	=	RELAXATION FACTOR
PHI(K)	=	EXPRESSION DEFINED IN EQ.(A-3)
PNREY	=	EXPONENT OF THE POWER-LAW MEAN VELOCITY REPRESENTATION
Q0	=	DISCHARGE RATE OF A DIFFUSING PLUME
QQ	=	CALCULATED DISCHARGE RATE OF A DIFFUSING PLUME
UMAX	=	FREESTREAM VELOCITY
U(K),W(K)	=	MEAN VELOCITY COMPONENTS IN X AND Z DIRECTIONS, RESPECTIVELY
WF	=	PARTICLE FALL VELOCITY
X0	=	X COORDINATE AT WHICH THE CONCENTRATION DISTRIBUTION IS APPROXIMATED WITH A GAUSSIAN DISTRIBUTION FUNCTION
X1	=	CORRECTION ON THE ORIGIN OF THE POINT SOURCE
X(II),Y(J),Z(K)	=	DISTANCES IN LONGITUDINAL, LATERAL, AND VERTICAL DIRECTIONS, RESPECTIVELY
XOUT(L)	=	X COORDINATE AT WHICH THE CALCULATED CONCENTRATION IS TO BE PRINTED
YK(J,K),ZK(K)	=	LATERAL AND VERTICAL DIFFUSIVITIES, RESPECTIVELY
ZDEL	=	BOUNDARY LAYER THICKNESS
ZSOUR	=	SOURCE HEIGHT

Fortran program

```
      PROGRAM DIFF
      DIMENSION CNO(52,85), CN1(2,52,85), ALPHA(85), BETAY1(52,85), BETA
     1Y2(52,85), BETAZ1(85), BETAZ2(85), PHI(85), A(52,85), B(52,85)
      DIMENSION CY(10), CZ(10), AA(10), XOUT(10)
      COMMON /DIFFA/ IMAX,JMAX,KMAX,II,KS,ZSOUR,JMAX1,KMAX1
      COMMON /DIFF1/ Y(85),Z(85),DY(85),DZ(85),U(85)
      COMMON /DIFFG/ X(1000),DX(1000),JMP,KMP,X1
      COMMON /DIFFV/ UMAX,W(85),AU(10),AN(10),AD(10),ZDEL,AUT(10),AWT(10
     1),AV,BV
      COMMON /DIFFK/ YK(52,85),ZK(85),A1,B1,PM,PN
      COMMON /DIFFC/ CC(52,85)
C
C ********************************************************************
C     NUMERICAL SOLUTION TO THE TURBULENT MASS DIFFUSION EQUATION
C     THIS PROGRAM USE THE SUCCESSIVE OVER-RELAXATION METHOD WITH
C     VARIABLE GRID SIZES.  THE GRID SYSTEM IS DESIGNED TO EXPAND
C     WITH THE SPREAD OF A DIFFUSING PLUME.  INPUT OF INITIAL
C     GRID SIZES ARE REQUIRED.  MEAN AND FLUCTUATING VELOCITIES
C     BEST FITTED WITH POLYNOMIALS ARE INPUT TO THE PROGRAM
C
C                          BY HSIEN TA LIU, FEB. 1972.
C                           COLORADO STATE UNIVERSITY
C
C ********************************************************************
C
C         ++++++++++++++++++++++++++++++++++++
C         +   CASE 3--OVER WIND WAVES, UMAX=30 FT/SEC   +
C         ++++++++++++++++++++++++++++++++++++
C
C     .... TO INPUT POLYNOMIAL COEFFICIENTS OF MEAN AND FLUCTUATING
C          VELOCITIES
C
      DATA (AU(I),I=1,4)/28.875483,.1422656,-.00603425,.0003246077/
      DATA (AD(I),I=1,4)/3.7236561,.2748965,-.001918430,-.0001723743/
      DATA (AN(I),I=1,4)/3.880227,-.0940964,.010716346,-.00027323418/
      DATA (AUT(I),I=1,8)/.12467753,-.27141622,.83020486,-1.4405735,1.18
     1378511,-.47698045,.088094810,-.005374B4/
      DATA (AWT(I),I=1,8)/.09531483,-.27082112,.899410519,-1.5752998,1.3
     178814,-.63452558,.14790938,-.013805482/
C
C     .... TO INPUT VALUES OF CONSTANTS AND PHYSICAL VARIABLES
C
      DATA AV,BV/.0025,.0025/
      DATA A1,B1,PM,PN/.0580,.0170,.85,.50/
      DATA Q0,X0,X1,DMIN,OMEGA,ZSOUR/1.,.3,.02,.008,1.25,.166667/
      DATA IMAX,JMAX,KMAX/80,52,85/
      DATA (XOUT(I),I=1,7)/1.04,1.83,3.76,5.84,7.75,11.76,15.76/
      X(1)=X0+X1
      GAMMA=0.
      WRITE (6,68)
C
C     .... INITIALIZATION
```

Fortran program - continued

```
C
      I=1
      WF=0.
      DO 1 K=1,KMAX
      DO 1 J=1,JMAX
      CN1(I,J,K)=.1E-200
      CN1(I+1,J,K)=.1E-200
      CNO(J,K)=.1E-200
    1 CONTINUE
      NI=3
      JMP=JMAX-1
      KMP=KMAX-1
      JMAX1=50
      KMAX1=83
      NG=0
      II=1
C
C     ... TO ASSIGN INITIAL GRID SIZES
C
      CALL GRID
C
C     .... TO START ITERATION
C
    2 JMM=JMAX1-1
      KMM=KMAX1-1
      N=0
      IF (II.GT.1) GO TO 21
    3 N=1
      IF (II.GT.1) GO TO 4
C
C     .... TO EVALUATE VELOCITY DISTRIBUTIONS
C
      CALL VELO (X(II))
C
C     .... TO EVALUATE DIFFUSIVITIES
C
      CALL YZK (X(II))
      GO TO 5
    4 CALL VELO (X(II-1))
      CALL YZK (X(II-1))
      GO TO 7
C
C     .... TO COMPUTE INITIAL CONDITIONS
C     ........ II=1 DESIGNATES INITIAL CONDITIONS
C
    5 CALL CZERO (U(KS),YK(1,KS),ZK(KS),QO,X(1))
      DO 6 J=2,JMAX1
      DO 6 K=2,KMAX1
      CN1(I+1,J,K)=CC(J,K)
    6 CONTINUE
      GO TO 33
C
```

Fortran program - continued

```
C     .... TO SOLVE THE FINITE-DIFFERENCE EQUATION, EQ.(A-8)
C
    7 DO 9 K=2,KMP
      BETAZ1(K)=(ZK(K-1)+ZK(K))/(DZ(K-1)*(DZ(K)+DZ(K-1)))
      BETAZ2(K)=(ZK(K+1)+ZK(K))/(DZ(K)*(DZ(K)+DZ(K-1)))
      PHI(K)=(W(K)-WF)/(DZ(K)+DZ(K-1))
      DO 8 J=2,JMP
      BETAY1(J,K)=YK(1,K)/(DY(J-1)*(DY(J-1)+DY(J))/2.)
    8 BETAY2(J,K)=YK(1,K)/(DY(J)*(DY(J-1)+DY(J))/2.)
    9 CONTINUE
      NG=0
      DO 11 K=2,KMM
      ALPHA(K)=DX(II-1)*(1.+GAMMA)/U(K)/2.
      DO 10 J=2,JMM
   10 A(J,K)=1.+ALPHA(K)*(1.-GAMMA)*(BETAY2(J,K)+BETAY1(J,K)+BETAZ2(K)+B
     1ETAZ1(K))
   11 CONTINUE
      DO 14 K=2,KMM
      DO 13 J=2,JMM
      IF (J.GT.2) GO TO 12
C
C     ........TO USE THE SYMMETRIC CONDITION AT Y=0
      CN1(I,J-1,K)=CN1(I,J+1,K)
   12 IF (K.GT.2) GO TO 13
C
C     ........TO USE THE LOWER BOUNDARY CONDITION AT Z=0
      CN1(I,J,K-1)=CN1(I,J,K+1)
   13 B(J,K)=CN1(I,J,K)+ALPHA(K)*(BETAY2(J,K)*(CN1(I,J+1,K)-CN1(I,J,K))-
     1BETAY1(J,K)*(CN1(I,J,K)-CN1(I,J-1,K))+BETAZ2(K)*(CN1(I,J,K+1)-CN1(
     2I,J,K))-BETAZ1(K)*(CN1(I,J,K)-CN1(I,J,K-1))-PHI(K)*(CN1(I,J,K+1)-C
     3N1(I,J,K-1)))
   14 CONTINUE
   15 DISMAX=0.
      DO 19 K=2,KMM
      DO 18 J=2,JMM
      IF (J.GT.2) GO TO 16
C
C     ........TO USE THE SYMMETRIC CONDITION AT Y=0
      CN1(I+1,J-1,K)=CNO(J+1,K)
   16 IF (K.GT.2) GO TO 17
C
C     ........TO USE THE LOWER BOUNDARY CONDITION AT Z=0
      CN1(I+1,J,K-1)=CNO(J,K+1)
   17 CN1(I+1,J,K)=OMEGA*(ALPHA(K)*(1.-GAMMA)/A(J,K)*(BETAY2(J,K)*CNO(J+
     11,K)+BETAY1(J,K)*CN1(I+1,J-1,K)+(BETAZ2(K)-PHI(K))*CNO(J,K+1)+(BET
     2AZ1(K)+PHI(K))*CN1(I+1,J,K-1))+B(J,K)/A(J,K))-(OMEGA-1.)*CNO(J,K)
C
C     .... TO CALCULATE VALUES OF DISPLACEMENT VECTOR
C
      IF (CN1(I+1,J,K).LT..1E-30) GO TO 18
      DISPL=ABS((CN1(I+1,J,K)-CNO(J,K))/CN1(I+1,J,K))
      IF (DISMAX.LT.DISPL) DISMAX=DISPL
```

Fortran program - continued

```
   18 CNO(J,K)=CN1(I+1,J,K)
   19 CONTINUE
      NN=N/25
      FN=FLOAT(N)/25.
      NN=FLOAT(NN)/FN
      IF (NN.NE.1) GO TO 20
      WRITE (6,77) DISMAX,DMIN,N,X(II),FACTOR,QQ,KS
C
C     .... TO EXTRAPOLATE FREE-BOUNDARY VALUES
C
   20 IF (DISMAX.GT.5.*DMIN) GO TO 63
   21 II1=I+1
      IF (N.EQ.0) II1=I
      DO 25 K=2,KMAX1
      IF (CN1(I+1,JMM,K).EQ.0) GO TO 25
      DO 24 J=1,NI
      JI=NI-J
      CY(J)=ALOG(ABS(CN1(II1,JMM-JI,K)))
      DO 24 JK=1,NI
      JII=NI-JK
      JIJ=JK+(J-1)*NI
      IF (J.GT.1) GO TO 22
      AA(JIJ)=1.
      GO TO 24
   22 IF (J.GT.2) GO TO 23
      AA(JIJ)=Y(JMM-JII)
      GO TO 24
   23 AA(JIJ)=Y(JMM-JII)**2
   24 CONTINUE
      CALL SIMQ (AA,CY,NI,IER)
      CYI=CY(1)+CY(2)*Y(JMAX1)+CY(3)*Y(JMAX1)**2
      CN1(II1,JMAX1,K)=EXP(CYI)
      IF (CN1(II1,JMAX1,K).GT.CN1(II1,JMM,K)) CN1(II1,JMAX1,K)=.1E-60
      CNO(JMAX1,K)=CN1(II1,JMAX1,K)
      IF (N.EQ.0) CC(JMAX1,K)=CNO(JMAX1,K)
   25 CONTINUE
      DO 29 J=2,JMAX1
      IF (CN1(I+1,J,KMM).EQ.0) GO TO 29
      DO 28 K=1,NI
      KI=NI-K
      CZ(K)=ALOG(ABS(CN1(II1,J,KMM-KI)))
      DO 28 JK=1,NI
      KII=NI-JK
      KIK=JK+(K-1)*NI
      IF (K.GT.1) GO TO 26
      AA(KIK)=1.
      GO TO 28
   26 IF (K.GT.2) GO TO 27
      AA(KIK)=Z(KMM-KII)
      GO TO 28
   27 AA(KIK)=Z(KMM-KII)**2
   28 CONTINUE
```

Fortran program - continued

```
      CALL SIMQ (AA,CZ,NI,IER)
      CZI=CZ(1)+CZ(2)*Z(KMAX1)+CZ(3)*Z(KMAX1)**2
      CN1(II1,J,KMAX1)=EXP(CZI)
      IF (CN1(II1,J,KMAX1).GT.CN1(II1,J,KMM)) CN1(II1,J,KMAX1)=CN1(II1,J
     1,KMM)*Z(KMM)/Z(KMAX1)*.08
      CNO(J,KMAX1)=CN1(II1,J,KMAX1)
      IF (N.EQ.0) CC(J,KMAX1)=CNO(J,KMAX1)
   29 CONTINUE
      IF (N.EQ.0) GO TO 3
      IF (DISMAX.LT.DMIN) GO TO 30
      GO TO 63
C
C     .... TO CHECK CONTINUITY CONDITION
C
   30 QQ=0.
      DO 31 J=2,JMM
      DO 31 K=2,KMM
   31 QQ=QQ+(CN1(I+1,J,K)+CN1(I+1,J+1,K)+CN1(I+1,J,K+1)+CN1(I+1,J+1,K+1)
     1)*DY(J)*DZ(K)/8.*(U(K)+U(K+1))
C
C     .... TO PRINT AND PUNCH RESULTS
C
      WRITE (6,77) DISMAX,DMIN,N,X(II),FACTOR,QQ,KS
      DO 32 MK=1,7
      IF (X(II).EQ.(XOUT(MK)+X1)) GO TO 33
   32 CONTINUE
      GO TO 57
   33 WRITE (6,72) X(II),N,JMAX1,KMAX1
      DO 44 WK=1,4
      GO TO (34,35,36,37), WK
   34 WRITE (6,83)
      GO TO 38
   35 WRITE (6,84)
      GO TO 38
   36 WRITE (6,82)
      GO TO 38
   37 WRITE (6,81)
   38 DO 43 K=2,KMAX1,10
      KK=K+9
      IF (KK.GT.KMAX1) KK=KMAX1
      GO TO (39,40,41,42), WK
   39 WRITE (6,71) Z(K),(U(KJ),KJ=K,KK)
      GO TO 43
   40 WRITE (6,71) Z(K),(W(KJ),KJ=K,KK)
      GO TO 43
   41 WRITE (6,71) Z(K),(ZK(KJ),KJ=K,KK)
      GO TO 43
   42 WRITE (6,71) Z(K),(YK(1,KJ),KJ=K,KK)
   43 CONTINUE
   44 WRITE (6,76)
      DO 51 L1=1,2
      IF (L1.EQ.2) GO TO 46
```

Fortran program - continued

```
      IF (II.EQ.1) GO TO 45
      WRITE (6,79)
      GO TO 47
   45 WRITE (6,78)
      GO TO 47
   46 IF (II.EQ.1) GO TO 52
      WRITE (6,80)
   47 DO 50 J=2,JMAX1,10
      JJ=J+9
      IF (JJ.GT.JMAX1) JJ=JMAX1
      WRITE (6,73)
      WRITE (6,74) (Y(JK),JK=J,JJ)
      DO 49 K=2,KMAX1,2
      IF (L1.EQ.2) GO TO 48
      WRITE (6,71) Z(K),(CC(JK,K),JK=J,JJ)
      GO TO 49
   48 WRITE (6,71) Z(K),(CN1(I+1,JK,K),JK=J,JJ)
   49 CONTINUE
      WRITE (6,76)
   50 CONTINUE
      WRITE (6,75)
   51 CONTINUE
   52 WRITE (6,76)
      IF (N.GT.400) GO TO 66
      IF (X(II).LT.1.8) GO TO 57
      PUNCH 69, X(II),JMAX1,KMAX1
      DO 53 J=2,JMAX,8
      JJ=J+7
      IF (JJ.GT.JMAX) JJ=JMAX
   53 PUNCH 70, (Y(JK),JK=J,JJ)
      DO 54 J=2,JMAX1,6
      JJ=J+5
      IF (JJ.GT.JMAX1) JJ=JMAX1
      PUNCH 67, (CN1(I+1,JK,KS),JK=J,JJ)
   54 CONTINUE
      PUNCH 69, X(II),JMAX1,KMAX1
      DO 55 K=2,KMAX,8
      KK=K+7
      IF (KK.GT.KMAX) KK=KMAX
   55 PUNCH 70, (Z(KJ),KJ=K,KK)
      DO 56 K=2,KMAX1,6
      KK=K+5
      IF (KK.GT.KMAX1) KK=KMAX1
      PUNCH 67, (CN1(I+1,2,KJ),KJ=K,KK)
   56 CONTINUE
   57 II=II+1
      IF (X(II).GT.(15.76+X1)) GO TO 66
C
C     .... TO CHECK NECESSITY FOR BROADENING OR EXPANSION OF THE GRID
C          SYSTEM
C
      IF (JMAX1.EQ.JMAX.OR.KMAX1.EQ.KMAX) GO TO 58
```

Fortran program - continued

```
      RATIO=CN1(I+1,2,KS)/CN1(I+1,2,KMAX1)
      RATIO1=CN1(I+1,2,KS)/CN1(I+1,JMAX1,KS)
      IF (RATIO.GT..1E13.OR.RATIO1.GT..1E13) GO TO 60
      JMAX1=JMAX1+1
      KMAX1=KMAX1+1
      GO TO 60
   58 CALL EXPAND
C
C     .... TO REDISTRIBUTE CONCENTRATION PROFILE ACCORDING TO THE NEWLY
C          EXPANDED GRID SYSTEM
C
      NG=1
      DO 59 K=2,KMAX,2
      DO 59 J=2,JMAX,2
      IF (K.GT.KMAX) GO TO 60
      IF (J.GT.JMAX) GO TO 60
      JK=J/2+1
      KJ=K/2+1
   59 CN1(I+1,JK,KJ)=CN1(I+1,J,K)
C
C     .... TO EVALUATE APPROXIMATE VALUES FOR THE NEXT ITERATION
C
   60 FACTOR=X(II-1)/X(II)
      IF (II.LT.6) CALL CZERO (U(KS),YK(1,KS),ZK(KS),Q0,X(II))
      DO 62 K=2,KMAX1
      DO 62 J=2,JMAX1
      IF (II.LT.6) GO TO 61
      CNO(J,K)=CN1(I+1,J,K)*FACTOR
      CC(J,K)=CNO(J,K)
      GO TO 62
   61 CNO(J,K)=CC(J,K)
   62 CN1(I,J,K)=CN1(I+1,J,K)
      IF (II.GT.IMAX) GO TO 66
      IF (NG.EQ.1) GO TO 2
      IF (RATIO.LT..1E13.OR.RATIO1.LT..1E13) GO TO 2
      GO TO 3
   63 N=N+1
      IF (N.GT.400) GO TO 66
      GO TO 15
   66 STOP
   67 FORMAT (6(E13.6))
   68 FORMAT (1H1)
   69 FORMAT (F14.5,6X,2I10)
   70 FORMAT (8F10.3)
   71 FORMAT (3X, 4HZ = ,E11.4,2X,10E11.3)
   72 FORMAT (/////5X, 21HCONCENTRATION AT X = ,F10.6, 30H AT DOWNSTREAM
     1 OF POINT SOURCE, 23H NUMBER OF ITERATION = ,I3,4X, 8HJMAX1 = ,I3
     2,4X, 8HKMAX1 = ,I3,//)
   73 FORMAT (50X, 35HTRANSVERSE DISTANCE FROM CENTERLINE,/)
   74 FORMAT (20X,10(F9.7,2X)/)
   75 FORMAT (50X, 40H++++++++++++++++++++++++++++++++++++++++)
```

Fortran program – continued

```
76 FORMAT (/)
77 FORMAT (10X,  9HDISMAX = ,E11.3,  7HDMIN = ,E11.3,  7H    N = ,I3,
  1 7H    X = ,F10.6,3X,  9HFACTOR = ,F10.6,  8H    QQ = ,F8.5,  8H    K
  2S = ,I3)
78 FORMAT (///60X, 18HINITIAL CONDITIONS,//)
79 FORMAT (//57X, 21HINITIAL APPROXIMATION,///)
80 FORMAT (///58X, 18HNUMERICAL SOLUTION,//)
81 FORMAT (////,60X, 19HDIFFUSIVITIES YK(K),//)
82 FORMAT (//,60X, 19HDIFFUSIVITIES ZK(K),//)
83 FORMAT (//,50X, 38HHORIZONTAL VELOCITY AT EACH GRID-POINT,//)
84 FORMAT (//,51X, 36HVERTICAL VELOCITY AT EACH GRID-POINT,//)
   END
```

```
      SUBROUTINE GRID
C
C****************************** SUBROUTINE GRID ******************************
C
      COMMON /DIFFA/ IMAX,JMAX,KMAX,II,KS,ZSOUR,JMAX1,KMAX1
      COMMON /DIFF1/ Y(85),Z(85),DY(85),DZ(85),U(85)
      COMMON /DIFFG/ X(1000),DX(1000),JMP,KMP,X1
C
C     .... THIS SUBROUTINE IS USED TO ASSIGN INITIAL GRID SIZES
C
      DATA (DY(JJ),JJ=1,52)/.002,.002,.002,.002,.0024,.0024,.0028,.0028,
     1.0032,.0032,.0036,.0036,.0040,.0040,.0040,.0040,.0044,.0044,.0044,
     2.0044,.0048,.0048,.0048,.0048,.0052,.0052,.0052,.0052,.0056,.0056,
     3.0056,.0056,.0058,.0058,.0060,.0060,.0062,.0062,.0064,.0064,.0066,
     4.0066,.0068,.0068,.0070,.0070,.0072,.0072,.0074,.0074,.0076,.0076/
      DATA (DZ(KK),KK=1,85)/.001001,.000999,.001,.0012,.0012,.0012,.0014
     1,.0016,.0018,.0020,.0022,.0024,.0026,.0028,.0030,.0033,.0036,.0040
     2,.0040,.0040,.0040,.0040,.0040,.0040,.0040,.0040,.0040,.0040,.0040
     3,.0040,.0040,.0040,.0042,.0042,.0044,.0044,.0044,.0044,.0044,.0044
     4,.0044,.0044,.0044,.0044,.0044,.0044,.0044,.0044,.0044,.0048,.0048
     5,.0052,.0052,.0056,.0056,.0060,.0060,.0064,.0064,.0068,.0068,.0072
     6,.0072,.0076,.0076,.0080,.0080,.0084,.0084,.0084,.0084,.0084,.0084
     7,.0084,.0084,.0084,.0084,.0084,.0084,.0084,.0084,.0084,.0084,.0084
     8,.0084/
      DATA (X(I),I=1,80)/.3,.301,.303,.305,.307,.31,.315,.32,.33,.345,.3
     16,.375,.39,.405,.42,.44,.46,.48,.50,.52,.54,.56,.60,.64,.68,.72,.7
     28,.84,.90,.96,1.04,1.12,1.2,1.3,1.4,1.5,1.6,1.70,1.83,1.95,2.1,2.2
     35,2.4,2.6,2.8,3.0,3.25,3.5,3.76,4.05,4.4,4.75,5.075,5.430,5.84,6.1
     45,6.55,6.95,7.35,7.75,8.13,8.52,8.91,9.31,9.71,10.11,10.52,10.92,1
     51.32,11.76,12.2,12.7,13.2,13.7,14.2,14.7,15.2,15.76,16.2,16.75/
      KS=50
      Y(2)=0.
      DO 1 J=3,JMAX
      Y(J)=Y(J-1)+DY(J-1)
    1 CONTINUE
```

Fortran program - continued

```
      Z(2)=.000001
      DO 2 K=3,KMAX
      Z(K)=Z(K-1)+DZ(K-1)
    2 CONTINUE
      Y(1)=Y(2)-DY(1)
      Z(1)=Z(2)-DZ(1)
      DY(JMAX)=DY(JMP)
      DZ(KMAX)=DZ(KMP)
      DO 3 I=2,IMAX
      X(I)=X(I)+X1
      IF (I.LT.80) GO TO 3
      DX(I)=.1
      X(I)=X(I-1)-DX(I-1)
    3 DX(I-1)=X(I)-X(I-1)
      IF (II.GT.1) GO TO 7
      WRITE (6,8)
      DO 4 K=1,KMAX,10
      KK=K+9
      IF (KK.GT.KMAX) KK=KMAX
    4 WRITE (6,11) (DZ(KJ),KJ=K,KK)
      WRITE (6,12)
      WRITE (6,9)
      DO 5 J=1,JMAX,10
      JJ=J+9
      IF (JJ.GT.JMAX) JJ=JMAX
    5 WRITE (6,11) (DY(JK),JK=J,JJ)
      WRITE (6,12)
      WRITE (6,10)
      DO 6 IJ=1,79,10
      IJJ=IJ+9
    6 WRITE (6,11) (X(IJI),IJI=IJ,IJJ)
    7 RETURN
C
    8 FORMAT (///,60X, 23H Z-DIRECTION INCREMENTS,//)
    9 FORMAT (////,60X, 22HY-DIRECTION INCREMENTS,///)
   10 FORMAT (////,50X, 44HDISTANCES FROM POINT SOURCE FOR EACH STATION,
     1//)
   11 FORMAT (10X,10F12.6)
   12 FORMAT (///)
      END


      SUBROUTINE VELO (X)
C
C******************************** SUBROUTINE VELO ***************************
C
      COMMON /DIFFA/ IMAX,JMAX,KMAX,II,KS,ZSOUR,JMAX1,KMAX1
      COMMON /DIFF1/ Y(85),Z(85),DY(85),DZ(85),U(85)
      COMMON /DIFFV/ UMAX,W(85),AU(10),AN(10),AD(10),ZDEL,AUT(10),AWT(10
```

Fortran program - continued

```
     1),AV,BV
C
C     .... THIS SUBROUTINE CALCULATES THE BEST FITTED VELOCITY
C          DISTRIBUTIONS AT SUCCESSIVE STATIONS
C
      ZDEL=AD(1)
      UMAX=AU(1)
      PNREY=AN(1)
      DO 1 I1=2,4
      XN=X**(I1-1)
      UMAX=UMAX+AU(I1)*XN
      PNREY=PNREY+AN(I1)*XN
    1 ZDEL=ZDEL+AD(I1)*XN
      PNREY=1./PNREY
      ZDEL=ZDEL/12.
      DO 2 K=2,KMAX1
      U(K)=UMAX*(Z(K)/ZDEL)**PNREY
      W(K)=(AV-BV*(Z(K)/ZDEL))*UMAX
      IF (W(K).LE.0.) W(K)=0.
      IF (U(K).GT.UMAX) U(K)=UMAX
    2 CONTINUE
      RETURN
      END
```

```
      SUBROUTINE YZK (X)
C
C******************************  SUBROUTINE YZK  ******************************
C
      COMMON /DIFFA/ IMAX,JMAX,KMAX,II,KS,ZSOUR,JMAX1,KMAX1
      COMMON /DIFF1/ Y(85),Z(85),DY(85),DZ(85),U(85)
      COMMON /DIFFV/ UMAX,W(85),AU(10),AN(10),AD(10),ZDEL,AUT(10),AWT(10
     1),AV,BV
      COMMON /DIFFK/ YK(52,85),ZK(85),A1,B1,PM,PN
C
C     .... THIS SUBROUTINE CALCULATES DIFFUSIVITIES AT SUCCESSIVE
C          STATIONS
C
      ZETA=ZDEL*.80
      XX=X
      IF (XX.GT.3.2) XX=3.2
      DO 3 K=2,KMAX1
      UP=AUT(1)
      WP=AWT(1)
      DO 1 I1=2,8
      ZN=(Z(K)/ZDEL)**(I1-1)
      UP=UP+AUT(I1)*ZN
    1 WP=WP+AWT(I1)*ZN
      ZKK=SQRT(1.25*(UP+WP)**2-2.*UP*WP)*UMAX
```

Fortran program - continued

```
      IF (Z(K).GT.ZETA) GO TO 2
      ZK(K)=A1*Z(K)**PM*ZKK
      ZK(K)=ZK(K)*ZDEL**.15
      YK(1,K)=B1*Z(K)**PN*ZKK*XX
      YK(1,K)=YK(1,K)/(ZDEL**PN)
      GO TO 3
    2 ZK(K)=A1*ZETA**PM*ZKK
      ZK(K)=ZK(K)*ZDEL**.15
      YK(1,K)=B1*ZETA**PN*ZKK*XX
      YK(1,K)=YK(1,K)/(ZDEL**PN)
    3 CONTINUE
      ZK(1)=0.
      RETURN
      END
```

```
      SUBROUTINE CZERO (U0,YK0,ZK0,Q0,X)
C
C******************************* SUBROUTINE CZERO ********************************
C
      COMMON /DIFFA/ IMAX,JMAX,KMAX,II,KS,ZSOUR,JMAX1,KMAX1
      COMMON /DIFF1/ Y(85),Z(85),DY(85),DZ(85),U(85)
      COMMON /DIFFC/ CC(52,85)
C
C     .... THIS SUBROUTINE CALCULATES CONCENTRATION PROFILES USING A
C     GAUSSIAN DISTRIBUTION FUNCTION
C
      YKVAR=2.*YK0*X/U0
      ZKVAR=2.*ZK0*X/U0
      DO 1 J=2,JMAX
      DO 1 K=2,KMAX
      CC(J,K)=Q0*EXP(-(Y(J)-Y(2))**2/(2.*YKVAR))/(2.*3.1416*U0*SQRT(YKVA
     1R*ZKVAR))*(EXP(-(1.*(Z(K)-ZSOUR))**2/(2.*ZKVAR))+EXP(-(1.*(Z(K)+ZS
     2OUR))**2/(2.*ZKVAR)))
    1 CONTINUE
      RETURN
      END
```

```
      SUBROUTINE SIMQ (A,B,N,KS)
C
C******************************* SUBROUTINE SIMQ *********************************
C
      DIMENSION A(1), B(1)
C
C     .... THIE SUBROUTINE SOLVES FOR COEFFICIENTS OF A SET OF
```

Fortran program - continued

```
C          SIMULTANEOUS EQUATIONS.  THESE COEFFICIENTS ARE USED TO
C          EXTRAPOLATE CONCENTRATIONS ON THE FREE SURFACE
C
      TOL=0.
      KS=0
      JJ=-N
      DO 8 J=1,N
      JY=J+1
      JJ=JJ+N+1
      BIGA=0
      IT=JJ-J
      DO 2 I=J,N
      IJ=IT+I
      IF (ABS(BIGA)-ABS(A(IJ))) 1,2,2
    1 BIGA=A(IJ)
      IMAX=I
    2 CONTINUE
      IF (ABS(BIGA)-TOL) 3,3,4
    3 KS=1
      RETURN
    4 I1=J+N*(J-2)
      IT=IMAX-J
      DO 5 K=J,N
      I1=I1+N
      I2=I1+IT
      SAVE=A(I1)
      A(I1)=A(I2)
      A(I2)=SAVE
    5 A(I1)=A(I1)/BIGA
      SAVE=B(IMAX)
      B(IMAX)=B(J)
      B(J)=SAVE/BIGA
      IF (J-N) 6,9,6
    6 IQS=N*(J-1)
      DO 8 IX=JY,N
      IXJ=IQS+IX
      IT=J-IX
      DO 7 JX=JY,N
      IXJX=N*(JX-1)+IX
      JJX=IXJX+IT
    7 A(IXJX)=A(IXJX)-(A(IXJ)*A(JJX))
    8 B(IX)=B(IX)-(B(J)*A(IXJ))
    9 NY=N-1
      IT=N*N
      DO 10 J=1,NY
      IA=IT-J
      IB=N-J
      IC=N
      DO 10 K=1,J
      B(IB)=B(IB)-A(IA)*B(IC)
      IA=IA-N
   10 IC=IC-1
```

Fortran program - continued

```
      RETURN
      END




      SUBROUTINE EXPAND
C
C****************************** SUBROUTINE EXPAND ******************************
C
      COMMON /DIFFA/ IMAX,JMAX,KMAX,II,KS,ZSOUR,JMAX1,KMAX1
      COMMON /DIFF1/ Y(85),Z(85),DY(85),DZ(85),U(85)
      COMMON /DIFFG/ X(1000),DX(1000),JMP,KMP
      COMMON /DIFFC/ CC(52,85)
C
C     .... THIS SUBROUTINE MANIPULATES THE EXPANSION OF THE GRID SYSTEM
C
      DZ(1)=DZ(1)+DZ(3)
      DY(1)=DY(1)+DY(3)
      Z(1)=Z(2)-DZ(1)
      Y(1)=Y(2)-DY(1)
      KS=KS/2+1
      DO 1 K=2,KMAX1,2
      IF (K.GT.KMAX1) GO TO 2
      KJ=K/2+1
      Z(KJ)=Z(K)
      IF (Z(KJ).EQ..1667) KS=KJ
      IF (KJ.LT.3) GO TO 1
      DZ(KJ-1)=Z(KJ)-Z(KJ-1)
    1 CONTINUE
    2 DO 3 J=2,JMAX1,2
      IF (J.GT.JMAX1) GO TO 4
      JK=J/2+1
      Y(JK)=Y(J)
      IF (JK.LT.3) GO TO 3
      DY(JK-1)=Y(JK)-Y(JK-1)
    3 CONTINUE
    4 JMAX1=JK-1
      KMAX1=KJ-1
      DO 5 K=KJ,KMP
      IF (K.LT.41) DZ(K)=DZ(KJ-1)
      IF (K.GT.40.AND.K.LT.51) DZ(K)=DZ(KJ-1)*1.1
      IF (K.GT.50.AND.K.LT.61) DZ(K)=DZ(KJ-1)*1.2
      IF (K.GT.60.AND.K.LT.71) DZ(K)=DZ(KJ-1)*1.3
      IF (K.GT.70.AND.K.LT.81) DZ(K)=DZ(KJ-1)*1.4
      IF (K.GT.80) DZ(K)=DZ(KJ-1)*1.5
      IF (DZ(K).GT..06) DZ(K)=.06
    5 Z(K+1)=Z(K)+DZ(K)
      DO 6 J=JK,JMP
      IF (J.LT.31) DY(J)=DY(JK-1)
      IF (J.GT.30.AND.J.LT.36) DY(J)=DY(JK-1)*1.1
```

Fortran program - continued

```
      IF (J.GT.35.AND.J.LT.41) DY(J)=DY(JK-1)*1.2
      IF (J.GT.40.AND.J.LT.46) DY(J)=DY(JK-1)*1.3
      IF (J.GT.45.AND.J.LT.51) DY(J)=DY(JK-1)*1.4
      IF (J.GT.50) DY(J)=DY(JK-1)*1.5
      IF (DY(J).GT..06) DY(J)=.06
    6 Y(J+1)=Y(J)+DY(J)
      DY(JMAX)=DY(JMP)
      DZ(KMAX)=DZ(KMP)
      WRITE (6,9)
      DO 7 K=1,KMAX,10
      KK=K+9
      IF (KK.GT.KMAX) KK=KMAX
    7 WRITE (6,11) (DZ(KJ),KJ=K,KK)
      WRITE (6,12)
      WRITE (6,10)
      DO 8 J=1,JMAX,10
      JJ=J+9
      IF (JJ.GT.JMAX) JJ=JMAX
    8 WRITE (6,11) (DY(JK),JK=J,JJ)
      WRITE (6,12)
      WRITE (6,12)
      RETURN
    9 FORMAT (///,60X, 23H Z-DIRECTION INCREMENTS,//)
   10 FORMAT (////,60X, 22HY-DIRECTION INCREMENTS,///)
   11 FORMAT (10X,10F12.6)
   12 FORMAT (////)
      END
```

APPENDIX C

UNCERTAINTY ANALYSIS

APPENDIX C

UNCERTAINTY ANALYSIS

Only experimental errors of random nature were considered in this uncertainty analysis. Systematic errors with fixed values may be corrected on the measurements. The random errors of U and z are expressed as standard deviations with normal probability distributions. The standard deviation of error for determination of vertical distance z was ±0.036 in. The accuracy of differential pressure measurements with a Tran Sonic pressure meter was approximately ±3% of full scale reading which is ±1.5% in terms of wind speed. To account for additional errors introduced by large velocity gradients and turbulent velocity fluctuations near the boundary, the standard deviation of pressure measurements was assumed to be ±5% (±2.5% in velocity) at the boundary, decreasing linearly to ±2% (±1% in velocity) at $z = \delta$.

The uncertainties in determination of displacement thickness δ_*, momentum thickness δ_2, and the exponent n of the power-law profile were estimated by random simulation. Small randomly varying quantities, which were assumed to be normally distributed with standard deviations given above, were added to the experimentally determined values of U and z. The parameters δ_*, δ_2 and n were then evaluated with the computer program for data reduction. The mean and standard deviation of these parameters were calculated by repeating the above procedure 100 times. Table C-1 lists the results of the uncertainty analysis.

TABLE C-1. RESULTS OF UNCERTAINTY ANALYSIS

Case	$x-x_s$ ft	U_∞ (ft/sec)	Lower Boundary Condition	Mean Values δ_* (in.)	Mean Values δ_2 (in.)	Mean Values n	Standard Deviation δ_* (in.)	Standard Deviation δ_* %	Standard Deviation δ_2 (in.)	Standard Deviation δ_2 %	Standard Deviation n	Standard Deviation n %
1	-0.25	9.85	Wind	0.510	0.348	0.179	0.0424	8.30	0.0340	9.80	0.0140	7.80
	15.76	10.56	Waves	0.658	0.470	0.148	0.0734	11.10	0.0612	13.00	0.0114	7.70
2	-0.25	18.42	Wind	0.584	0.389	0.202	0.0890	15.20	0.0797	20.50	0.0268	13.20
	15.76	19.80	Waves	1.353	0.842	0.245	0.0854	6.30	0.0632	7.50	0.0176	7.16
3	-0.25	28.87	Wind	0.789	0.468	0.250	0.0792	10.00	0.0663	14.20	0.0311	12.40
	15.76	30.92	Waves	1.521	0.865	0.248	0.0847	5.60	0.0632	7.40	0.0173	7.00
4	-0.25	18.22	Mech.	0.793	0.483	0.161	0.0898	11.30	0.0777	16.10	0.0195	12.10
	15.76	19.78	Waves	1.463	0.826	0.191	0.0813	5.60	0.0611	7.40	0.0095	5.00
5	-0.25	18.88	Flat	0.553	0.385	0.160	0.0568	10.30	0.0484	12.60	0.0154	9.60
	15.76	20.08	Plate	0.916	0.681	0.156	0.0724	7.90	0.0586	8.60	0.0125	8.20

TABLES

TABLE 4-1. NUMERICAL VALUES OF PHYSICAL VARIABLES FOR TEST PROBLEMS

(a) Test Problem I

Physical Variables	Numerical Values	Increments in Z-Direction (ft)		Increments in Y-Direction (ft)		Increments in X-Direction (ft)	
U	16.40 (ft/sec)	Δz = 32.81	$0 < z < 721.78$	Δy = 32.81	$0 < y < 524.93$	Δx = 104.99	$0 < x < 314.96$
K	107.64 (ft^2/sec)	Δz = 65.62	$721.78 < z < 1246.72$	Δy = 65.62	$524.93 < y < 1181.10$	Δx = 209.97	$314.96 < x < 944.88$
z_s	656.17 (ft)	Δz = 131.23	$1246.72 < z < 2296.59$	Δy = 131.23	$1181.10 < y < 2755.91$	Δx = 419.95	$944.88 < x < 2204.72$
Q	0.1 (unit/sec)	Δz = 262.47	$2296.59 < z$	Δy = 212.47	$2755.91 < y$	Δx = 839.90	$2204.72 < x$

(b) Test Problem II

Physical Variables	Numerical Values	Physical Variables	Numerical Values	Physical Variables	Numerical Values
U_1	16.40 (ft/sec)	m	0.205	β	1.0
z_1	656.17 (ft)	n	0.340	$\sqrt{(\overline{v'^2}/\overline{w'^2})}$	1.8
Q	1.0 (unit/sec)	A	0.39		
z_s	0.0 (ft)	B	0.86		

TABLE 6-1. DESCRIPTIONS OF MASS DIFFUSION EXPERIMENTS

Water Depth	6 in.
Source Height	2 in.
Diameter of Source	.25 in.
Thermal Stratification	Neutral
Source Substance	Dioctyl Phthalate Particles
Method of Source Generation	Atomization
Particle Fall Velocity	Less than .1 in./sec
Particle Exit Velocity	Matched with Local Ambient Velocity

Case	Freestream Velocity U_∞(ft/sec)	Lower Boundary Condition
1	∿ 10	Wind Waves
2	∿ 20	Wind Waves
3	∿ 30	Wind Waves
4	∿ 20	Mechanical Waves
5	∿ 20	Flat Plate*

*Covered with #1½ E floor sandpaper made by Norton at an equivalent level to a water surface.

FIGURES

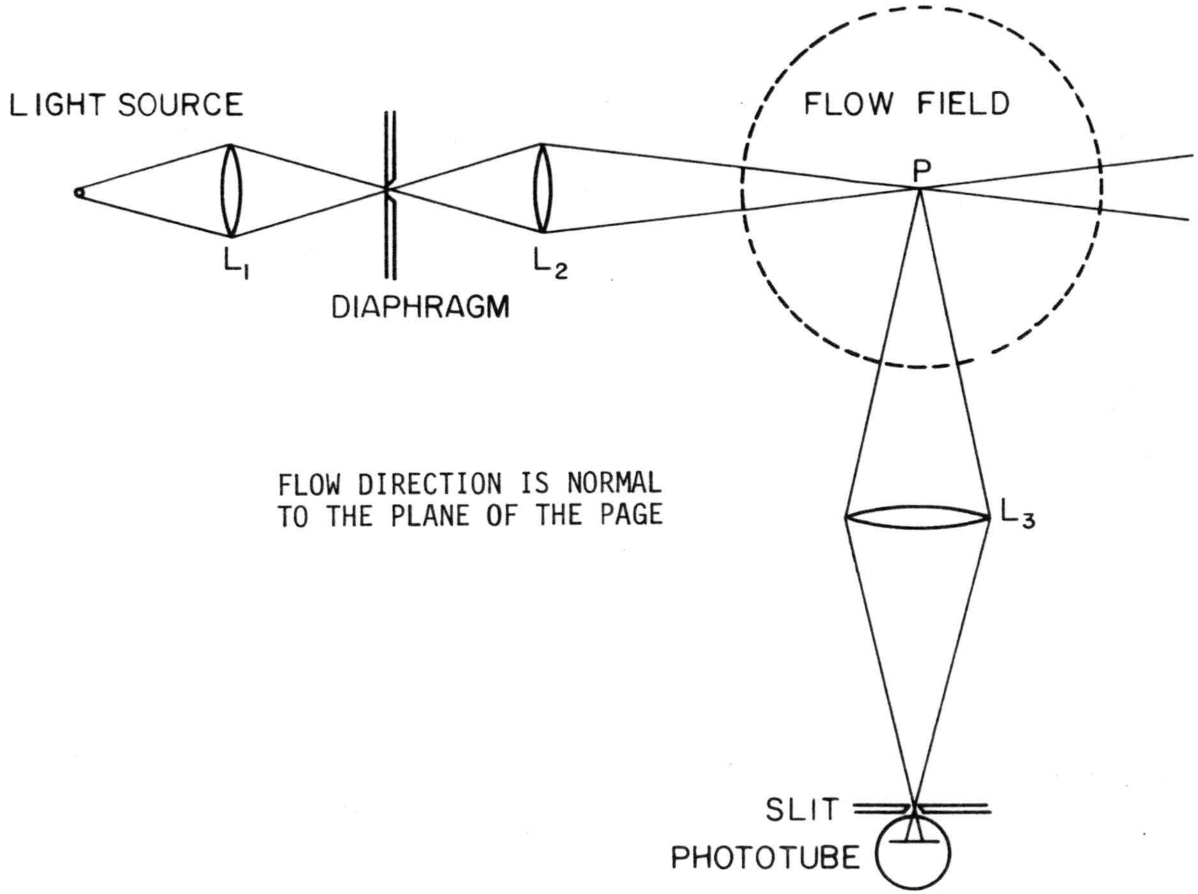

Figure 2-1. Schematic arrangement of an optical system developed by Rosensweig et al. (1961).

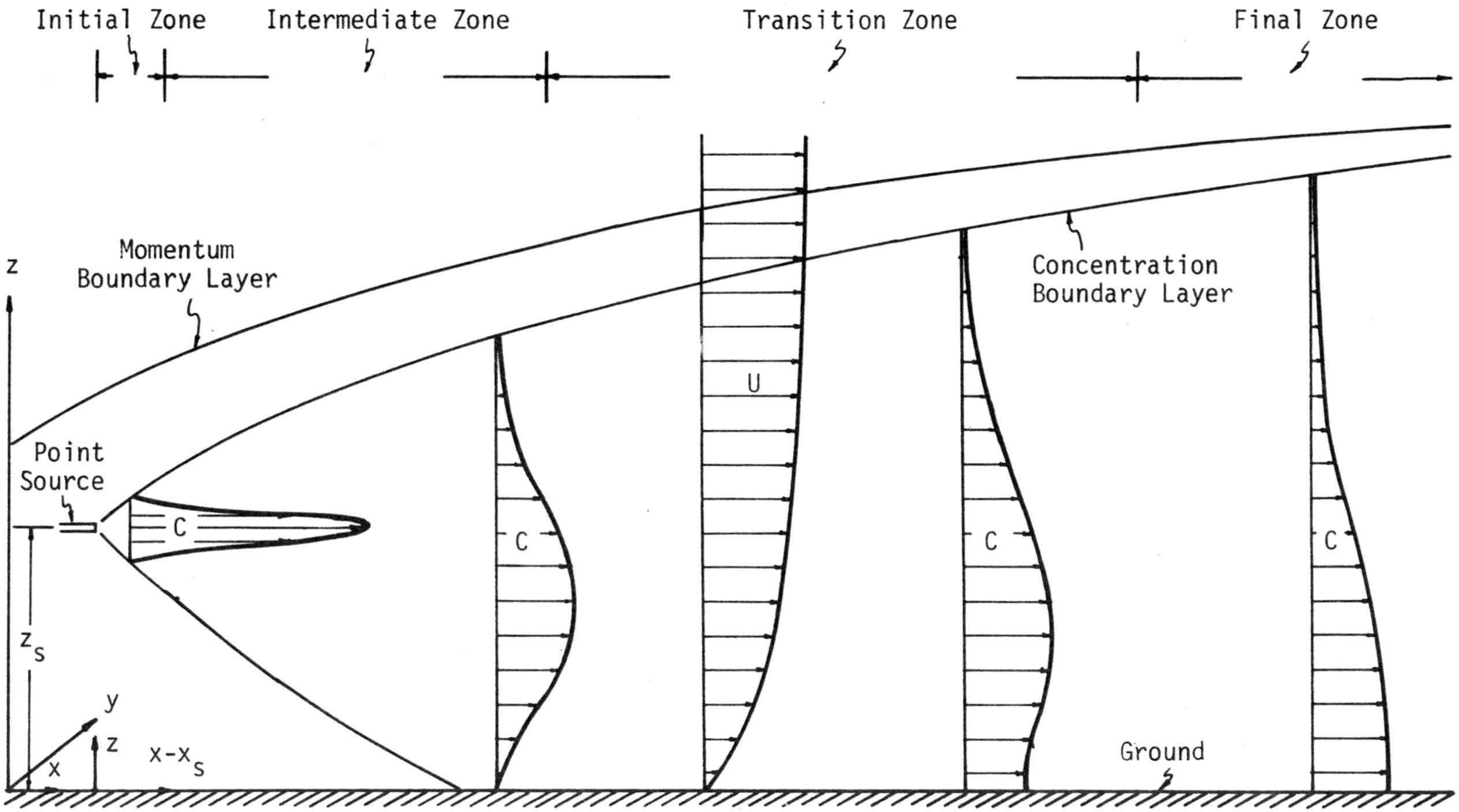

Figure 3-1. Graphical description of the diffusion field.

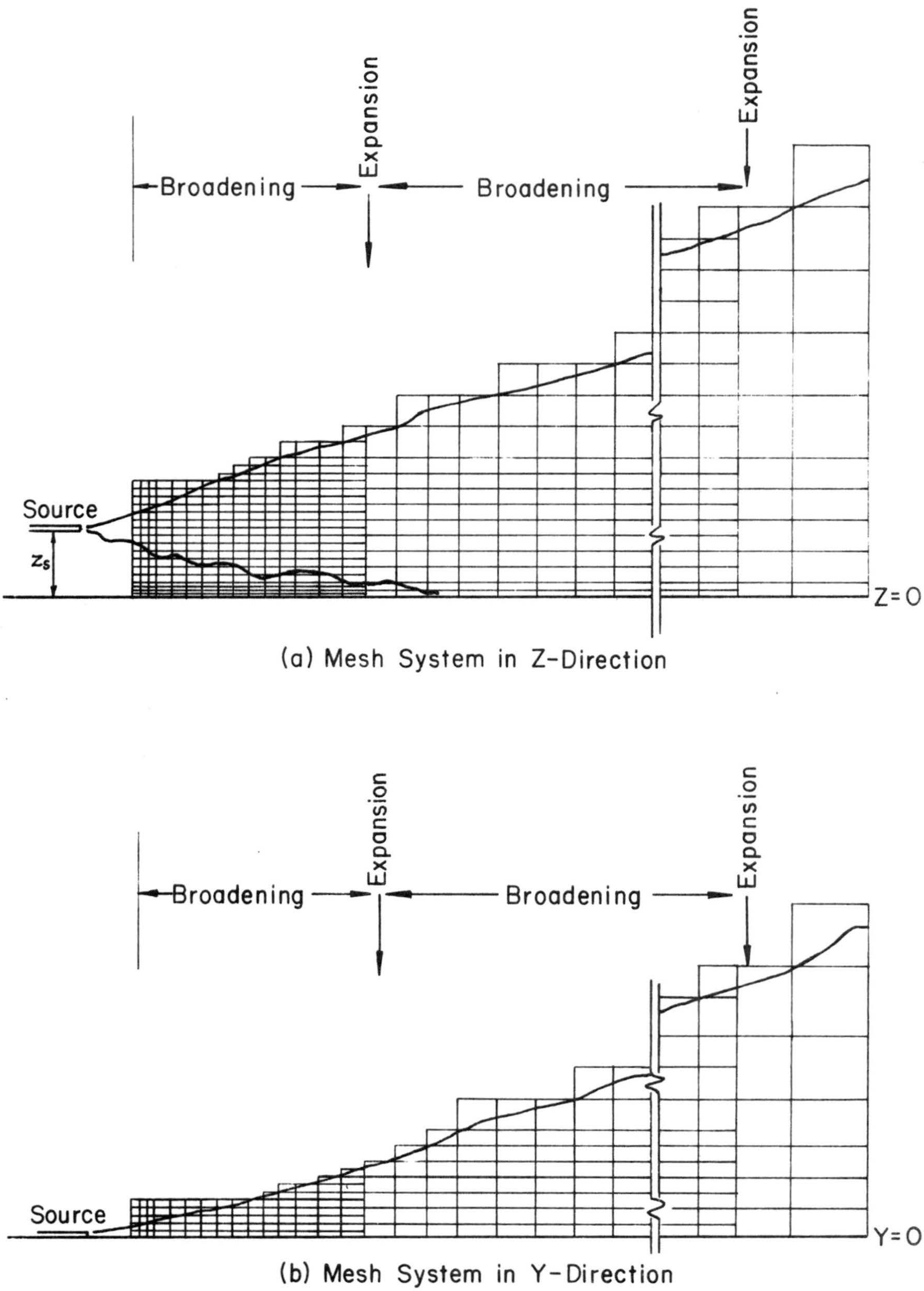

Figure 4-1. Mesh system for numerical calculations.

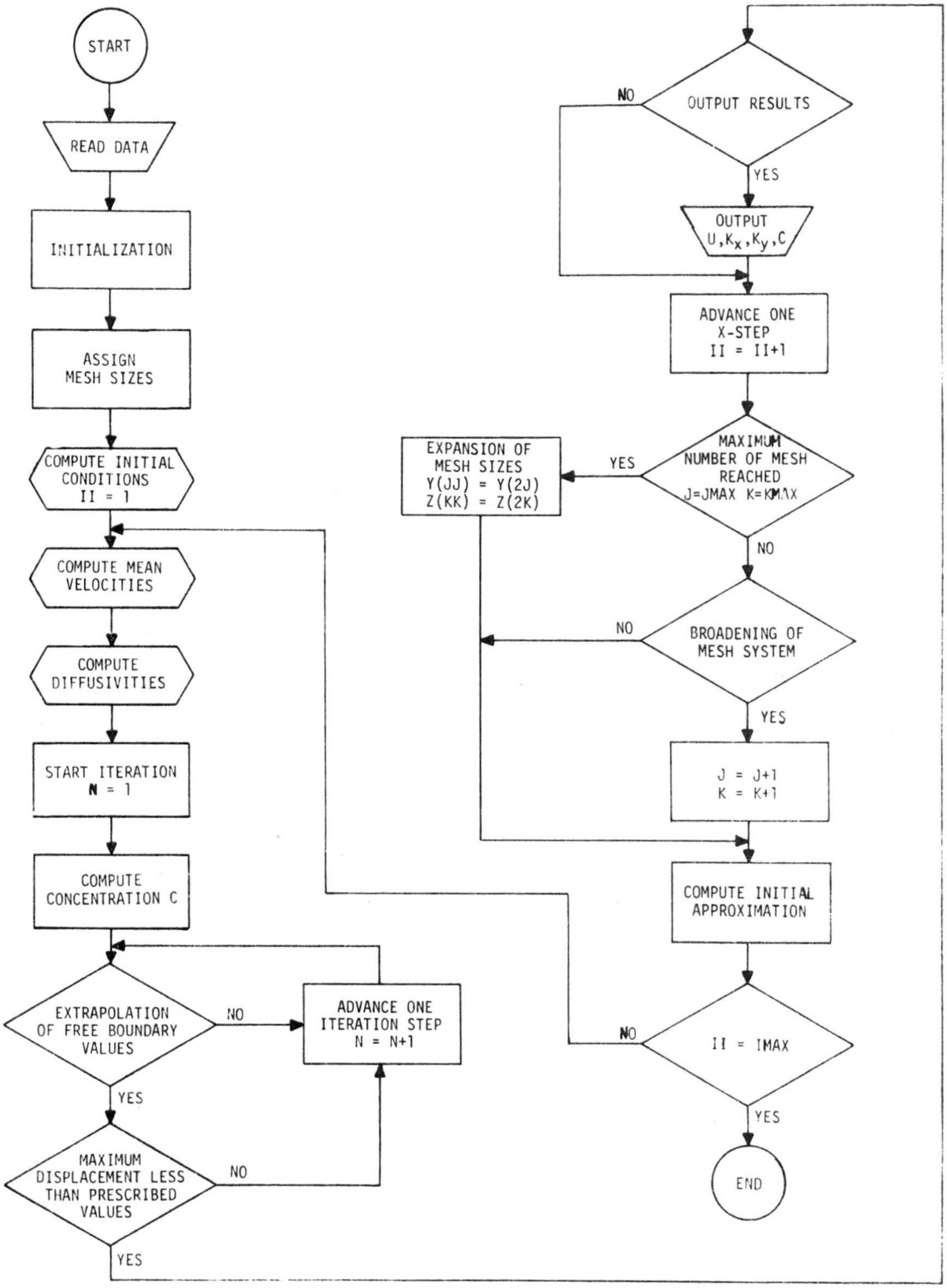

Figure 4-2. Flow chart for numerical solution of the diffusion equation.

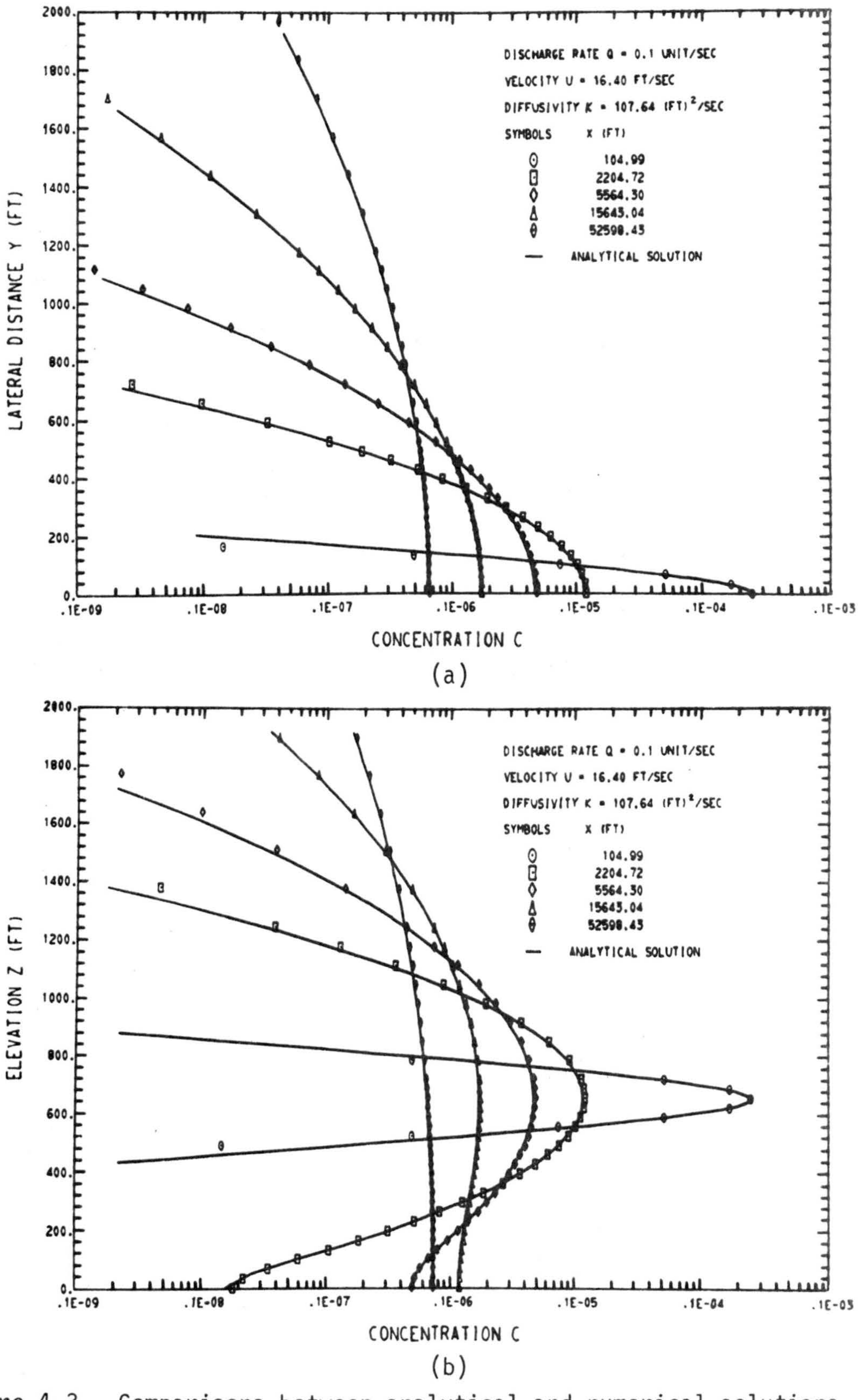

Figure 4-3. Comparisons between analytical and numerical solutions-Test problem I.

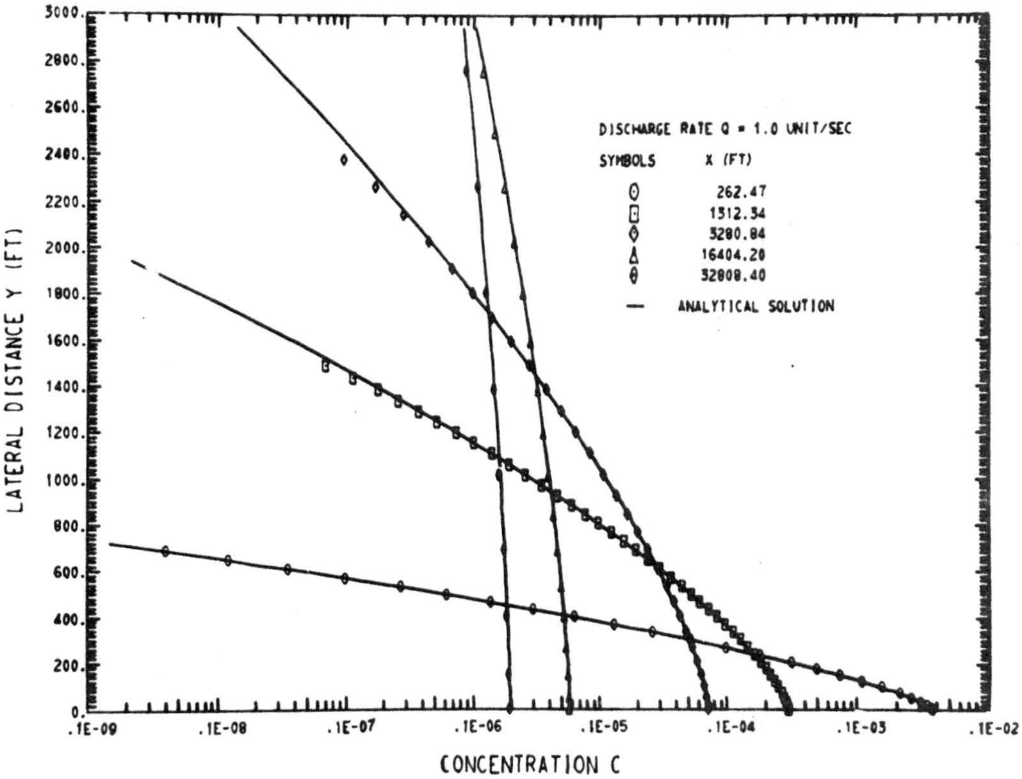

(a)

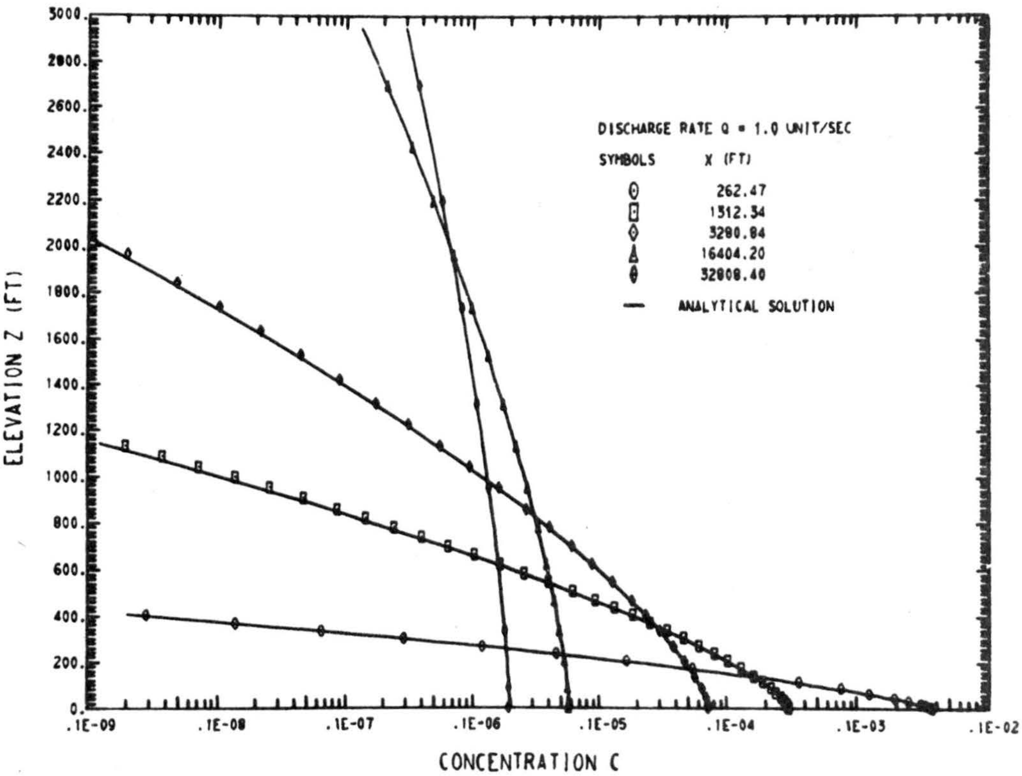

(b)

Figure 4-4. Comparisons between analytical and numerical solutions-Test problem II.

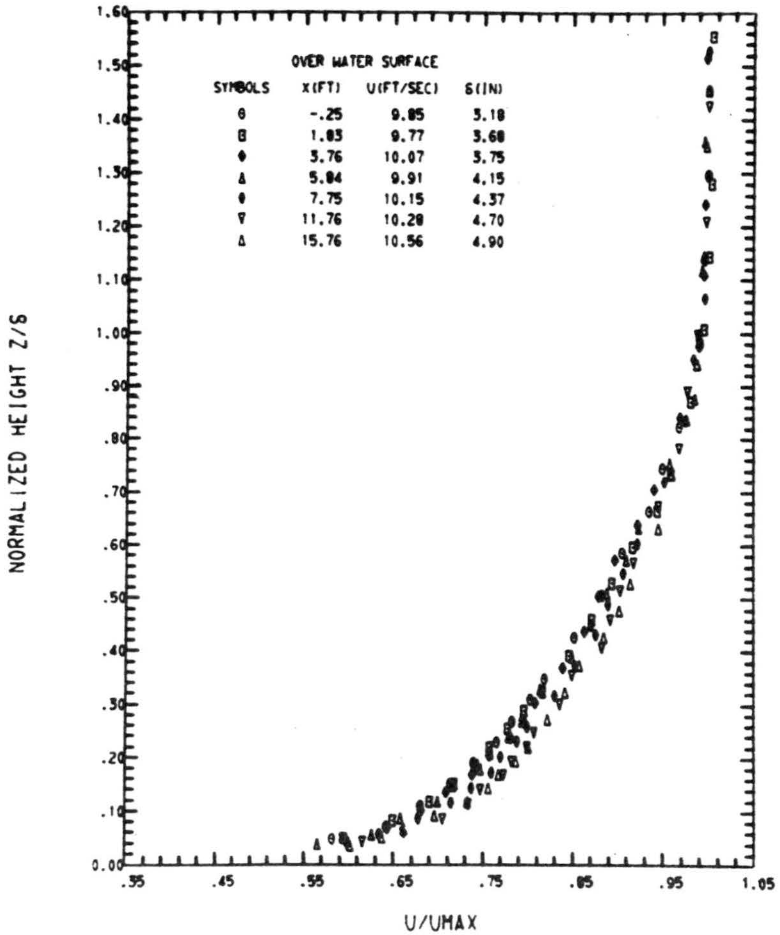

(a) Over Wind Waves $U_\infty \simeq 10$ fps

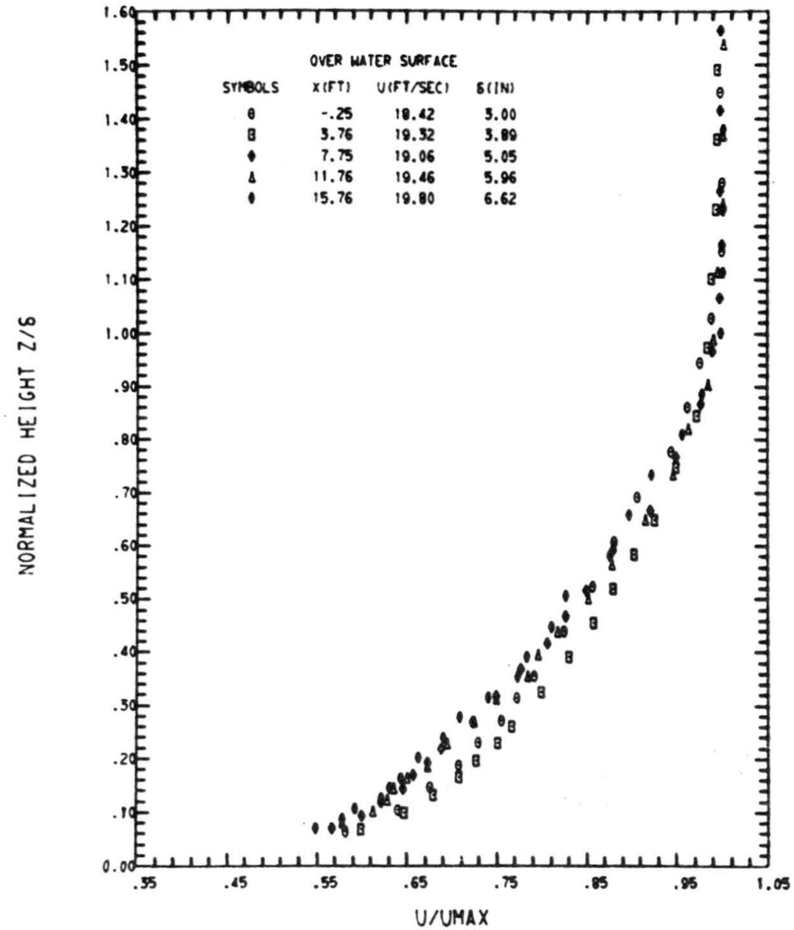

(b) Over Wind Waves $U_\infty \simeq 20$ fps

Figure 4-5. Normalized mean velocity distributions.

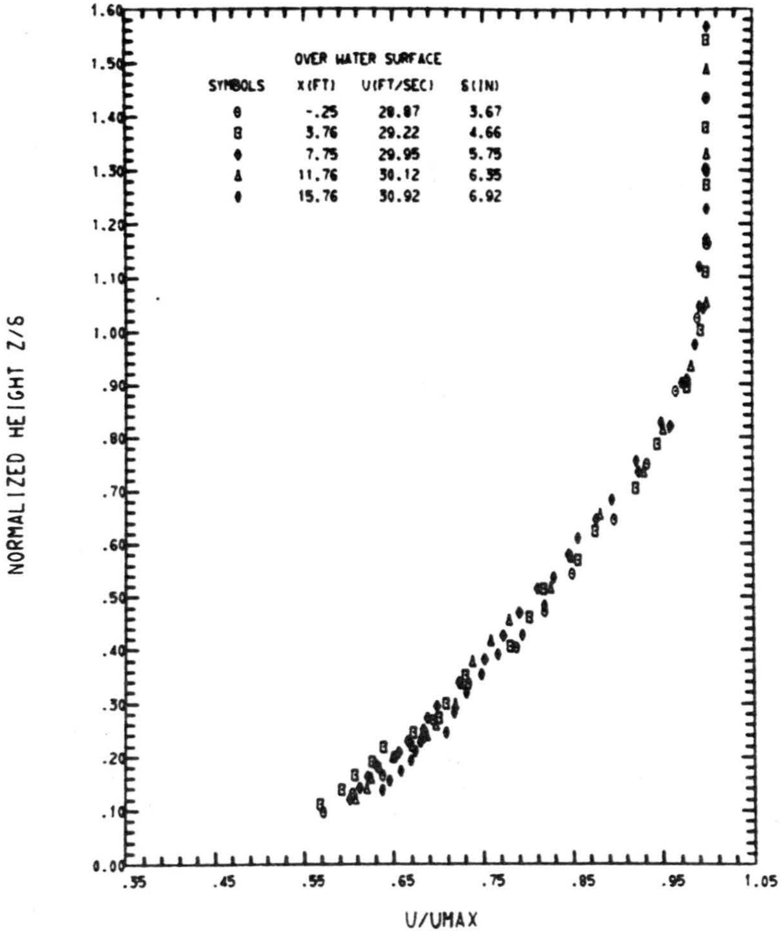

(c) Over Wind Waves $U_\infty \simeq$ 30 fps

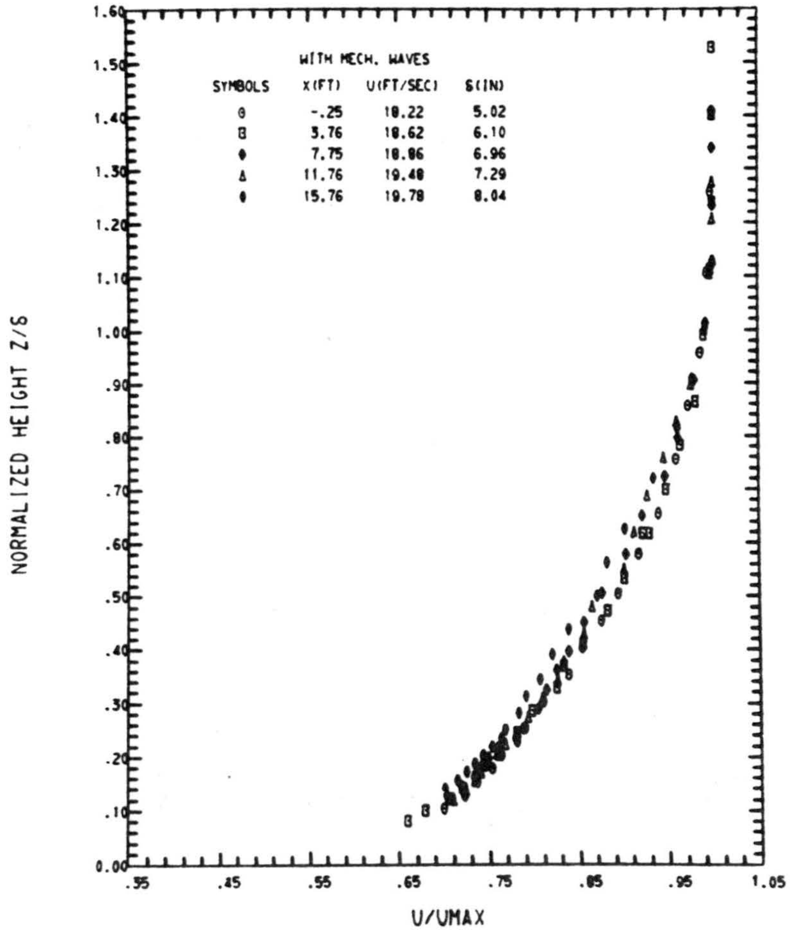

(d) Over Mechanical Waves $U_\infty \simeq$ 20 fps

Figure 4-5. Normalized mean velocity distributions (continued).

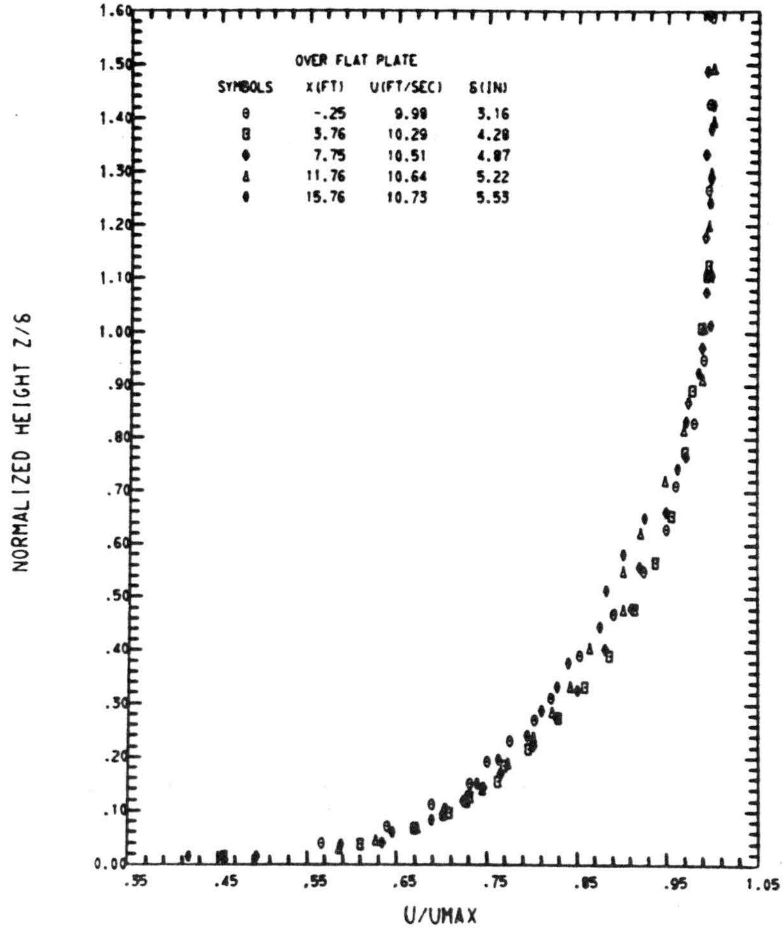

(e) Over Flat Plate $U_\infty \simeq 10$ fps

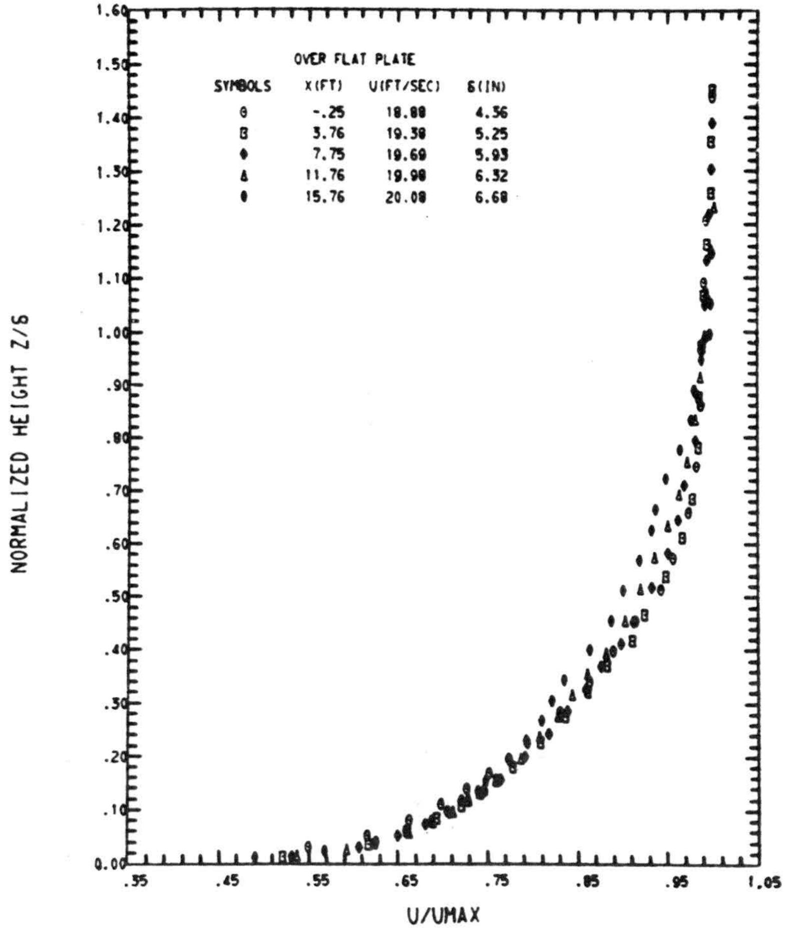

(f) Over Flat Plate $U_\infty \simeq 20$ fps

Figure 4-5. Normalized mean velocity distributions (continued).

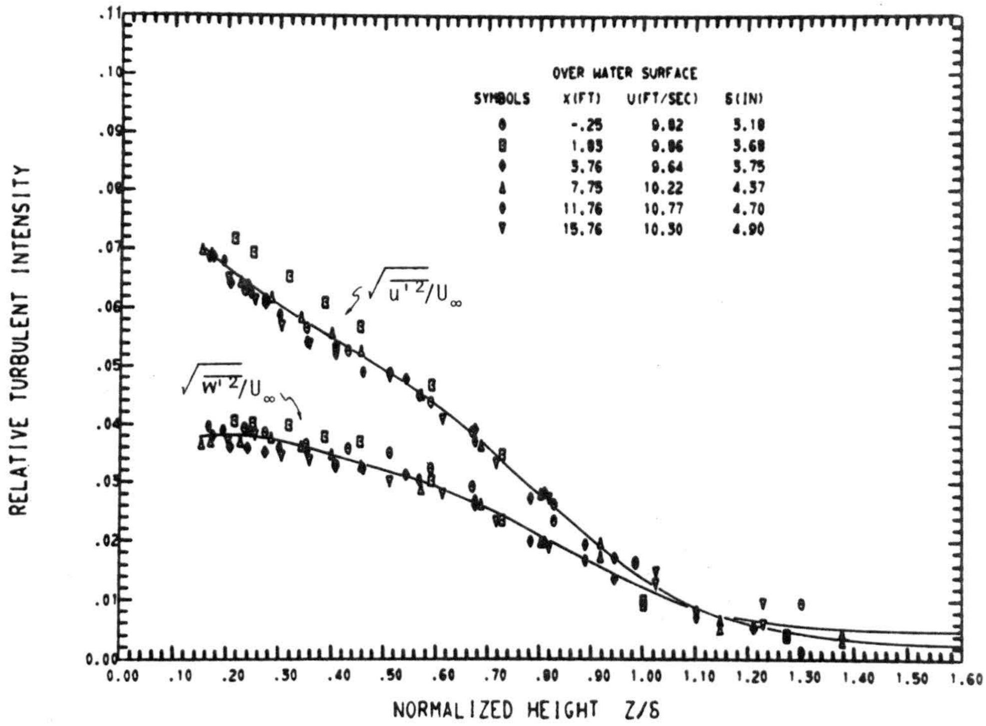

(a) Over Wind Waves $U_\infty \simeq 10$ fps

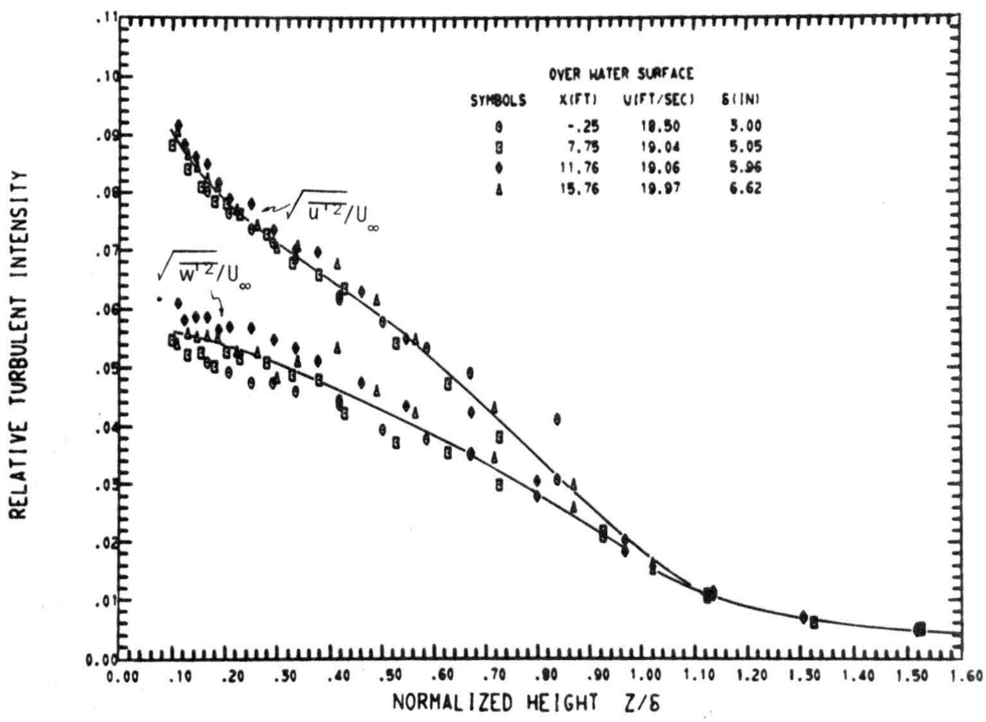

(b) Over Wind Waves $U_\infty \simeq 20$ fps

Figure 4-6. Measurements of relative turbulent intensity.

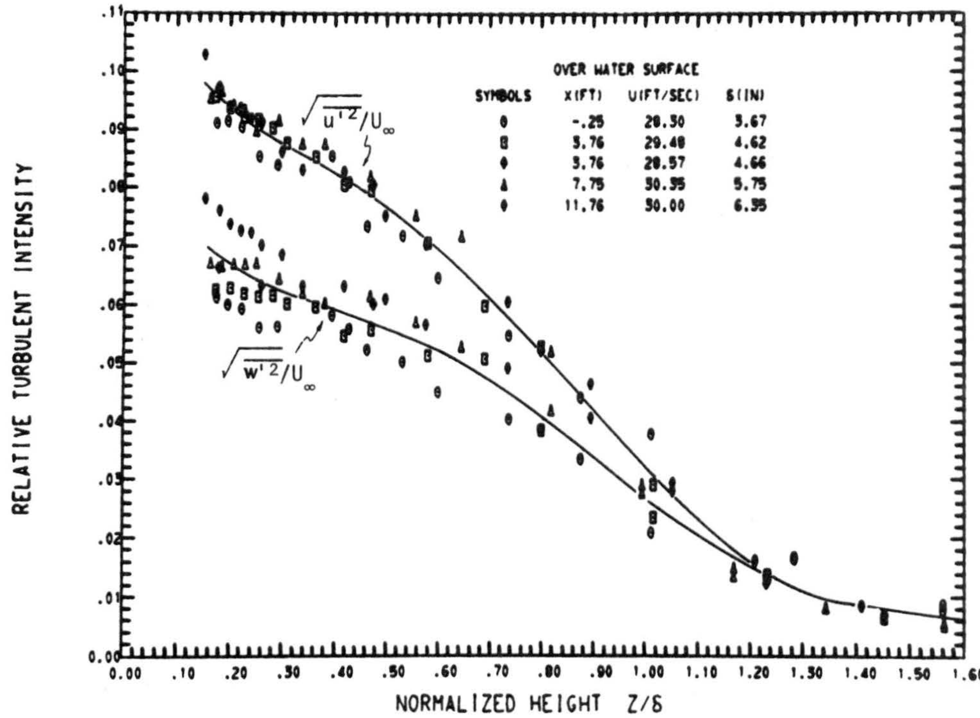

(c) Over Wind Waves $U_\infty \simeq 30$ fps

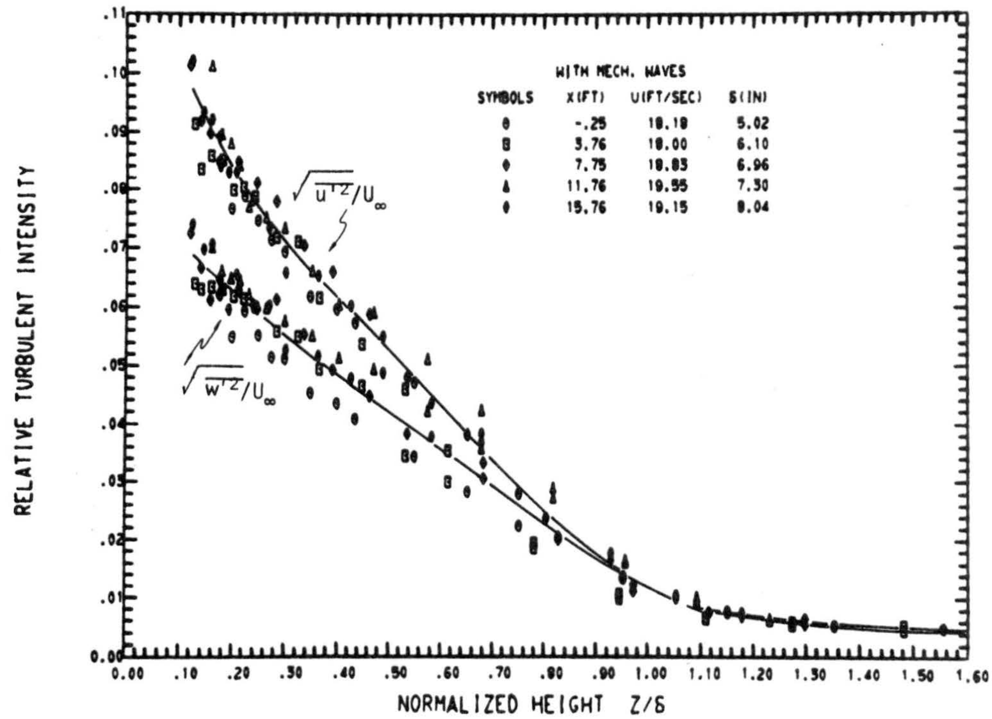

(d) Over Mechanical Waves $U_\infty \simeq 20$ fps

Figure 4-6. Measurements of relative turbulent intensity (continued).

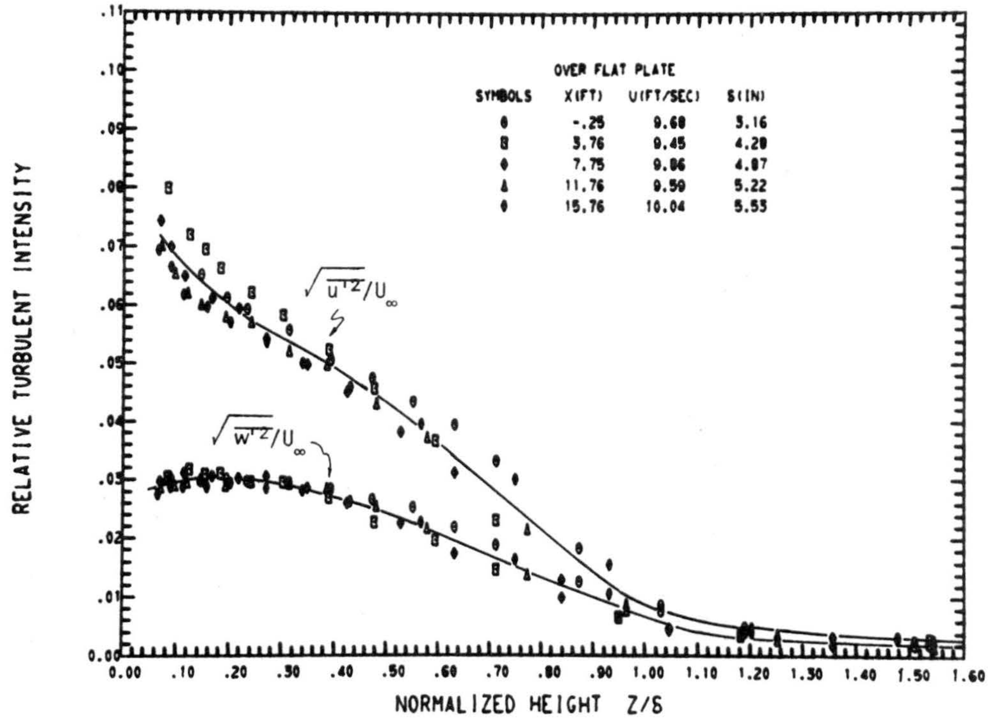

(e) Over a Flat Plate $U_\infty \simeq 10$ fps

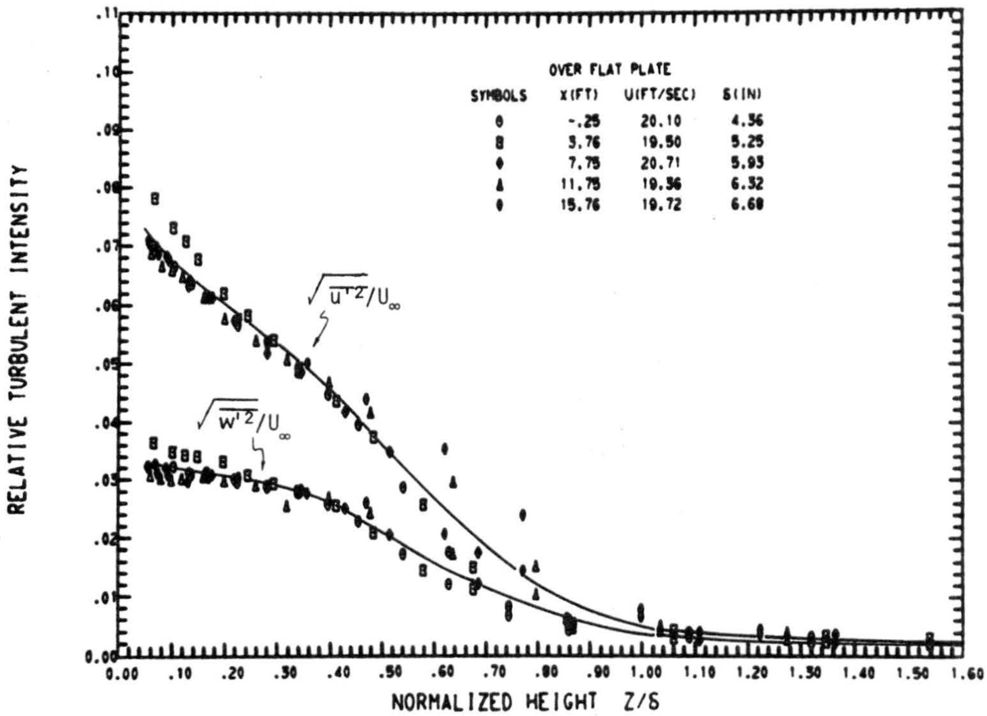

(f) Over a Flat Plate $U_\infty \simeq 20$ fps

Figure 4-6. Measurements of relative turbulent intensity (continued).

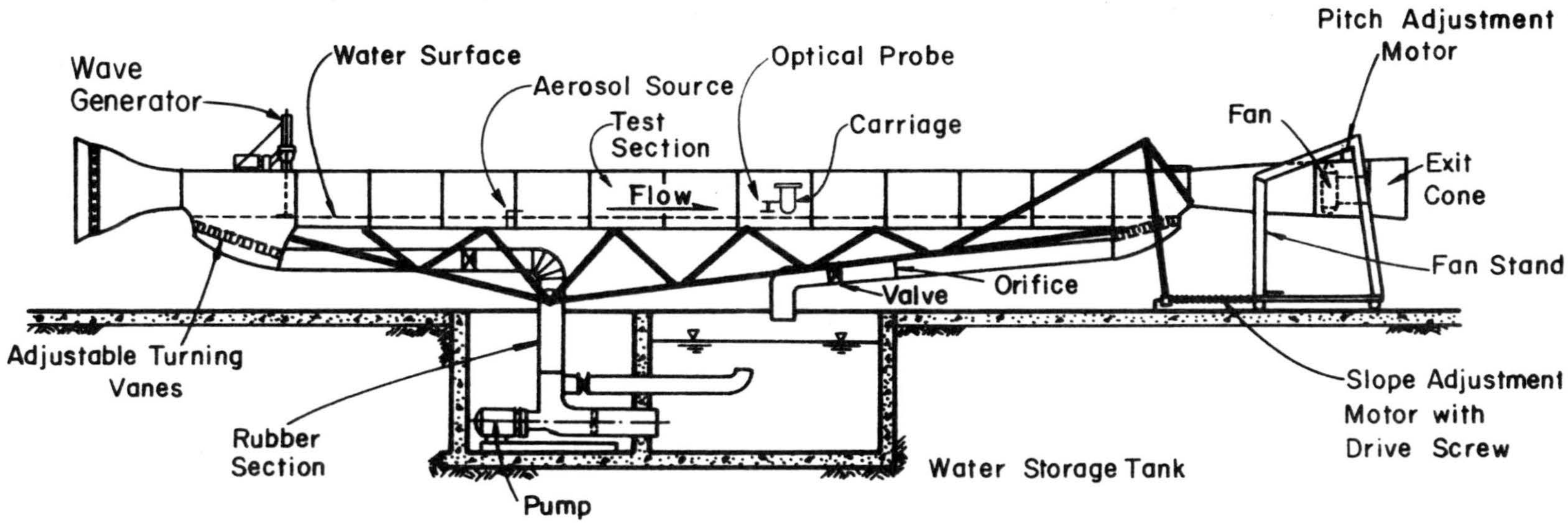

Figure 5-1. Schematic drawing of the wind-water tunnel.

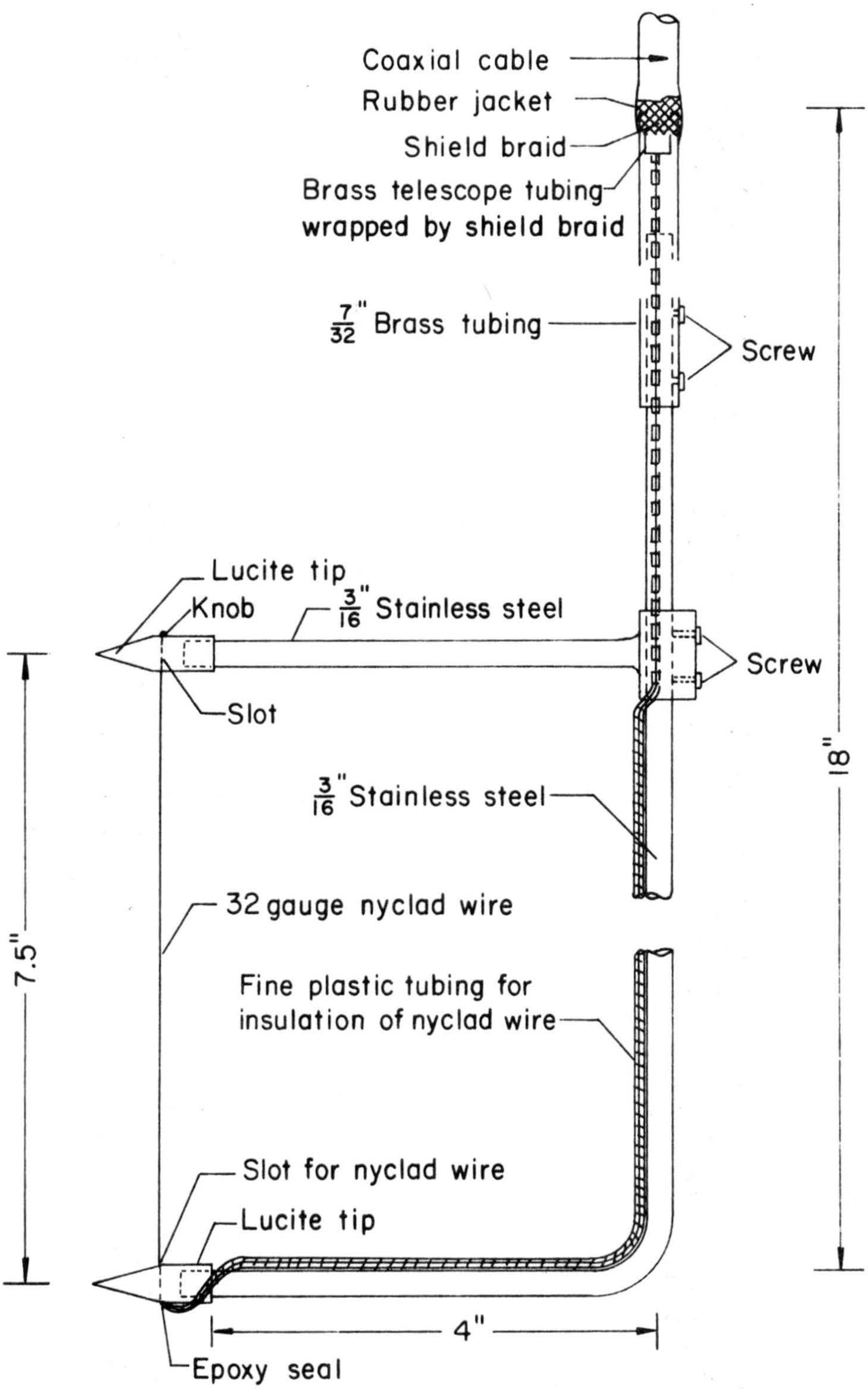

Figure 5-2. Schematic drawing of the capacitance wave gauge.

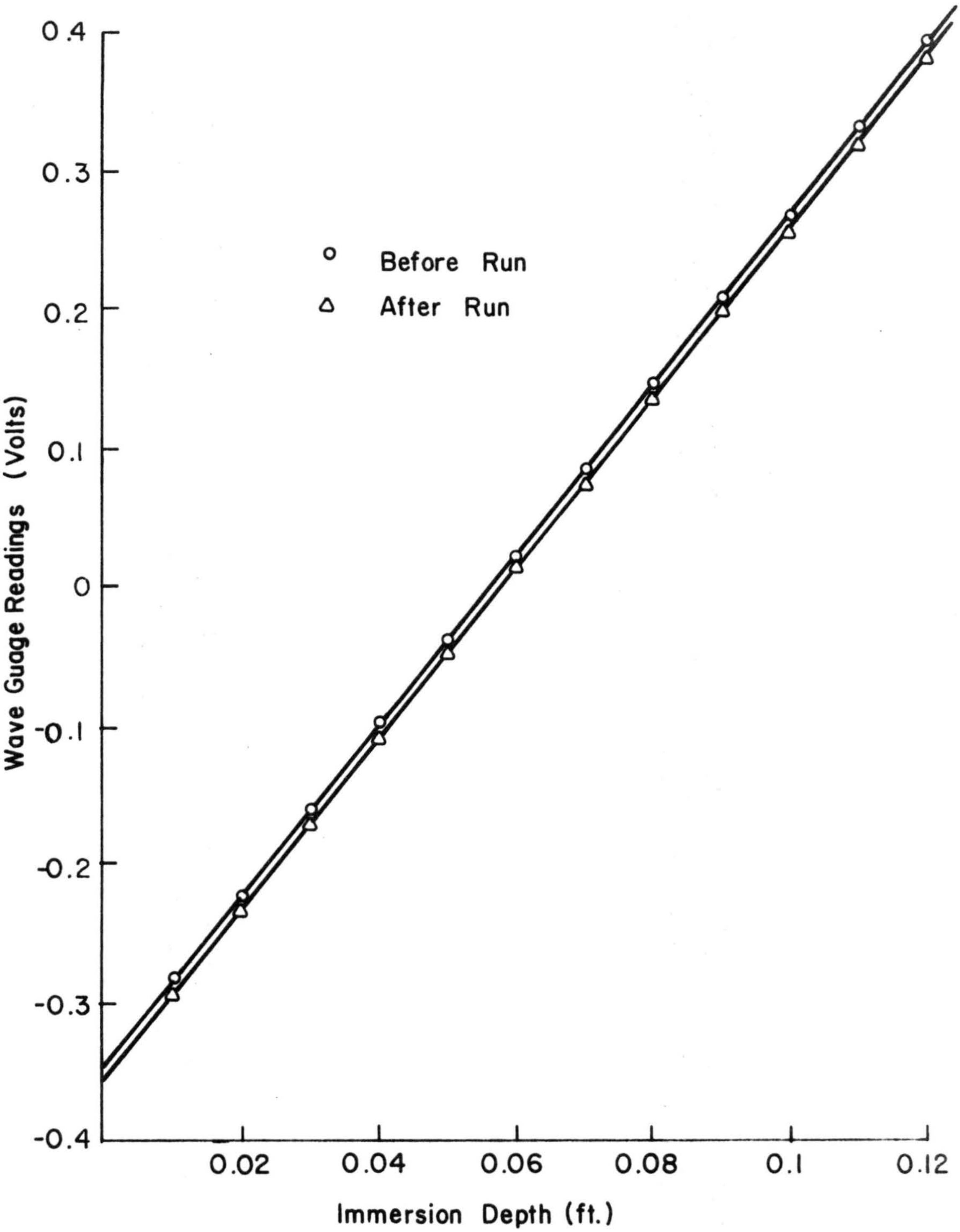

Figure 5-3. Typical calibration curves for the wave gauge.

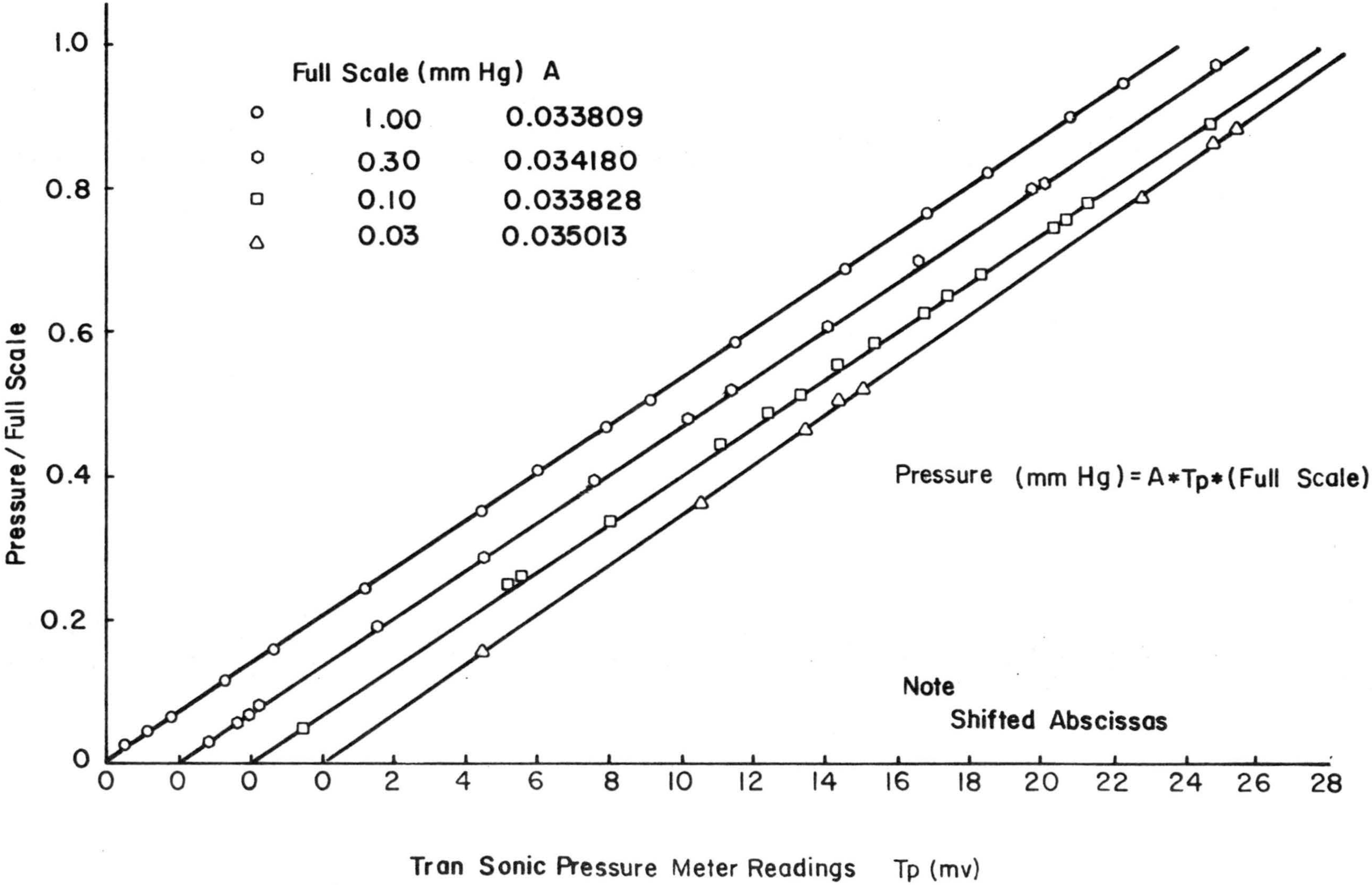

Figure 5-4. Calibration curves for the Tran Sonic pressure meter.

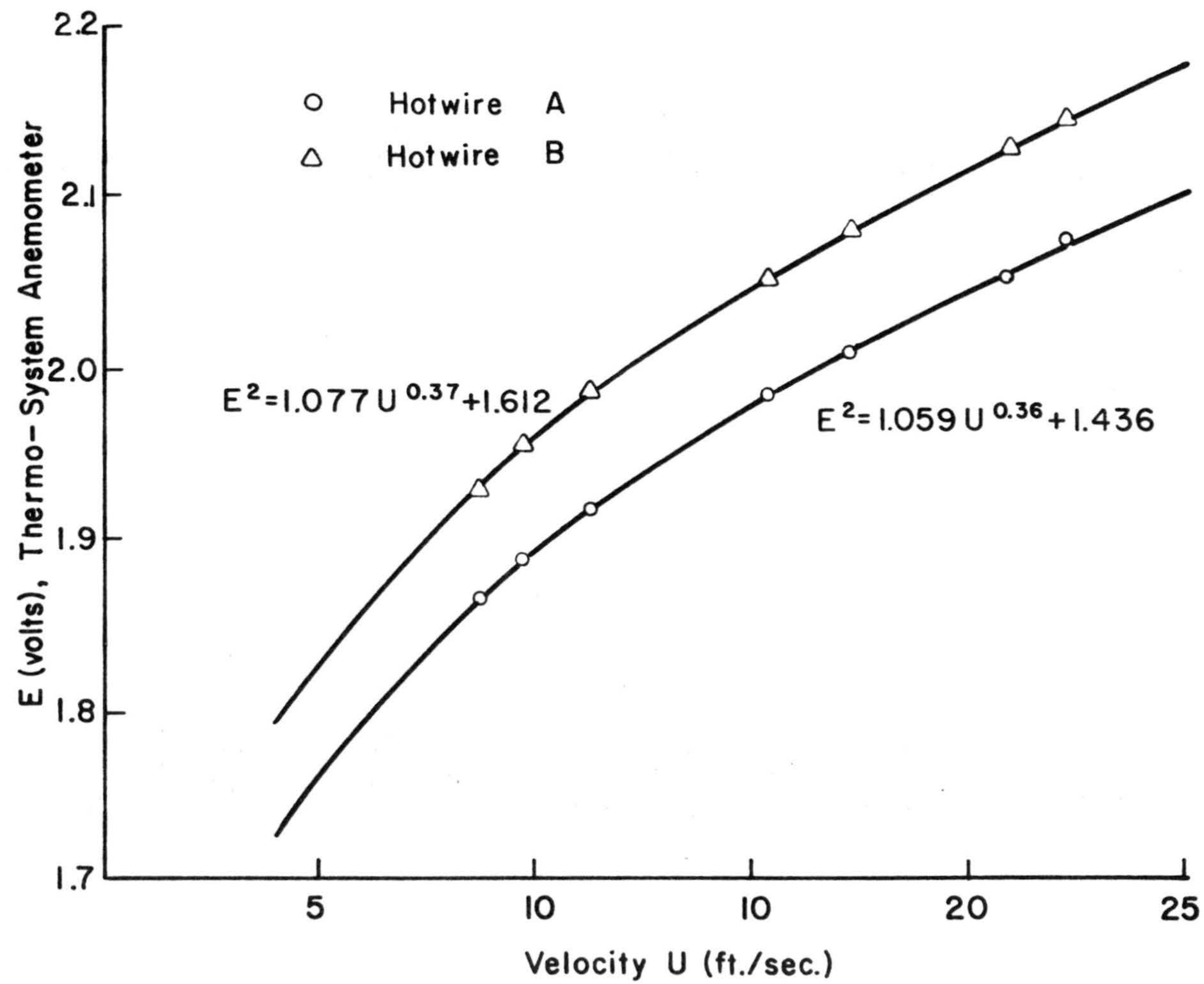

Figure 5.5 Typical calibration curves for the cross-wire anemometer.

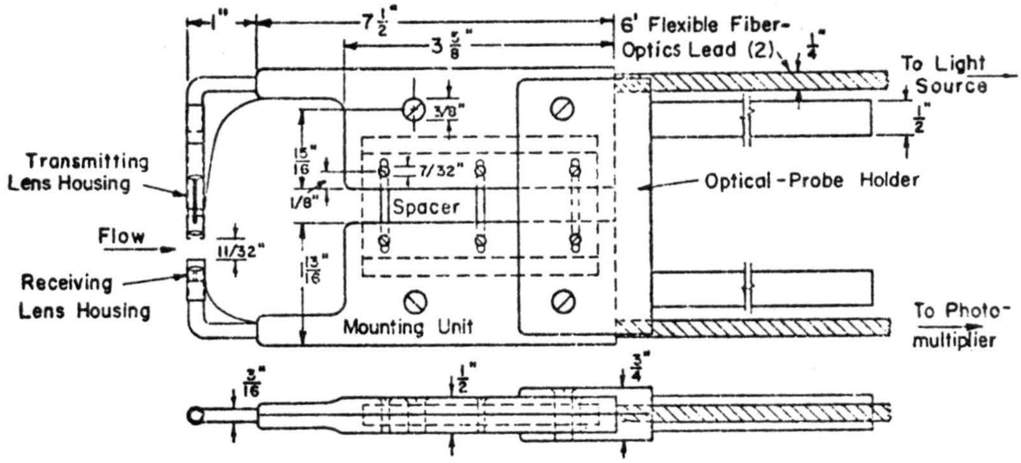

a. Physical Arrangement of the Optical Probe

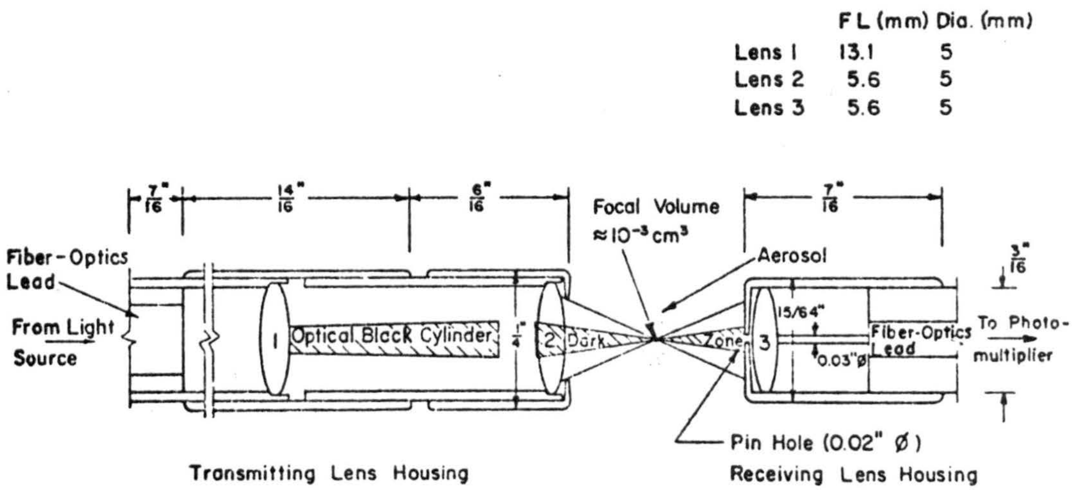

b. Details of Optical Probe Gap

Figure 5-6. Optical probe details.

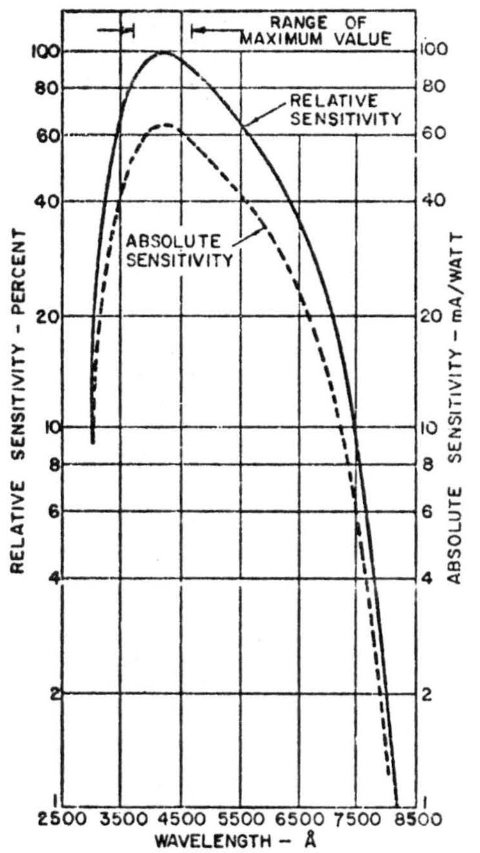

a. Spectral Response Characteristics of the Photomultiplier.

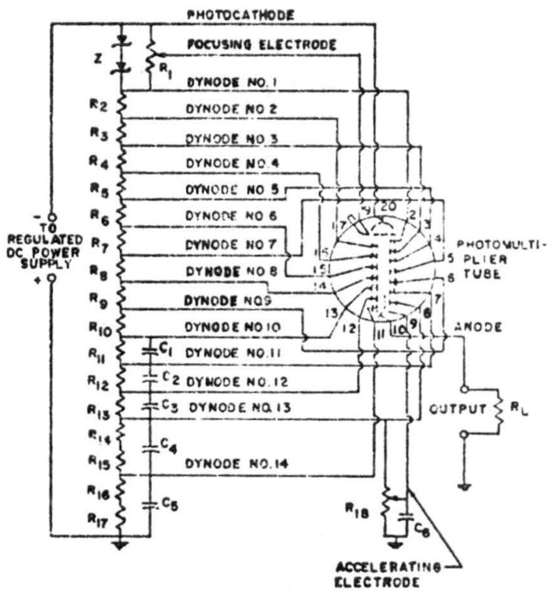

C_1: 25 pF, 20%, 600 volts (dc working), ceramic disc
C_2: 50 pF " " " "
C_3: 100pF " " " "
C_4: 250pF " " " "
C_5: 500pF " " " "
C_6: 100pF, 20%, 1000 volts " "
R_1: 5 megohms, 20%, 1/2 watt, adjustable
R_2 through R_{11}: 22000 ohms, 5%, 1 watt
R_{12}: 27000 ohms, 5%, 2 watts
R_{13}: 33000 ohms " "
R_{14}: 22000 ohms " "
R_{15}: 18000 ohms " "
R_{16}: 22000 ohms " "
R_{17}: " " "
R_{18}: 10 megohms, 2 watts, adjustable
R_L: 0~ 2500 Ohms
Z : (1)- 150 V, 1 W zener diode, or equivalent
(1)- 180V, " " "

b. Voltage Divider Circuitry for use with the Photomultiplier.

Figure 5-7. RCA 7265 photomultiplier characteristics and circuitry.

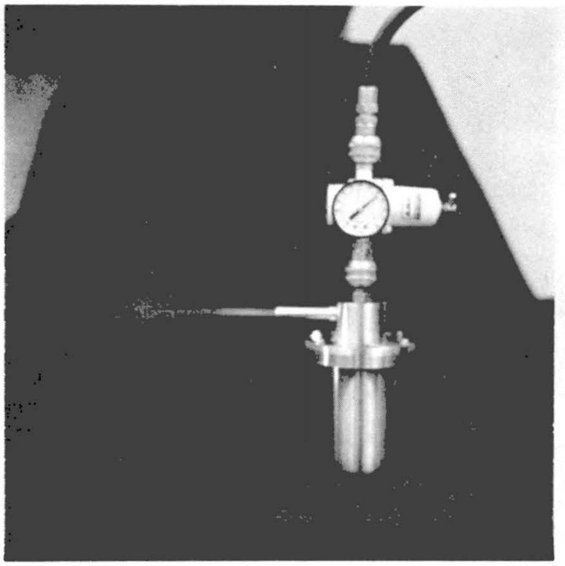

(a) Aerosol Generator or DOP Atomizer

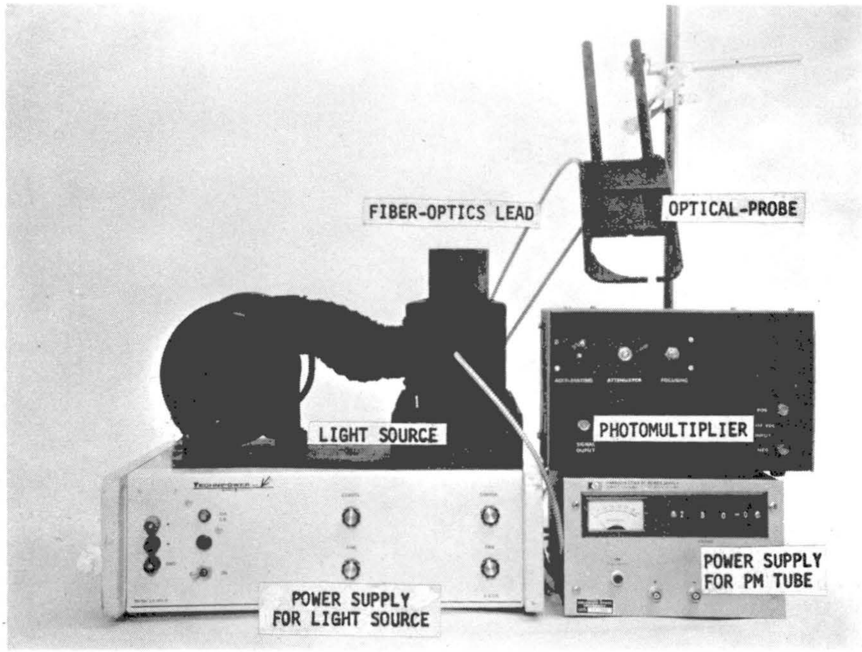

(b) Components of the Optical Device

Figure 5-8. Apparatus for concentration measurements.

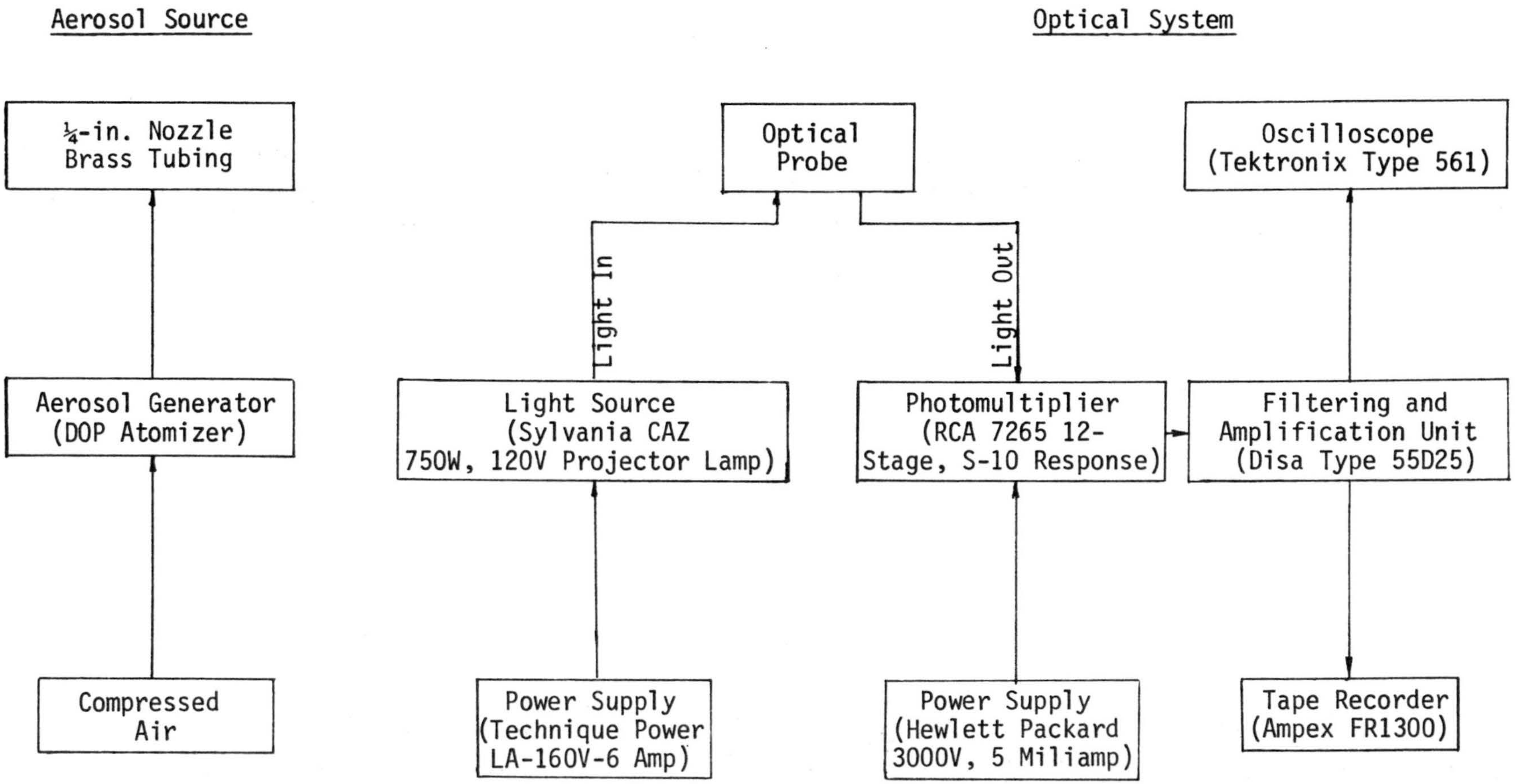

Figure 5-9. Block diagram for the optical device and aerosol generator.

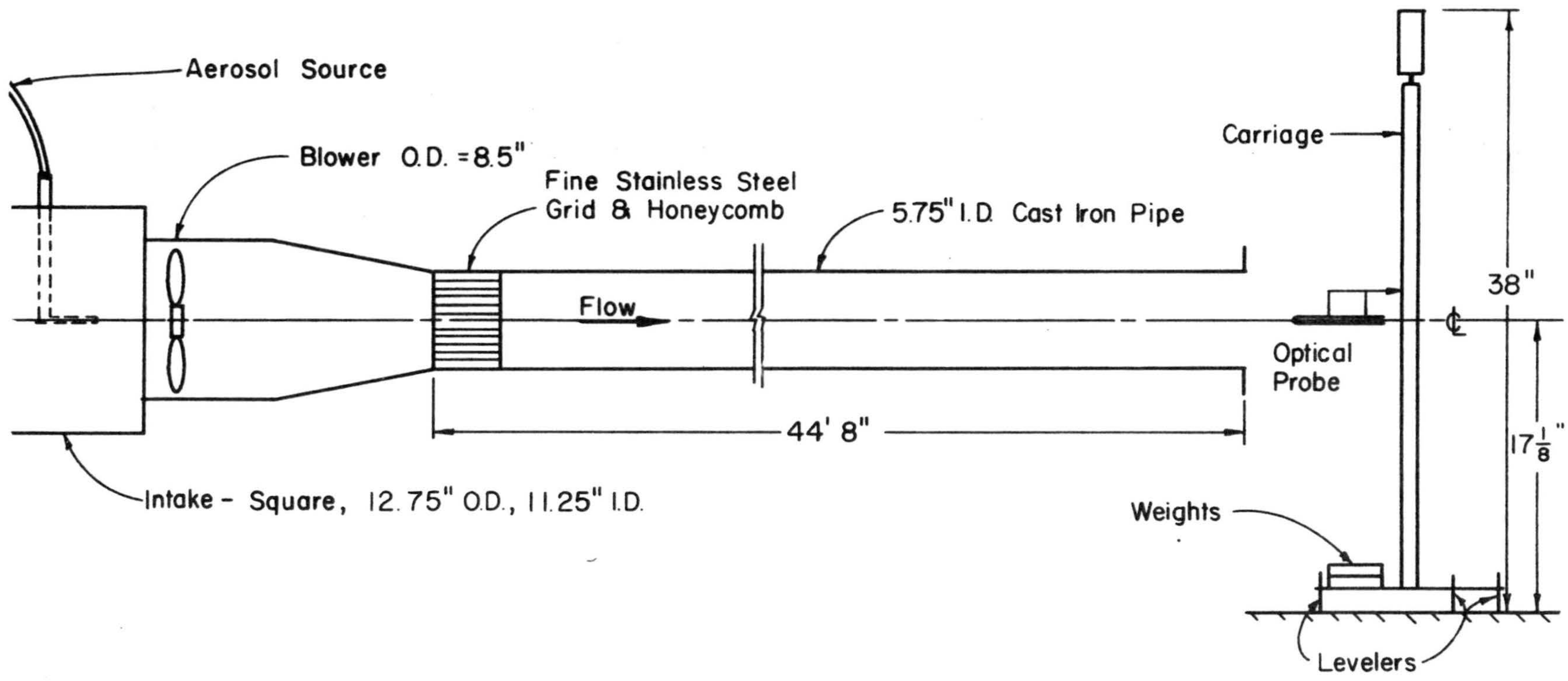

Figure 5-10. Arrangement for calibration of the optical device.

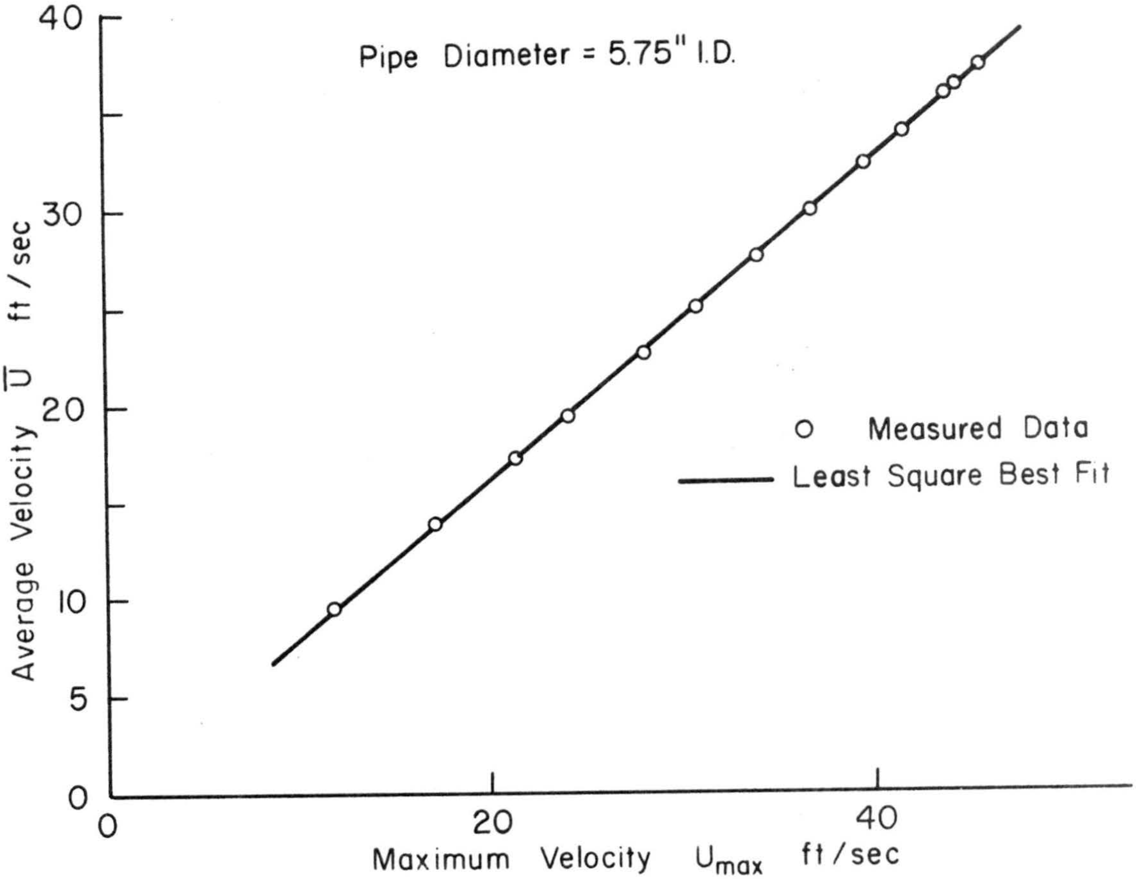

Measured data		Least Square Best Fit	
Maximum Velocity U_{max}	Average Velocity $\overline{U}$	Average Velocity $\overline{U}_{cal}$	Relative Error
45.80	37.17	37.23	.0017
44.55	36.21	36.17	-.0012
43.92	35.73	35.65	-.0022
41.86	34.07	33.96	-.0031
39.84	32.35	32.31	-.0013
37.03	30.06	29.99	-.0023
34.19	27.56	27.67	.0039
30.95	24.87	25.00	.0054
28.20	22.59	22.75	.0067
24.20	19.40	19.47	.0034
21.43	17.21	17.19	-.0008
17.21	13.77	13.72	-.0033
11.89	9.48	9.36	-.0135

Best Fit Equation: $\overline{U}_{cal} = .821 \times U_{max} - .4040$

Figure 5-11. Relationship between average and maximum velocities of the calibration pipe.

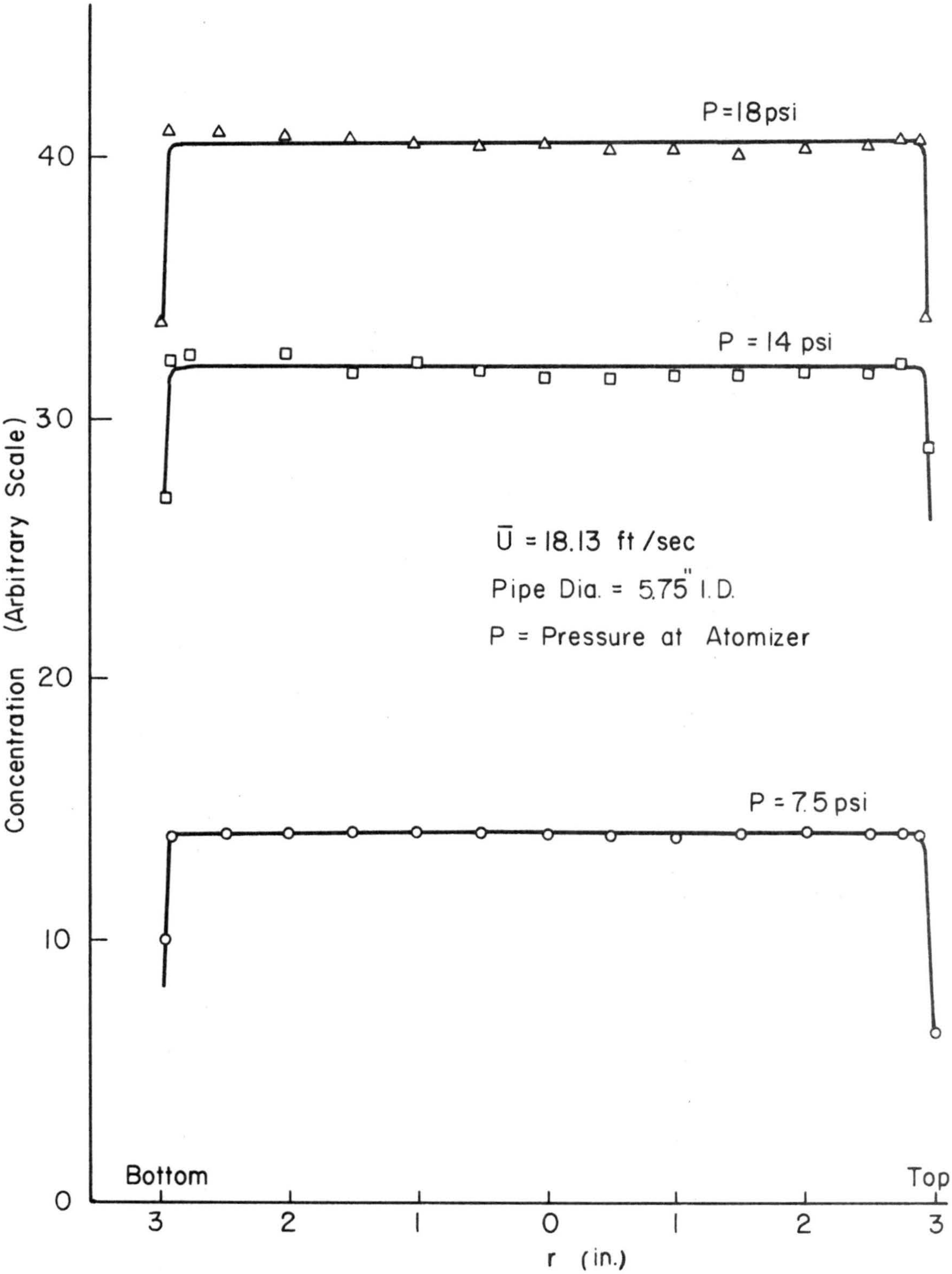

Figure 5-12. Concentration profiles across the outlet of the calibration pipe.

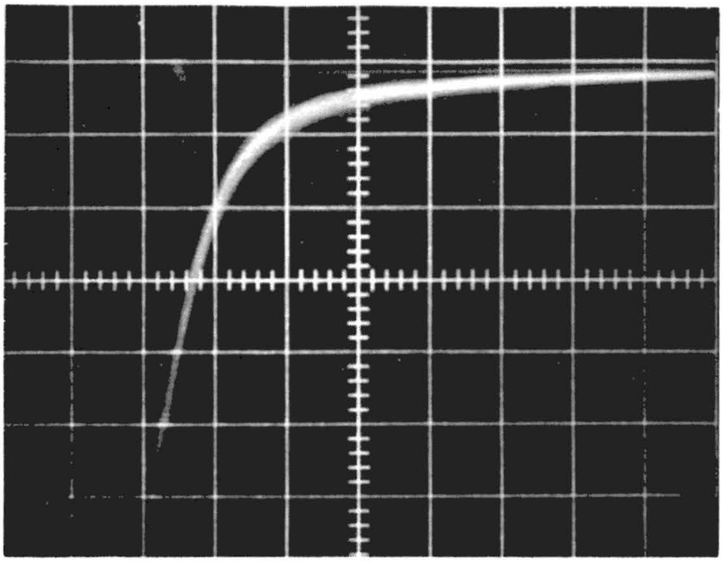

(a) Stroboscope Fequency = 300 Hz
Vertical Scale = 0.2 volt/div.
Horizontal Scale = 2 x 10^{-6} sec

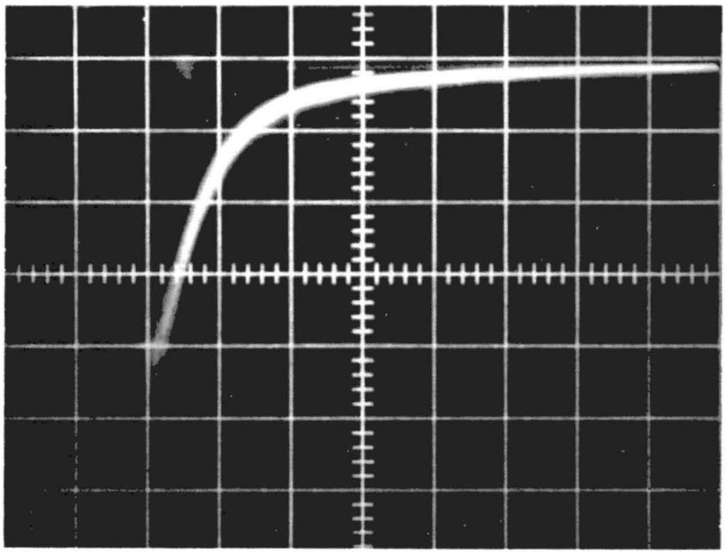

(b) Stroboscope Frequency = 417 Hz
Vertical Scale = 0.2 volt/div.
Horizontal Scale = 2 x 10^{-6} sec

Figure 5-13. Oscillograms for estimating frequency response of the optical device.

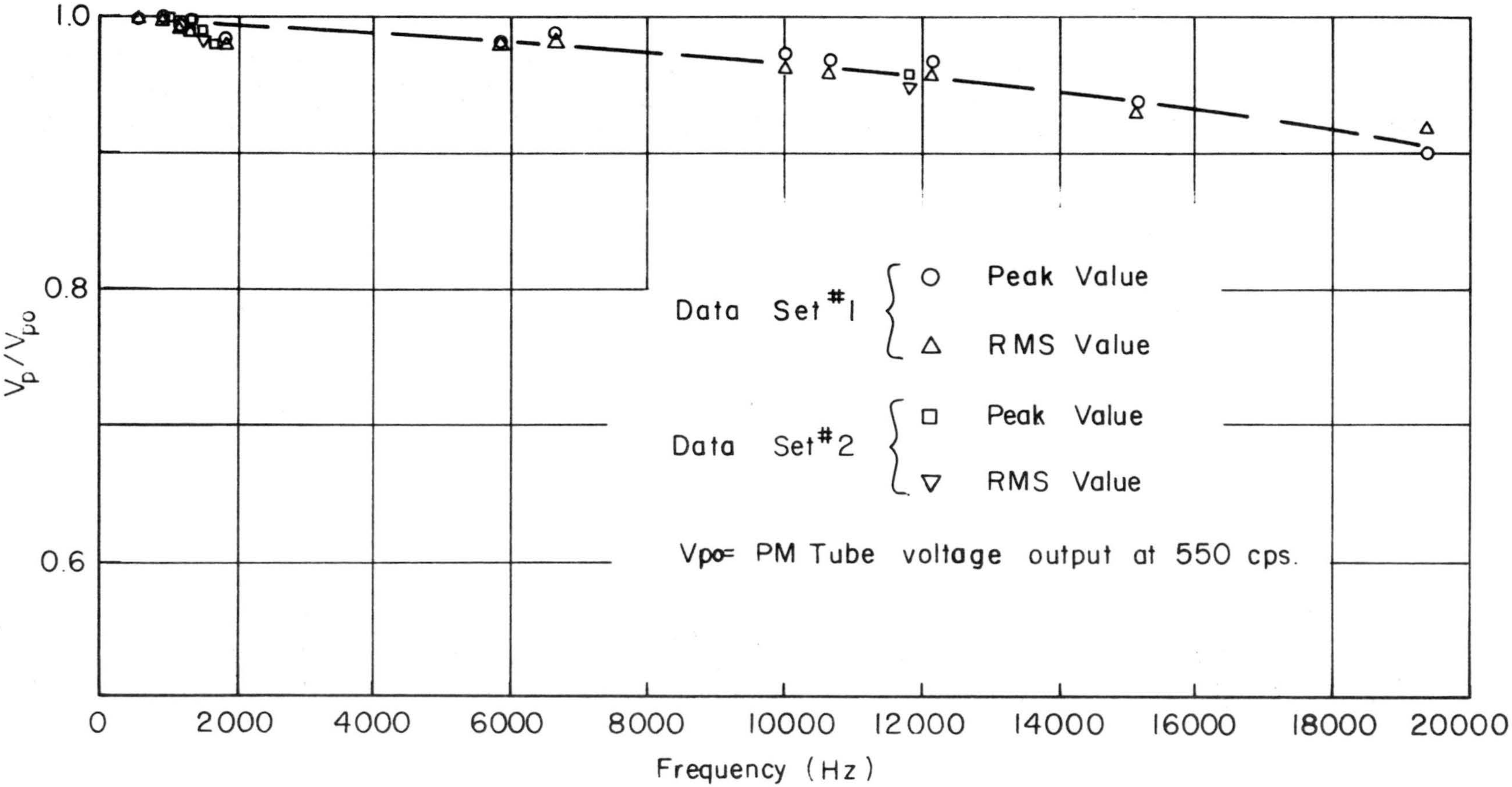

Figure 5-14. Signal attenuation of the optical device with respect to frequency.

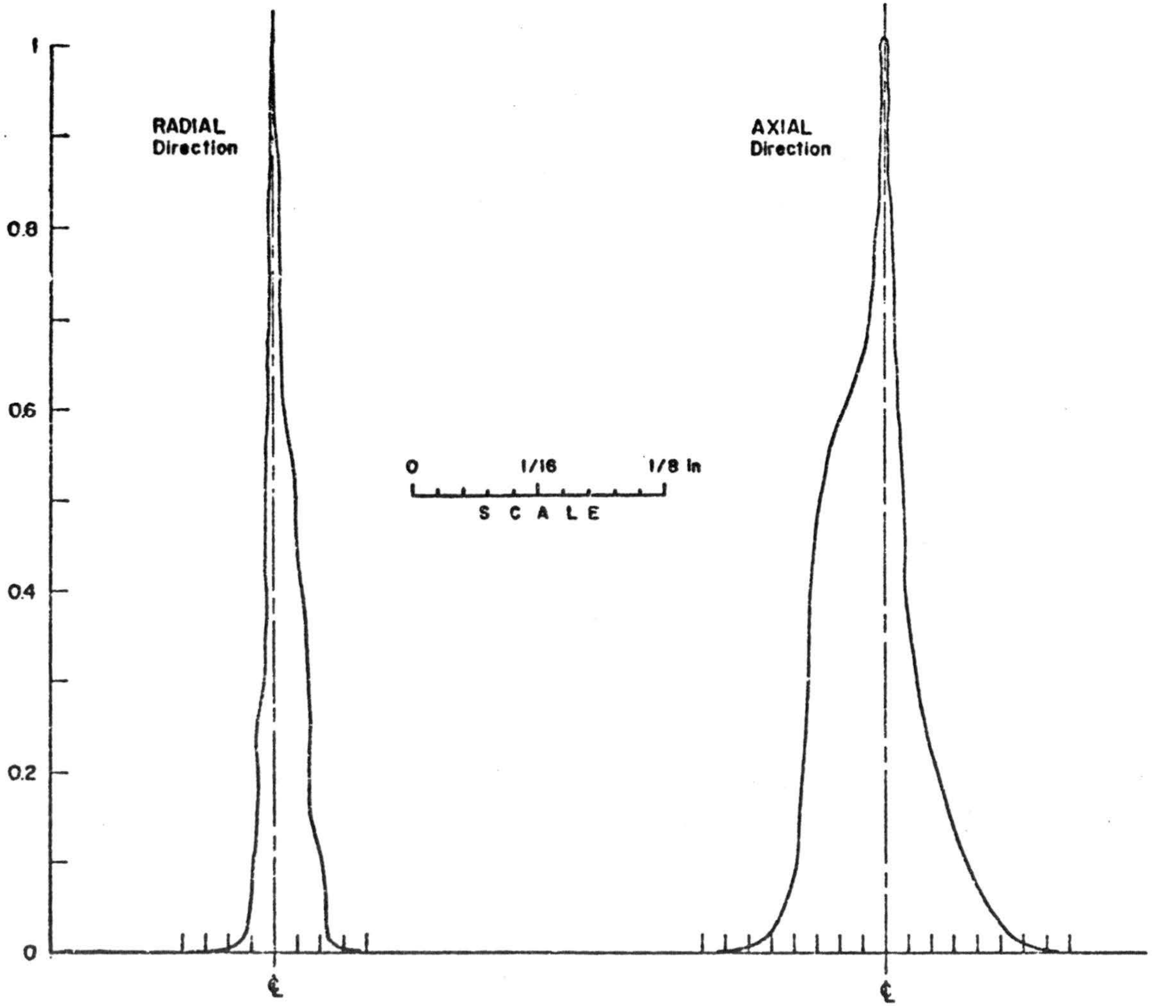

Figure 5-15. Envelopes of PM output curves for calculation of focal volume.

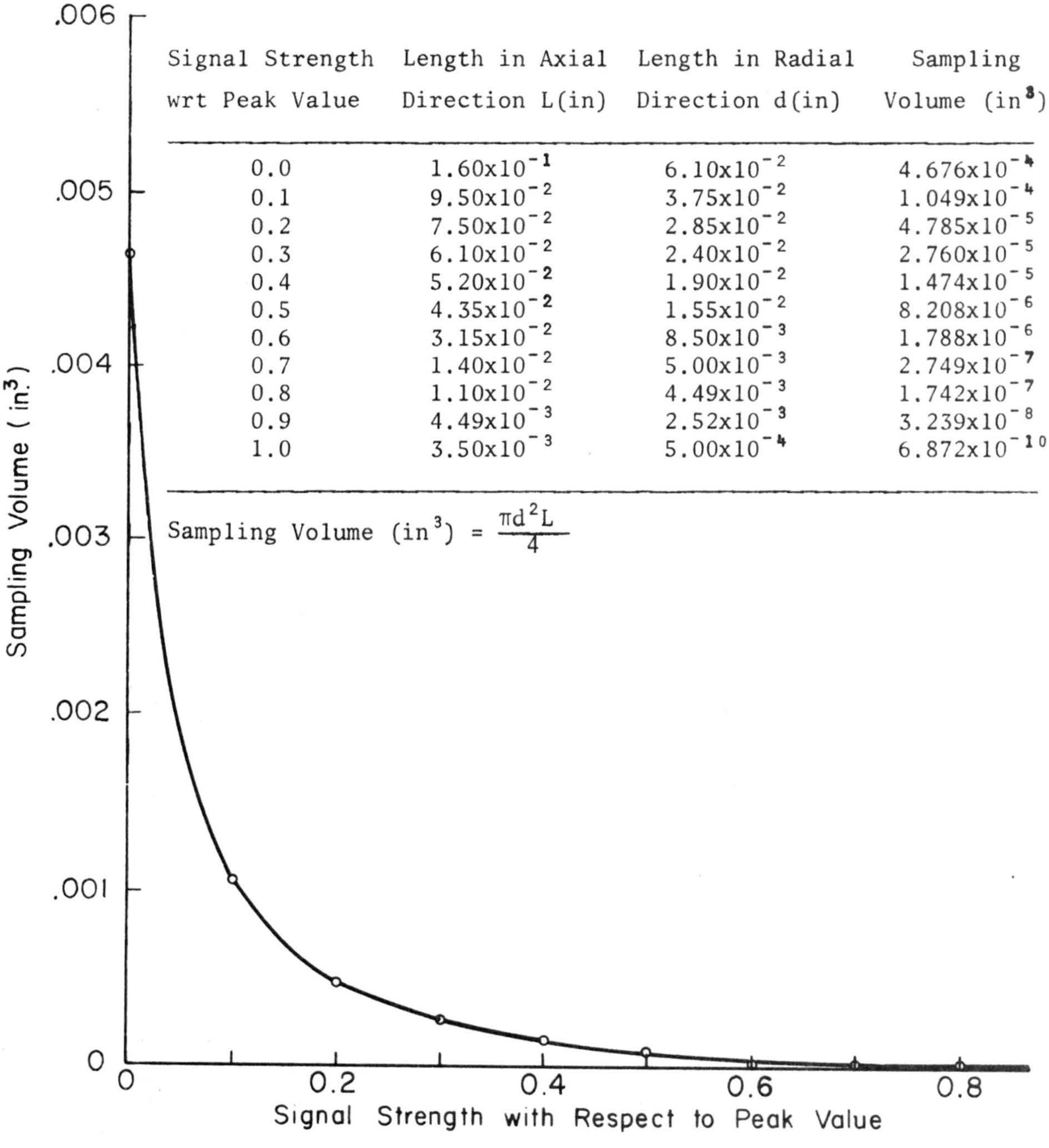

Signal Strength wrt Peak Value	Length in Axial Direction L(in)	Length in Radial Direction d(in)	Sampling Volume (in^3)
0.0	1.60×10^{-1}	6.10×10^{-2}	4.676×10^{-4}
0.1	9.50×10^{-2}	3.75×10^{-2}	1.049×10^{-4}
0.2	7.50×10^{-2}	2.85×10^{-2}	4.785×10^{-5}
0.3	6.10×10^{-2}	2.40×10^{-2}	2.760×10^{-5}
0.4	5.20×10^{-2}	1.90×10^{-2}	1.474×10^{-5}
0.5	4.35×10^{-2}	1.55×10^{-2}	8.208×10^{-6}
0.6	3.15×10^{-2}	8.50×10^{-3}	1.788×10^{-6}
0.7	1.40×10^{-2}	5.00×10^{-3}	2.749×10^{-7}
0.8	1.10×10^{-2}	4.49×10^{-3}	1.742×10^{-7}
0.9	4.49×10^{-3}	2.52×10^{-3}	3.239×10^{-8}
1.0	3.50×10^{-3}	5.00×10^{-4}	6.872×10^{-10}

$$\text{Sampling Volume (in}^3) = \frac{\pi d^2 L}{4}$$

Figure 5-16. Sampling volume sizes of the optical-probe.

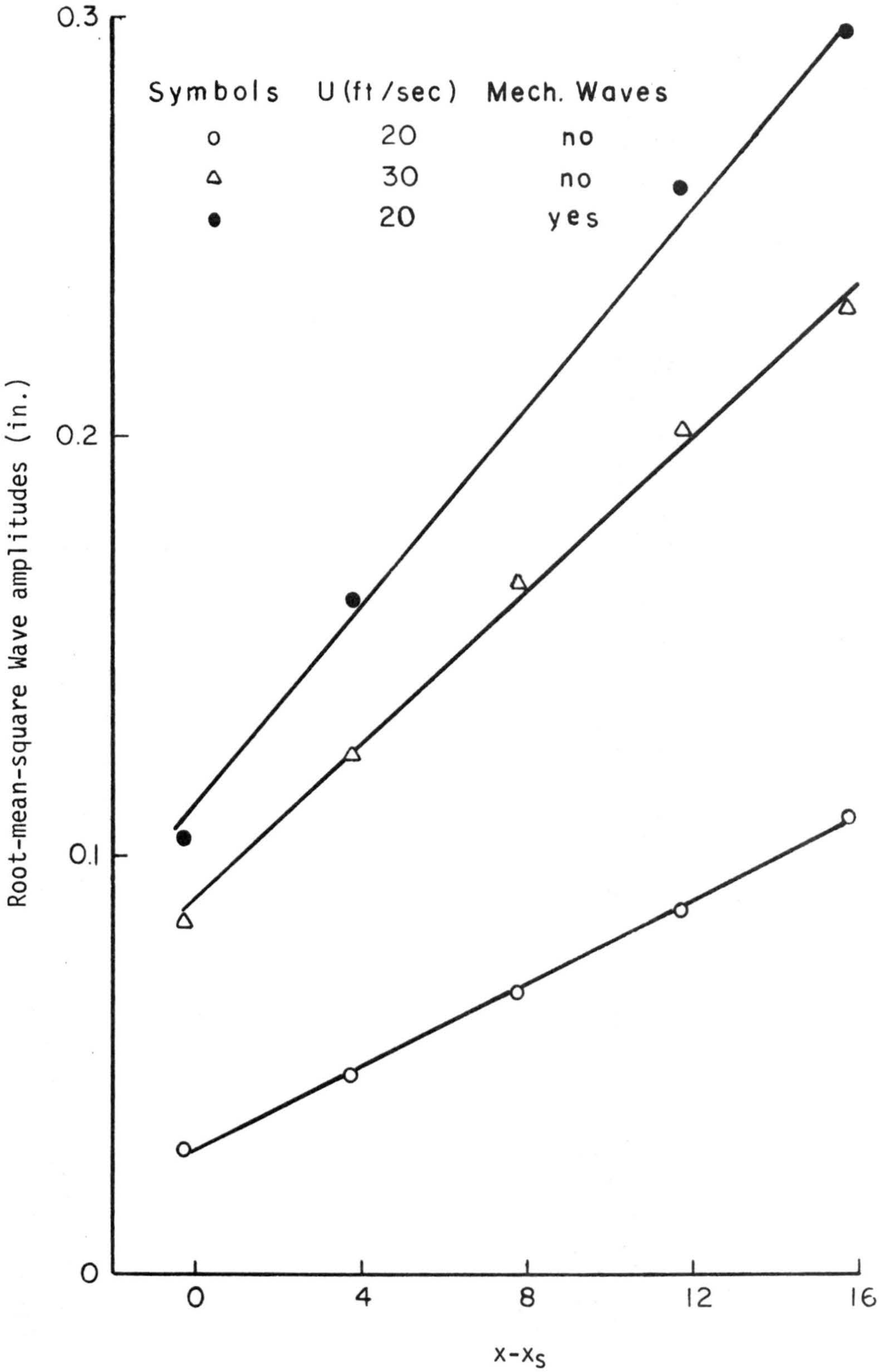

Figure 6-1. Root-mean-square wave amplitudes.

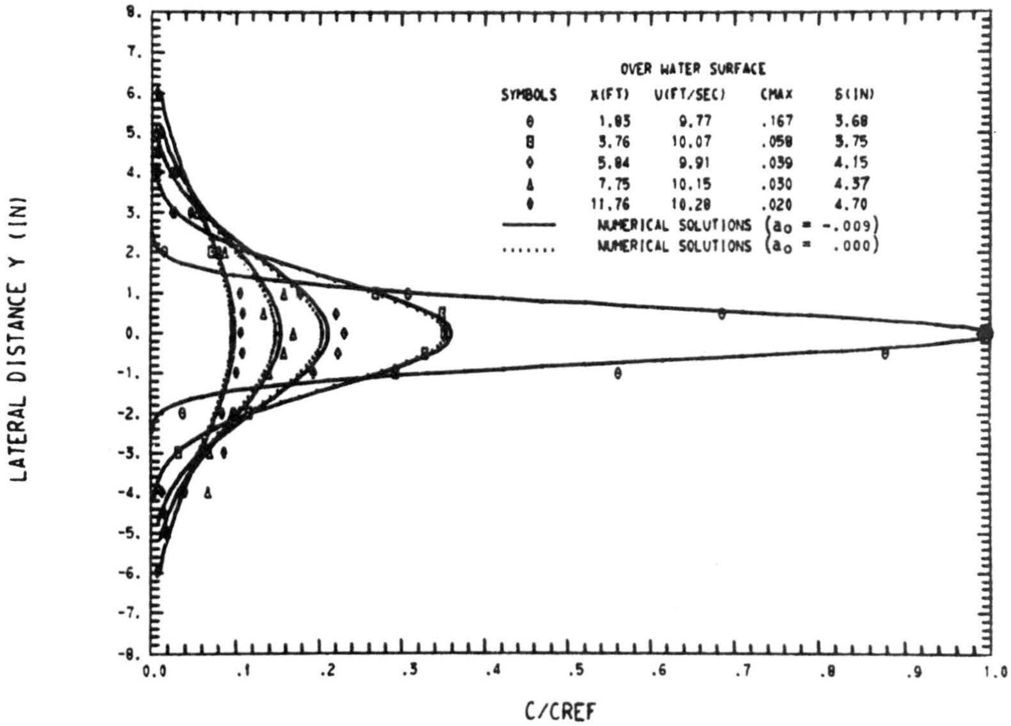

(a)

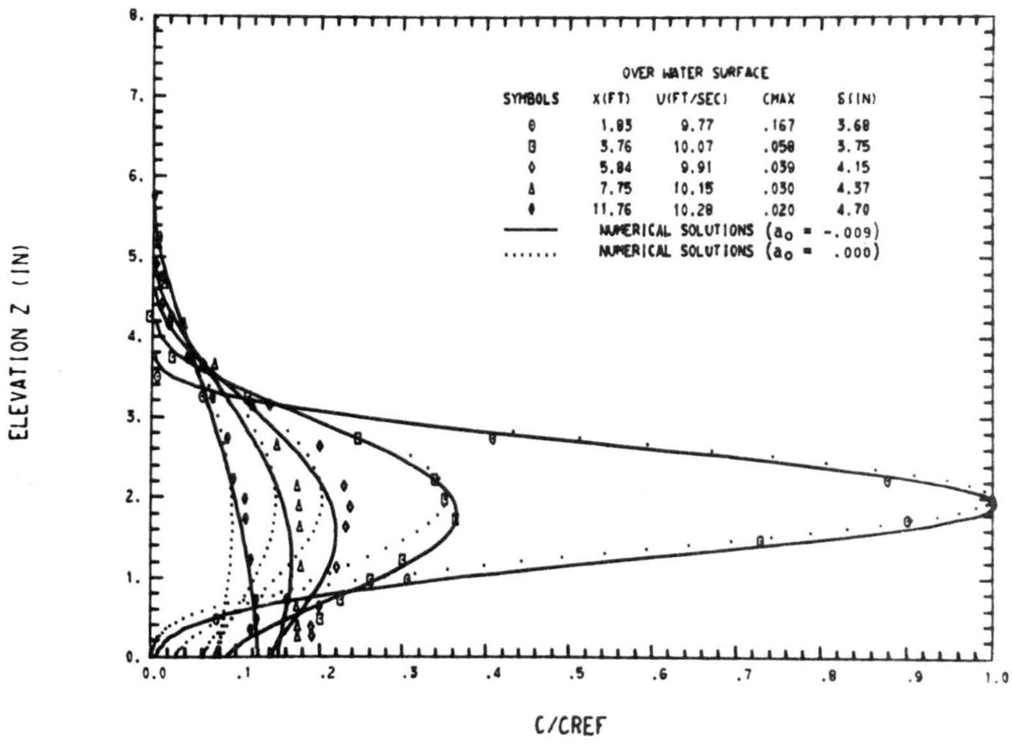

(b)

Figure 6-2. Mean concentration distributions over wind waves, $U_\infty \approx 10$ fps.

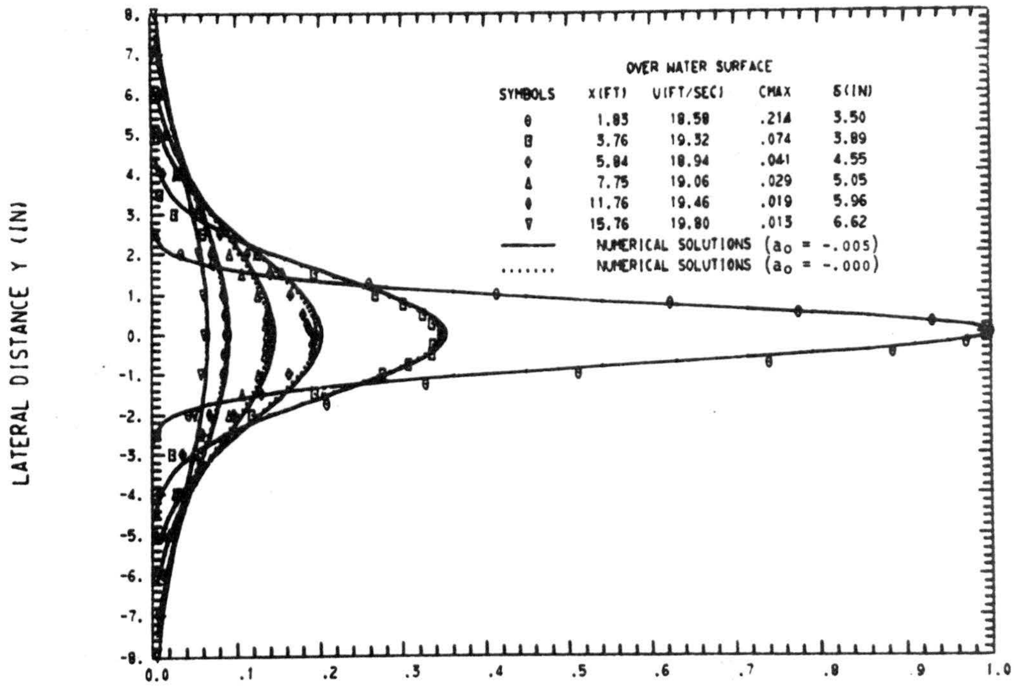

(a)

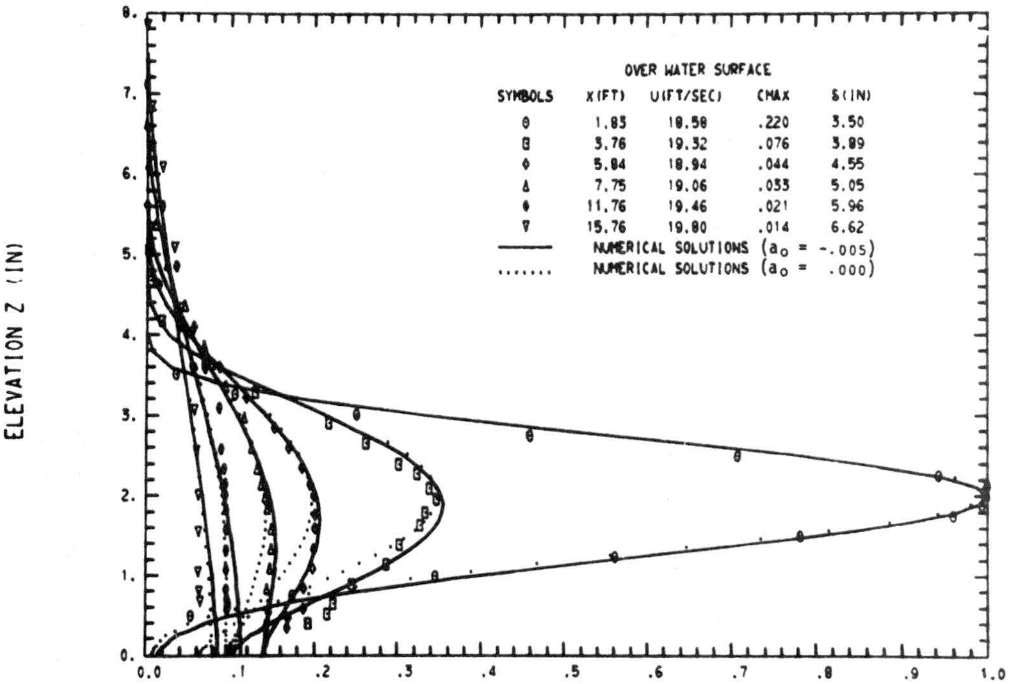

(b)

Figure 6-3. Mean concentration distributions over wind waves, $U_\infty \simeq 20$ fps.

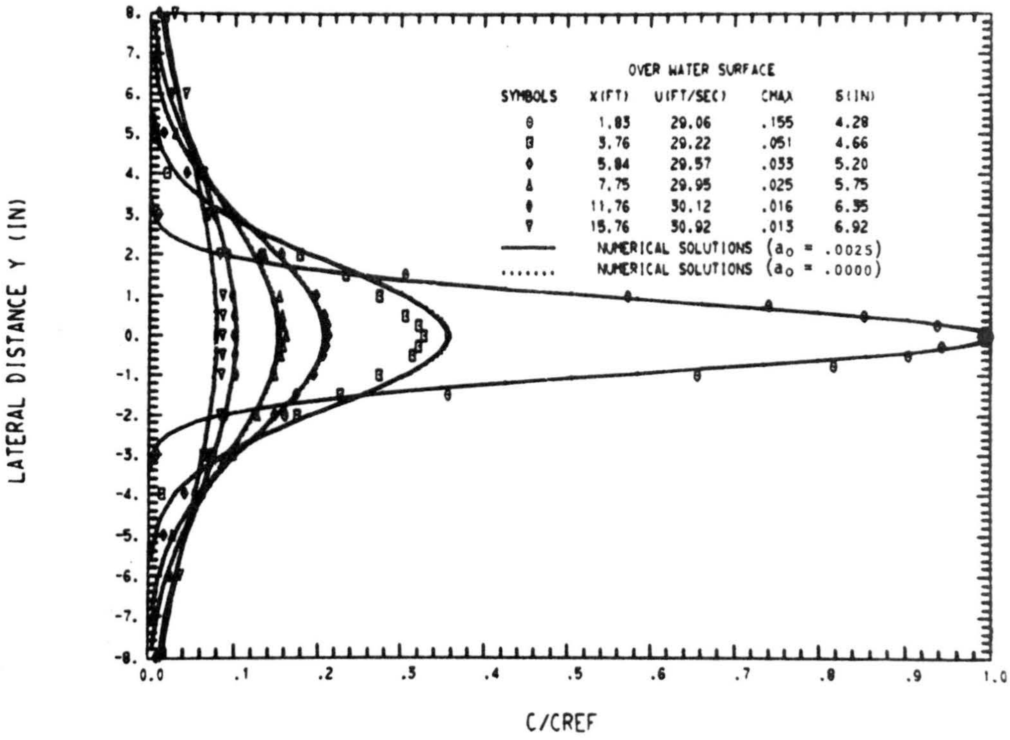

(a)

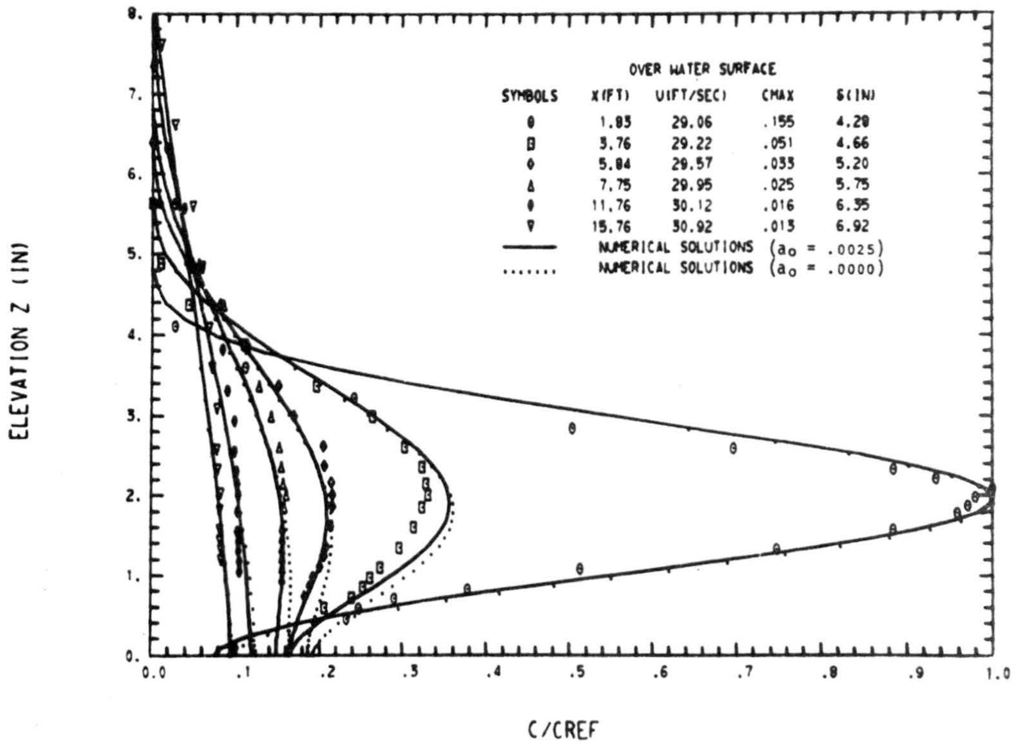

(b)

Figure 6-4. Mean concentration distributions over wind waves, $U_\infty \simeq 30$ fps.

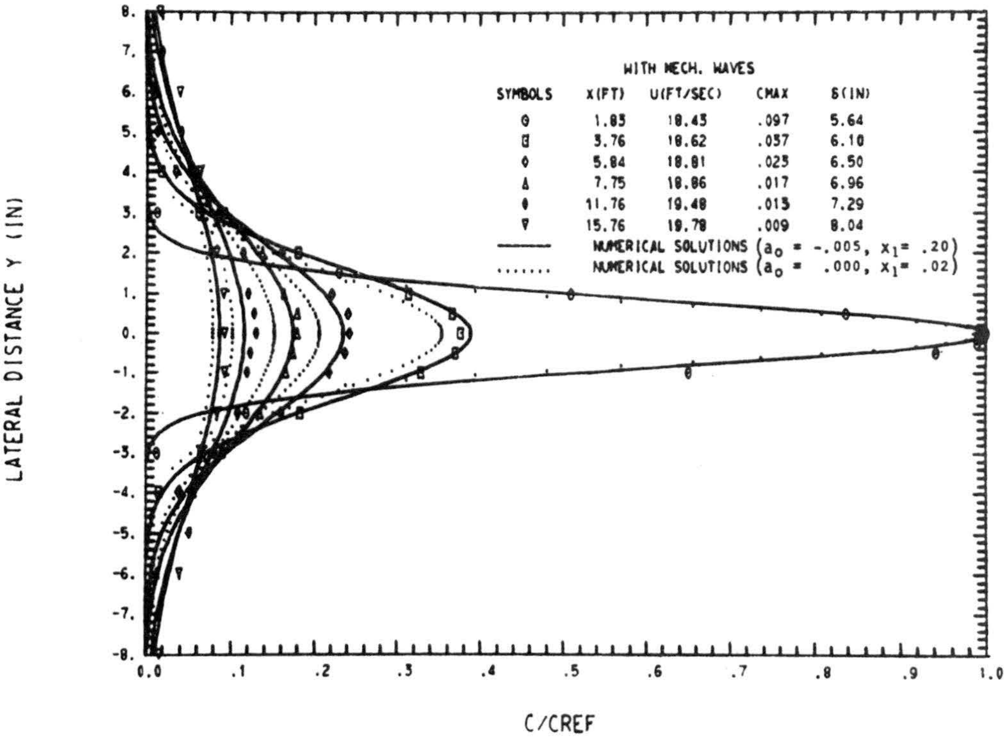

(a)

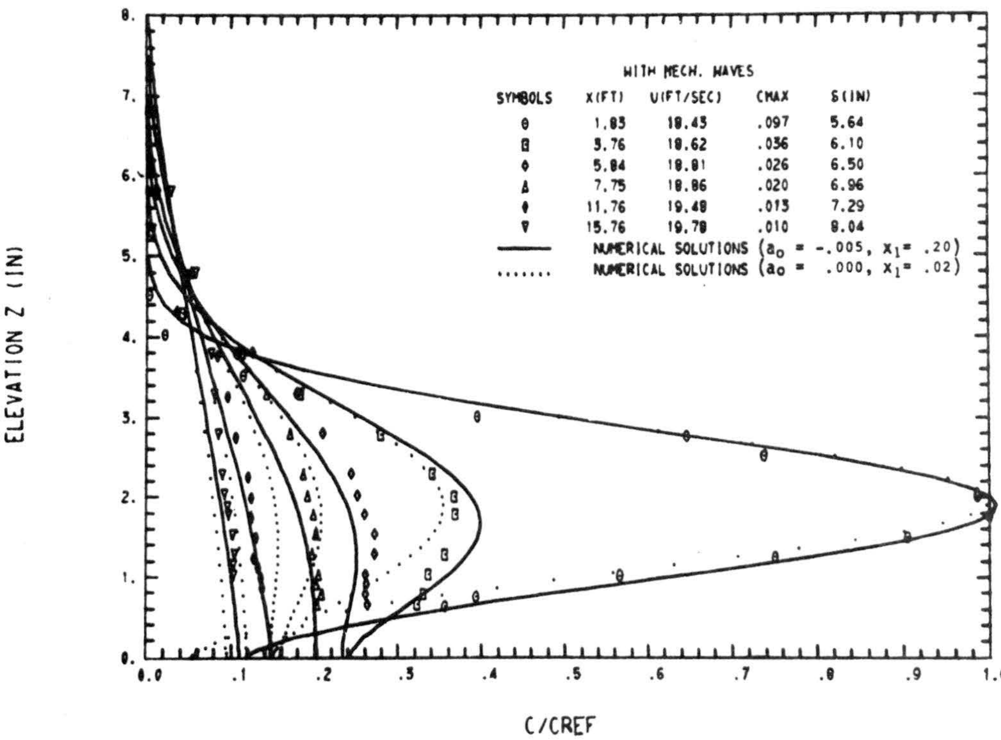

(b)

Figure 6-5. Mean concentration distributions over mechanical waves, $U_\infty \simeq 20$ fps.

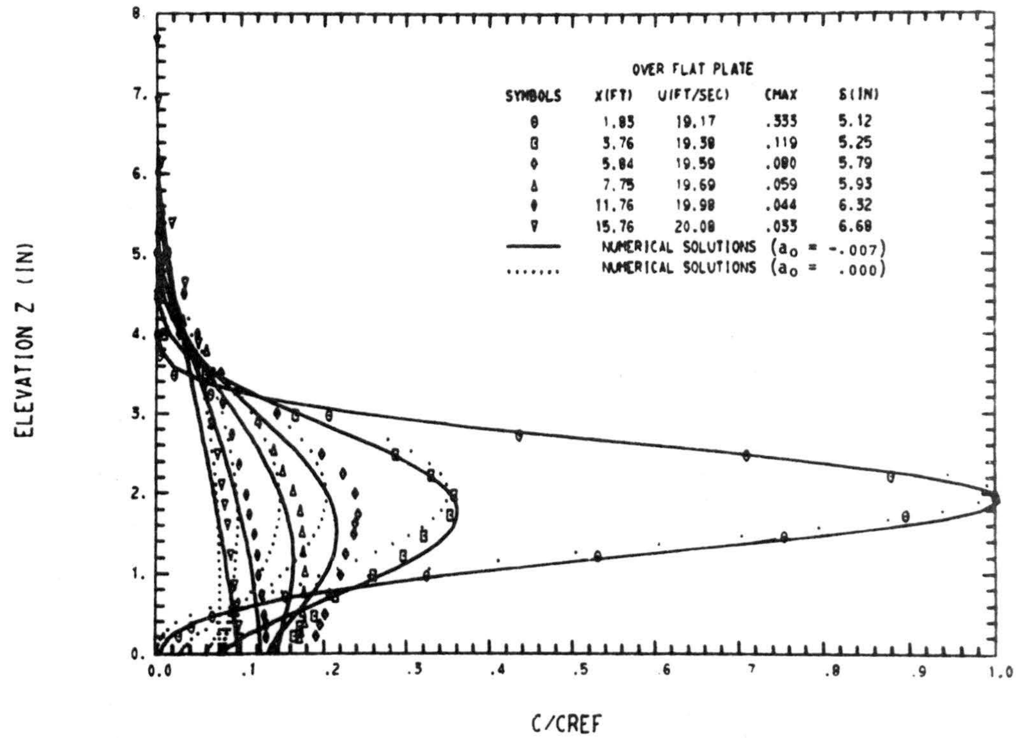

(a) Vertical Mean Concentration Distributions

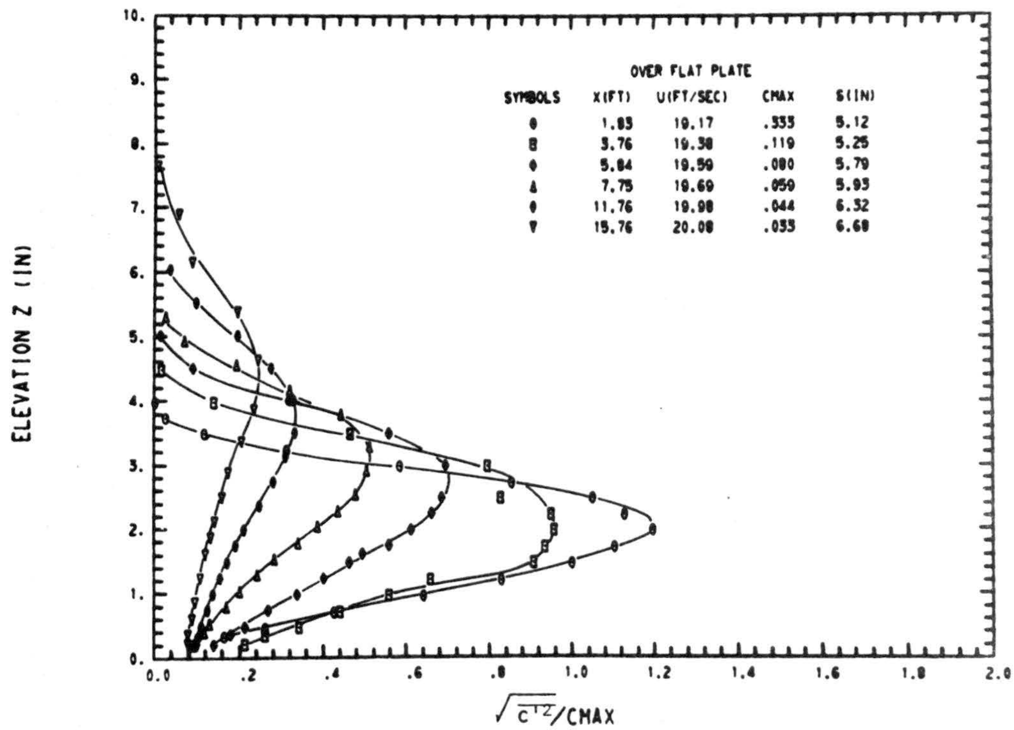

(b) Vertical Relative RMS Concentration Distributions

Figure 6-6. Concentration distributions over a flat plate, $U_\infty \simeq 20$ fps.

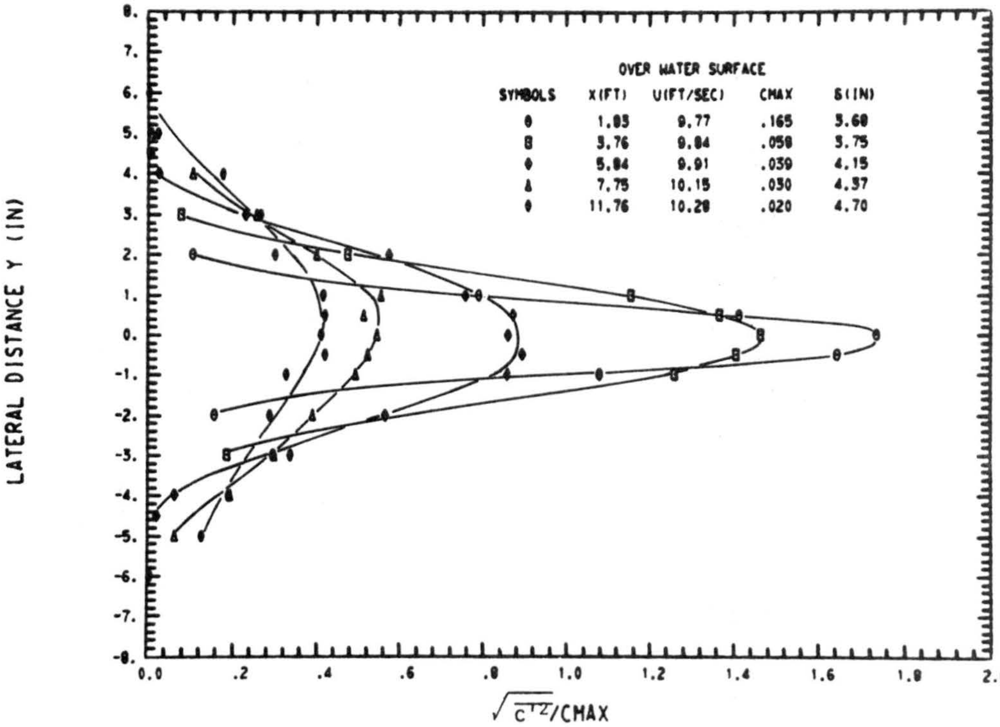

(a)

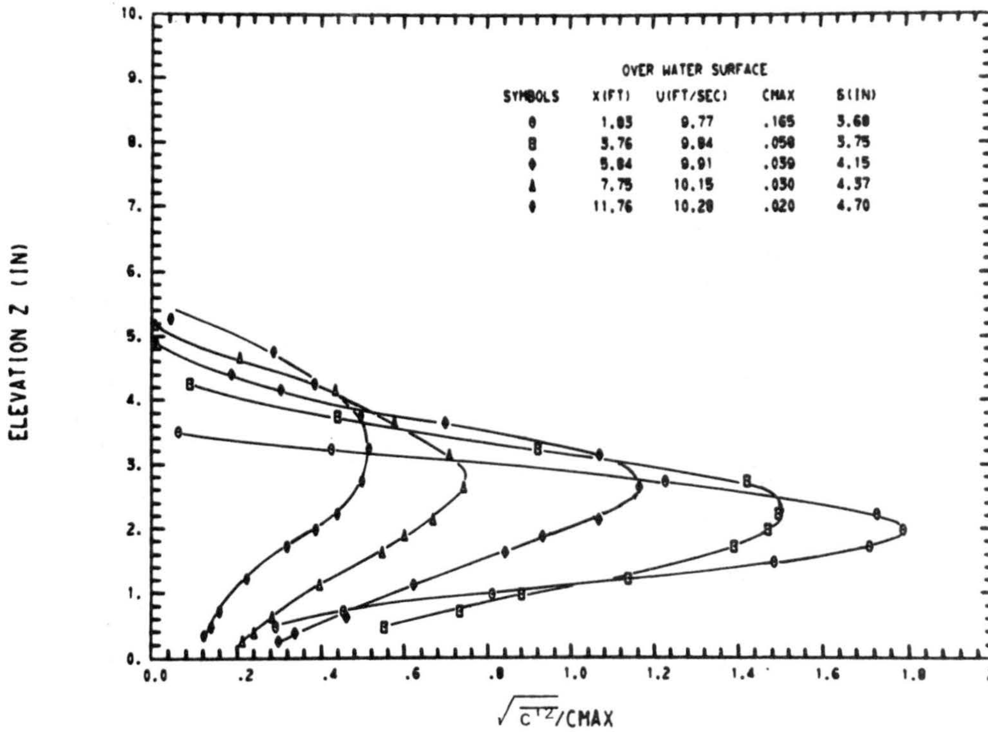

(b)

Figure 6-7. Relative rms concentration distributions over wind waves, $U_\infty \simeq 10$ fps.

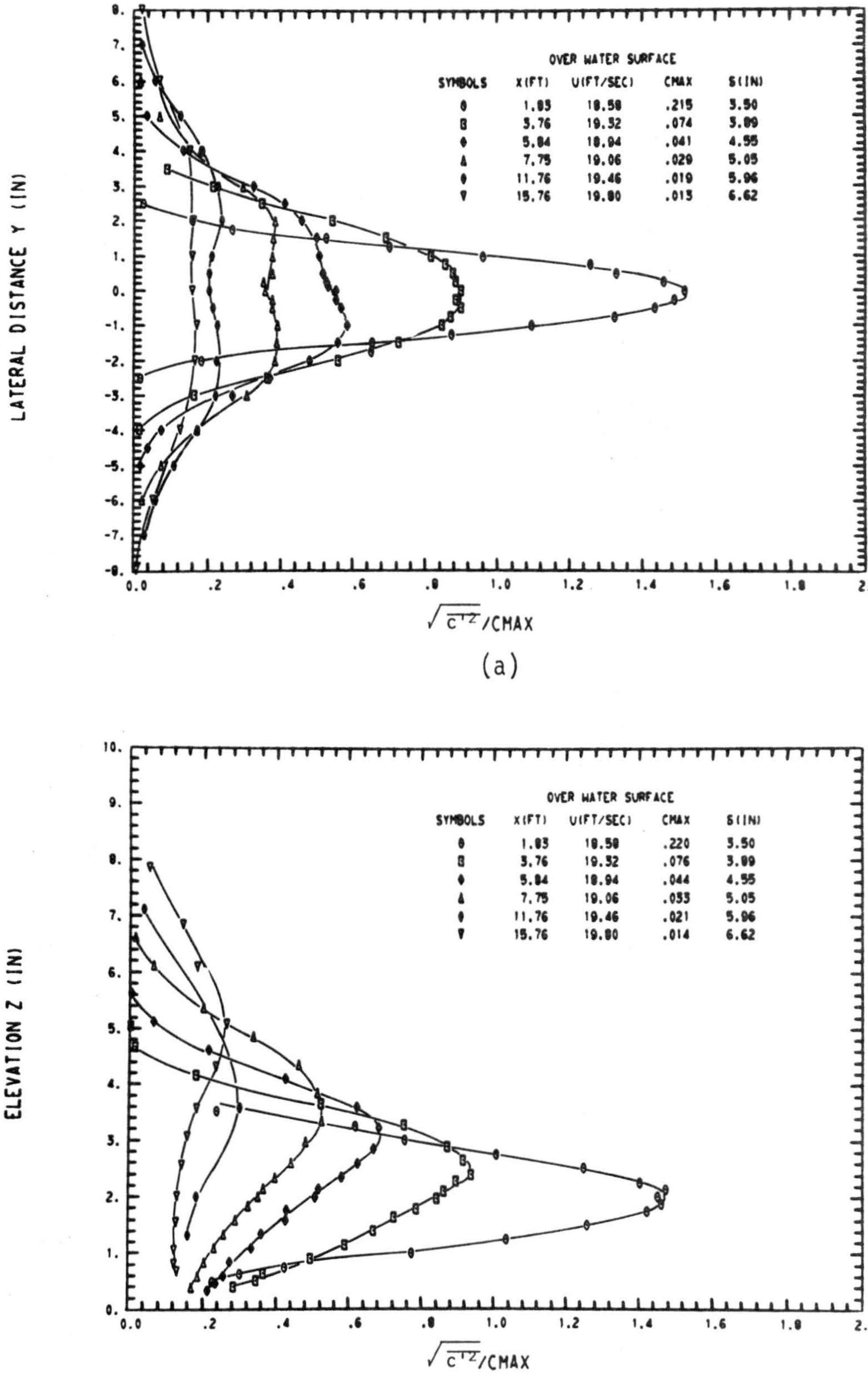

Figure 6-8. Relative rms concentration distributions over wind waves, $U_\infty \simeq 20$ fps.

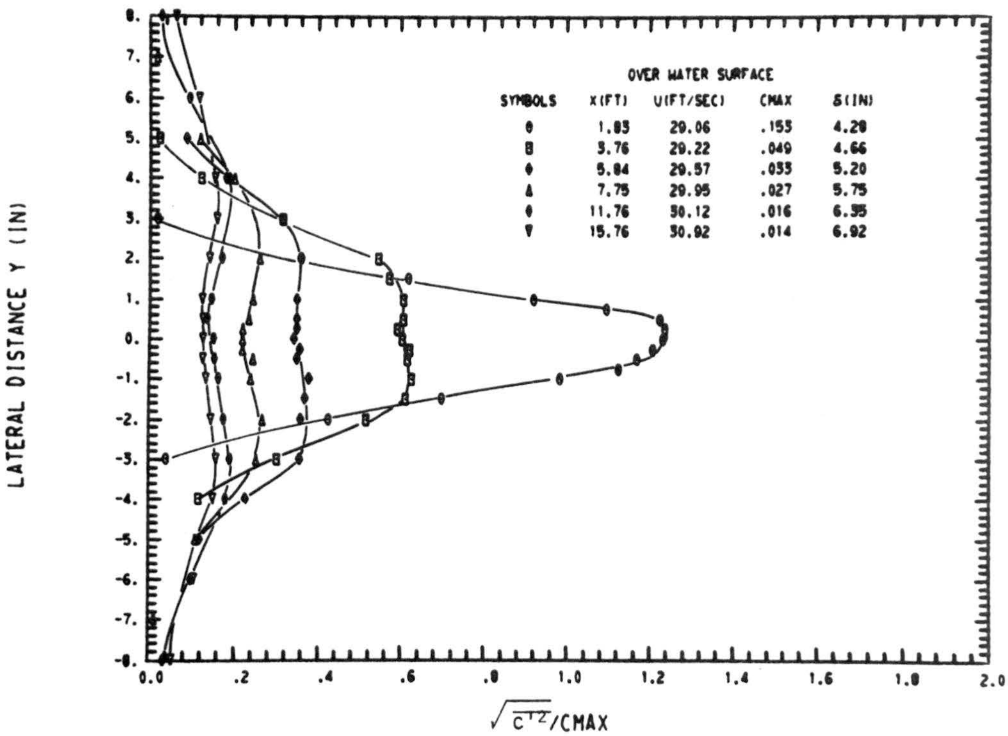

(a)

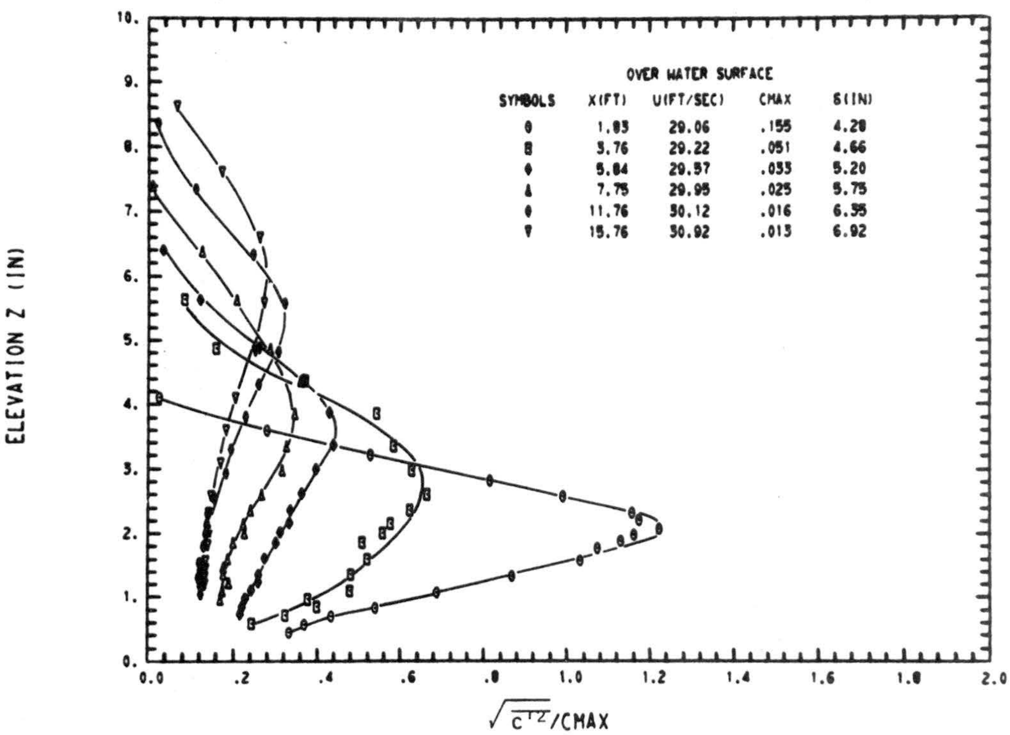

(b)

Figure 6-9. Relative rms concentration distributions over wind waves, $U_\infty \simeq 30$ fps.

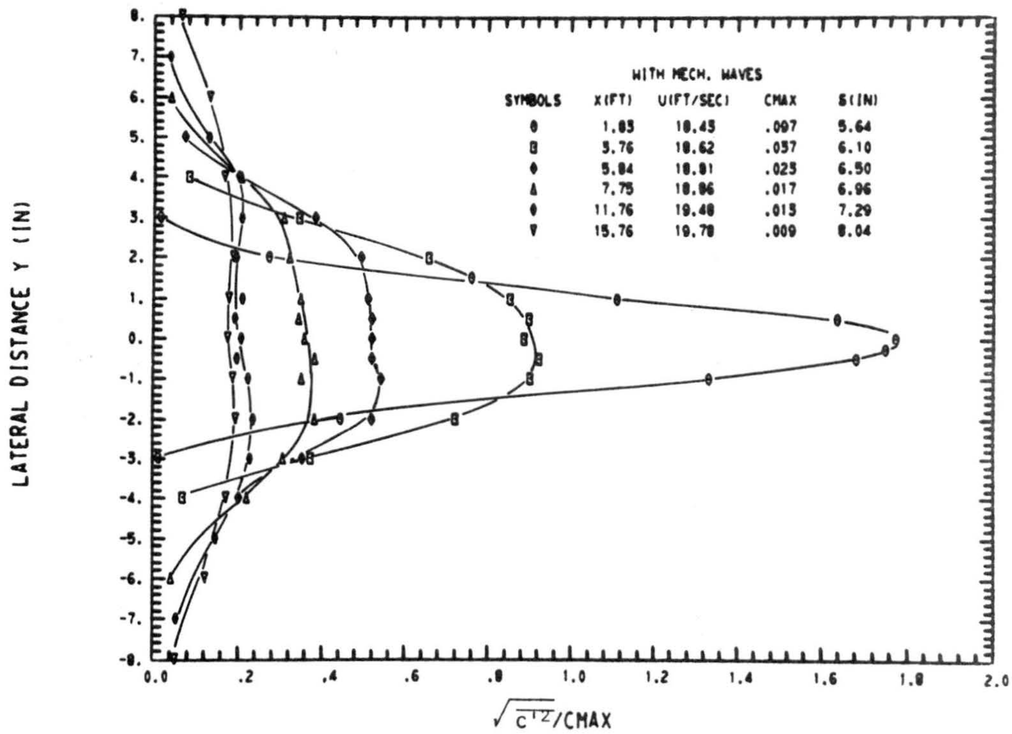

(a)

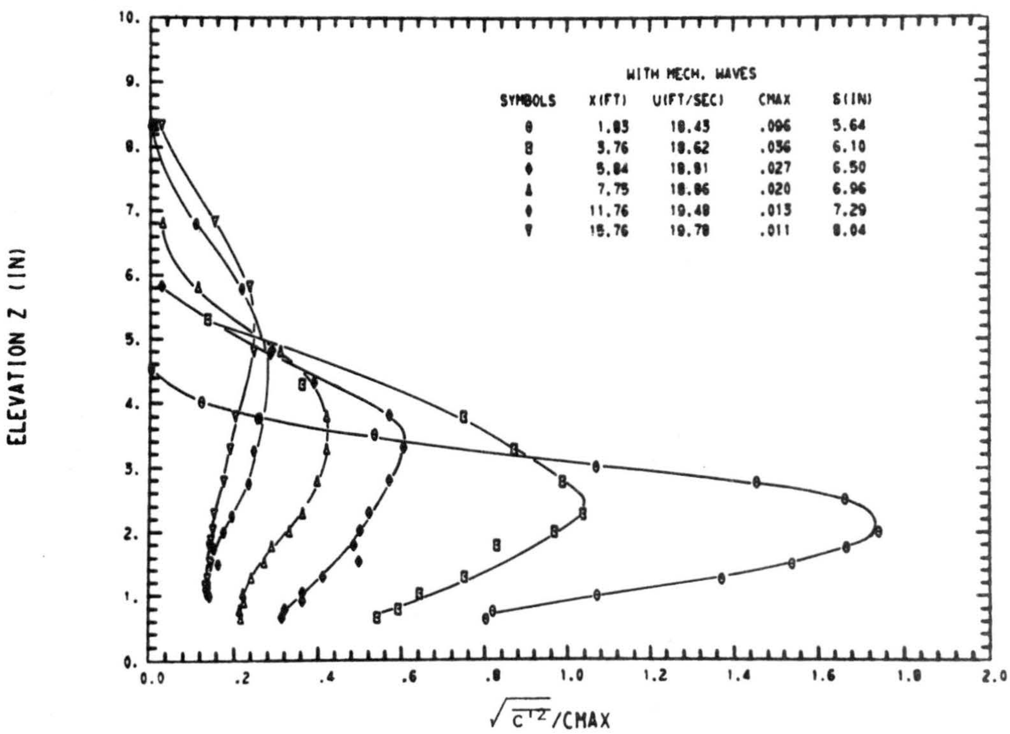

(b)

Figure 6-10. Relative rms concentration distributions over mechanical waves, $U_\infty \simeq 20$ fps.

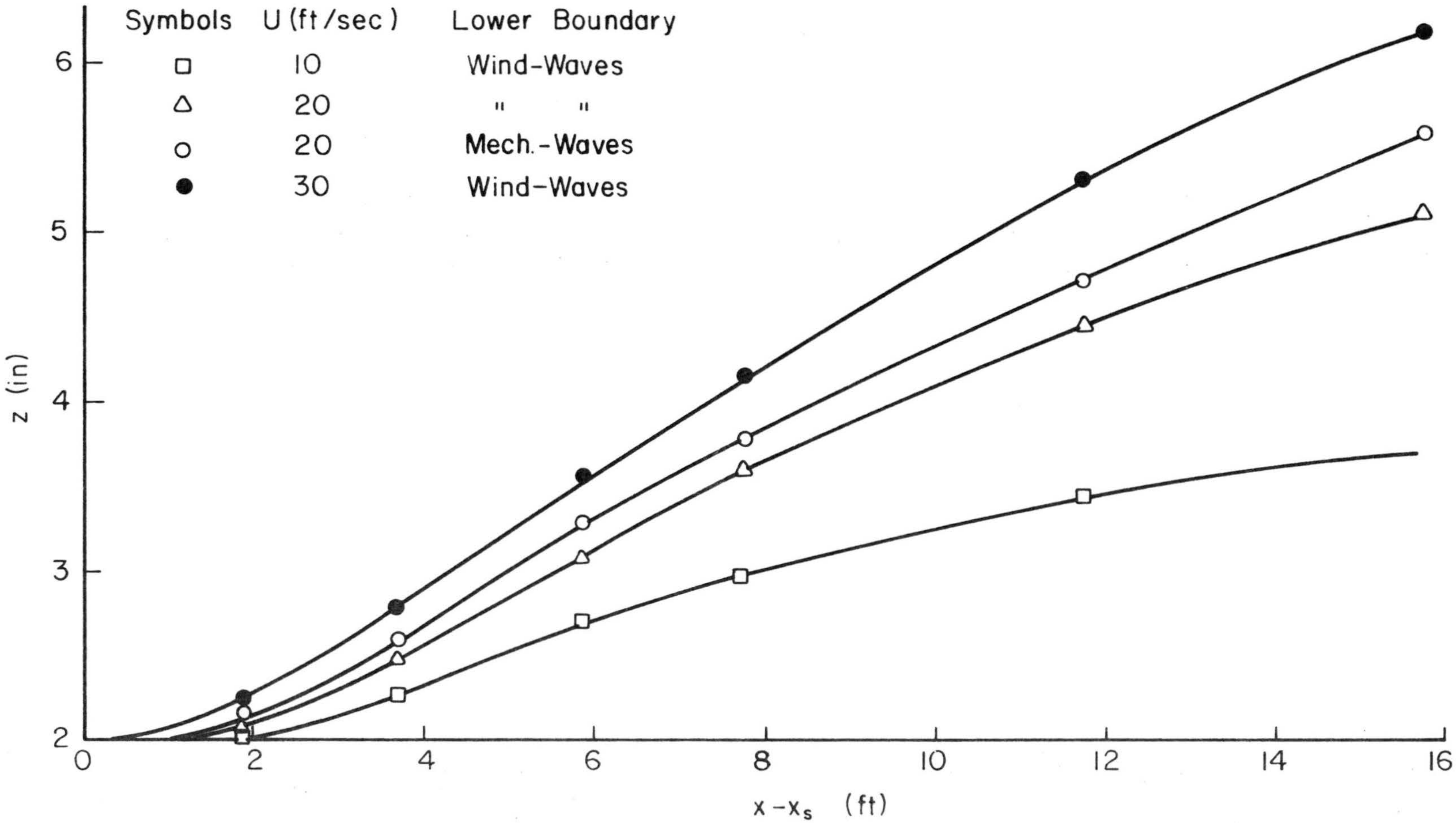

Figure 6-11. Trajectories of maximum rms concentration at successive stations on the x-z plane through $y = y_s$.

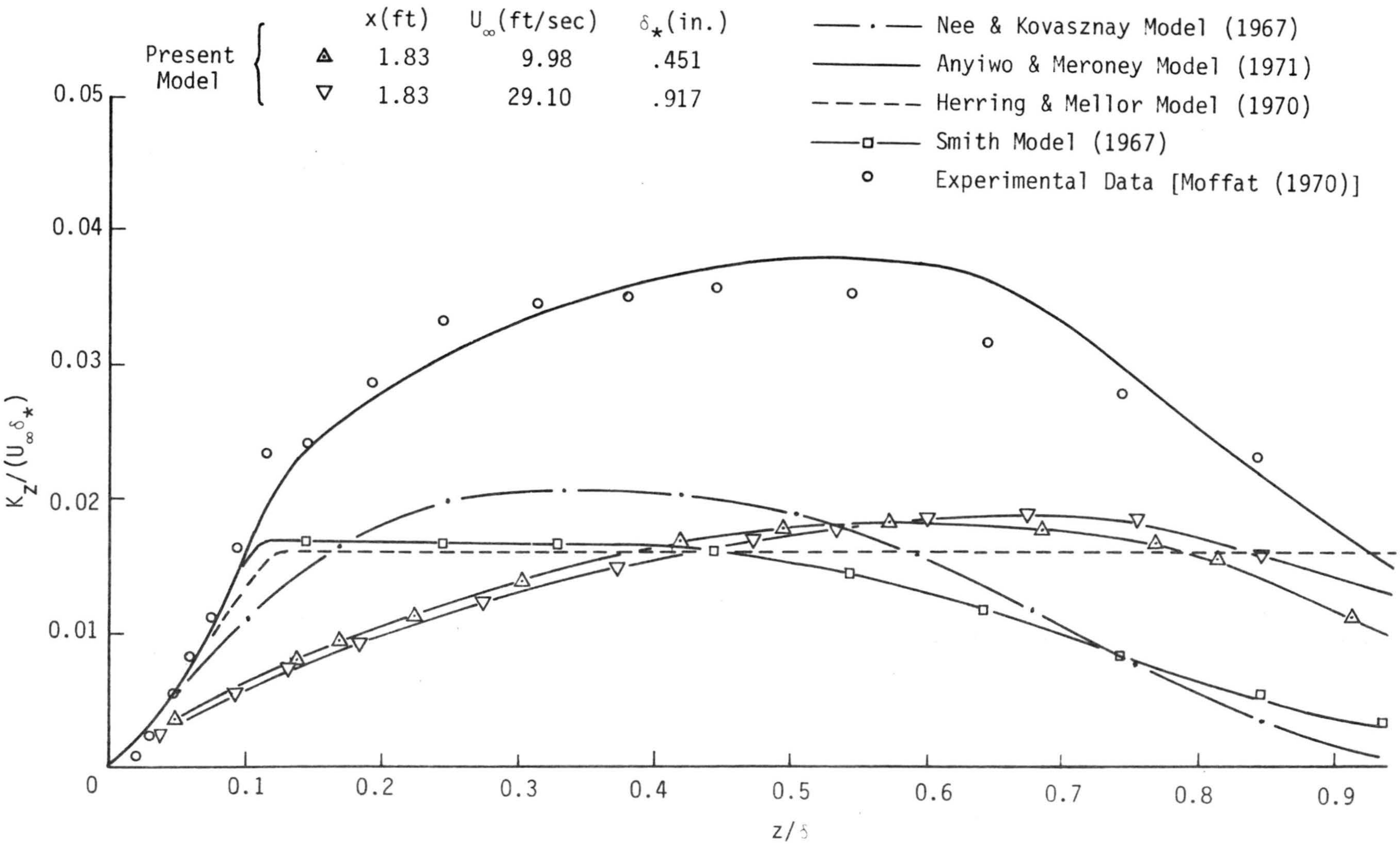

Figure 6-12. Comparisons of vertical diffusivity models.